Travelling Waves in Distributed Control

by

Ing. Dan Martinec

supervised by *Prof. Ing. Michael Šebek, DrSc.*

Dissertation

Presented to the *Department of Control Engineering,*
Faculty of Electrical Engineering of
Czech Technical University in Prague
in Partial Fulfillment of the Requirements
for the Degree of

Doctor

in Ph.D. programme
Electrical Engineering and Information Technology
in the branch of study
Control Engineering and Robotics

Czech Technical University in Prague
December 2015

Do Good.
And Good
will come to you.

– Buddhist proverb

I would like to dedicate this thesis to my parents for their endless support and love during my studies filled with moments of bliss and moments of despair. You are the best parents that one can wish for. Words cannot express the gratitude and love I feel to you.

Konej dobro.
A dobro
se ti vrátí.

– Buddhistické přísloví

Tuto práci bych rád věnoval mým rodičům pro jejich neutuchající podporu a lásku během mého studia plného okamžiků štěstí ale i zoufalství. Jste ti nejlepší rodiče, které si každý může přát. Slova nedokáží vyjádřit vděk a lásku, co k Vám cítím.

Acknowledgements

It has been a privilege to study on the Department of Control Engineering. I consider myself lucky that I could collaborate with many wonderful people. It is not easy to leave this group since I have so many fond memories connected to this department. There are a lot of things that I am grateful for. It is not possible to name it all here, but I would like to personally thank the persons that shaped my study most.

Czech Technical University in Prague   *Dan Martinec*
December 2015

Declaration

This doctoral thesis is submitted in partial fulfillment of the requirements for the degree of doctor (Ph.D.). The work submitted in this dissertation is the result of my own investigation, except where otherwise stated. I declare that I worked out this thesis independently and I quoted all used sources of information in accord with Methodical instructions about ethical principles for writing academic thesis. Moreover I declare that it has not already been accepted for any degree and is also not being concurrently submitted for any other degree.

Czech Technical University in Prague   *Dan Martinec*
December 2015

Abstract

The thesis develops a novel approach, the so-called travelling-wave approach, for the analysis and control of a linear multi-agent system. The approach takes advantage of the wave-like behaviour of a multi-agent system by decomposing the outputs of the agents into two waves travelling through the system in opposite directions. The main advantage of the approach is that it splits the bidirectional interactions between the agents into two non-interacting waves. This allows us to study the interactions between two neighbouring agents without the necessity to consider the effect of other agents in the system. Such a local analysis then allows us to infer system properties, such as the string stability of even a large scale system, which is difficult to carry out with the traditional approaches. Another benefit of the travelling-wave approach is that it allows us to design a feedback controller, which significantly shortens the transient of the system.

The most challenging issue of the approach is that it employs irrational transfer functions, which are less mathematically studied than rational transfer functions. For instance, even the current state-of-the-art programs are not able to carry out the inverse Laplace transform of an irrational transfer function. Therefore, a part of the thesis focuses on the development of algorithms for the rational approximation of irrational transfer functions. The programs carrying out the approximation are published online on the webpage of Matlab Central and have already been downloaded by dozens of users.

Key words: multi-agent system, string stability, travelling wave, wave transfer function

Abstrakt

Disertační práce představuje nový, tzv. vlnový, přístup, který je použit pro analýzu a řízení lineárních multi-agentních systémů. Základní myšlenka tohoto přístupu spočívá ve využití vlnového chování multi-agentního systému a rozložení výstupního signálu agenta do dvou postupných vln, které se šíří v opačných směrech. Hlavní výhodou potom je, že dokážeme rozložit obousměrnou interakci mezi agenty do dvou postupných vln, které spolu neinteragují. To nám umožní prostudovat vzájemnou interakci mezi dvěma sousedícími agenty bez toho, že bychom museli vzít do úvahy interakce mezi ostatními agenty v systému. Tato lokální analýza je výhodná v tom, že nám umožní odvodit vlastnosti, jako například stringovou stabilitu, i většího systému, což je velmi složité se současnými metodami. Vlnový přístup dále umožňuje navrhnout zpětnovazební regulátor, který kvalitativně zlepší rychlost odezvy celého systému.

Největší komplikací tohoto přístupu je, že pracuje s iracionálními přenosovými funkcemi, které nejsou matematicky prostudovány tak dobře jako racionální přenosové funkce. Například, ani ty nejlepší současné programy nedokáží vypočítat inverzní Laplaceovu transformaci iracionální přenosové funkce. Část práce se proto zabývá i algoritmy, které iracionální přenosové funkce aproximují pomocí racionálních přenosových funkcí. Programy, které tuto aproximaci vypočítají, jsou zveřejněny na stránkách Matlab Central a již byly staženy desítkami uživatelů.

Klíčová slova: multi-agentní systém, stringová stabilita, postupná vlna, vlnová přenosová funkce

Acronyms

ATF   Agent transfer function
AWTF   Asymmetric wave transfer function
BTF   Boundary transfer function
CRHP   Closed-right half plane
FIR   Finite impulse response
MSE   Mean square error
ORHP   Open-right half plane
WTF   Wave transfer function

Contents

Contents

Contents

1 Introduction

1.1 Motivation

The distributed control is a broad and active field of research. The need for it comes from the mobile robotics mainly due to the current advances in miniaturization. The aim is to represent and control a large set of interacting autonomous agents to reach a common goal. The motivation may vary from purely practical (re-position large group of agents without collisions) through economical (lower fuel consumption of vehicular platoons) to feasibility issues, when a single agent is not able to fulfil the task (mapping of a large area). As the number of agents in the system increases, the control becomes more challenging since the centralized information is usually not available to all the agents. Although each agent usually has its own local controller and performs well as individual, the interaction with other agents may trigger unexpected phenomena such as: dramatic increase of the required control effort (called string instability or harmonic instability), or in some cases, even the asymptotic instability of the whole distributed system. Sometimes, the control of the distributed system is counter-intuitive since the system performance may be dramatically improved or deteriorated by adding or removing just one communication link between the agents.

The distributed system can be found in a many, seemingly unrelated, areas such as: formation of agents (platoon of vehicles, sensor network, fleet of unmanned boats), biological systems (neural and ecological networks), social systems (Facebook), technological systems (energy networks, traffic in cities) etc. The internet itself represents a massive distributed system. Many of online applications are beautiful applications of the distributed

control theory in practice, such as (Google PageRank, Netflix, BitTorrent, Skype etc., see [Chiang (2012)]).

Nowadays, the distributed control is a very active field of research, particularly in the control community. At least one third of the papers, but usually more, are related to the distributed control or networks of agents on the top control-community conferences such as Conference on Decision and Control (CDC), American Control Conference (ACC) or European Control Conference (ECC). The same applies to the top control-community journals such as Automatica or IEEE Transactions on Automatic Control. Recently, a new journal has been founded (IEEE Transactions on Control of Network Systems), which is dedicated entirely to the distributed control.

1.2 State of the art

1.2.1 Laplacian approach for analysis of multi-agent systems

General graph topology

The traditional approach for the analysis of a linear multi-agent system with a general graph topology is based on the algebraic graph theory. A thorough introduction into this field is given for instance in (Ren et al., 2007), [Olfati-Saber et al. (2007)] or [Mesbahi and Egerstedt (2010)]. The analysis of nonlinear systems is usually carried out either by the Lyapunov function, see [Moreau (2005)] and [Zhang et al. (2012)], or by the examination of the passivity of the multi-agent system, see for instance [Chopra and Spong (2006)], [Arcak (2007)], [Zelazo and Mesbahi (2011)] or [Yamamoto and Smith (2013)].

The simplest and most studied interaction topology of a multi-agent system is a path graph. It represents interactions in a system where each agent, except of the first and last ones, interacts with two neighbouring agents. It is used, for instance, as a model of vehicular platoons

[Eyre et al. (1998)], [Swaroop and Hedrick (1999)], discretized flexible structures [Singhose et al. (1996)] or [Dwivedy and Eberhard (2006)], or spatially-discretized models of long electrical transmission lines [Dhaene and Zutter (1992)]. A path graph is also called a chain graph, see for instance [Egerstedt et al. (2012)] or [Cao et al. (2012)].

Path graph topology - vehicular platooning

Regarding control strategies, among the first treatments of vehicular platooning were papers by [Levine and Athans (1966)] and [Melzer and Kuo (1971)]. They examined a centralized control approach with a single global controller governing all vehicles. However, [Jovanovic and Bamieh (2005)] later showed that one has to be careful about the stability of the system, since it might degrade with an increasing number of vehicles. Nevertheless, more attention is paid to fully or partially distributed control, wherein each vehicle is controlled by its own on-board controller with only limited knowledge about the platoon. Among the first papers dealing with such distributed control was the work by [Chu (1974)]. Basic questions about the feasibility and performance of such systems were introduced by [Cosgriff (1969)] and later formalized by [Swaroop and Hedrick (1996)] under the term *string stability*.

The string stability, or more precisely string instability, is a phenomenon that causes higher control demands on the members of a vehicular platoon that are farther from the source of regulation error, see the definitions in [Eyre et al. (1998)], [Ploeg et al. (2014)] or [Swaroop and Hedrick (1996)]. The string stability is a useful analytic tool that is used for the performance assessment of various distributed control strategies, see for instance [Seiler et al. (2004)], [Barooah and Hespanha (2005)] and [Shaw and Hedrick (2007)]. However, it is important to stress out that it does not guarantee that the vehicles do not crash into each other. Similar analytical measures of system performance are harmonic stability [Tangerman et al. (2012)] and flock stability [Cantos and Veerman (2014)]. A fundamental limitation of many distributed algorithms with only local information about the platoon is the inability to maintain coherence in

a large-scale platoon subjected to stochastic disturbances [Bamieh et al. (2012)]. However, the coherence can be improved by introducing optimal non-symmetric localized feedback [Lin et al. (2012)].

A common goal of each platooning algorithm is to drive the platoon with a reference velocity and inter-vehicle distances. Many distributed algorithms have been introduced in the platooning field. The most simple algorithm, relying only on the measurement of the distance to the immediately preceding vehicle, is the so-called *predecessor following algorithm*. A straightforward extension is the so-called *bidirectional control algorithm*, which additionally measures the distance to the immediate follower. Depending on the weight between the two distance measurements, we distinguish either *symmetric*, see e.g. [Lestas and Vinnicombe (2007)], [Middleton and Braslavsky (2010)], [Barooah and Hespanha (2005)] [Hao and Barooah (2012b)], or *asymmetric*, see [Barooah et al. (2009)], bidirectional control.

In order to assure that the vehicles in the platoon are able to track the leader moving with a constant velocity, we need to satisfy the Internal Model Principle [Wieland et al. (2011)], [Lunze (2012)], which, in this case, means the presence of two integrators in the open-loop model of each vehicle. It was shown in [Seiler et al. (2004)] that the string instability is unavoidable for the agents with two integrators and the predecessor following algorithm. Later, it was shown in [Hao and Barooah (2012a)] that the same asymmetry for all states used for coupling causes a nonzero lower bound on the distributed-system eigenvalues, which guarantees the controllability of a system with even a large number of agents, see [Barooah et al. (2009)]. The disadvantage of such an asymmetric bidirectional control of agents with two integrators, as shown in [Tangerman et al. (2012)] and [Herman et al. (2015a)], is that the system is harmonically unstable, meaning that the H_∞ norm of transfer functions between the agents scales exponentially with the number of agents in the system. The asymmetric bidirectional controllers were generalized in [Hao et al. (2012)] and [Cantos and Veerman (2014)] by assuming nonequal asymmetries between the output states used in the bidirectional controller.

Another topic of interest is the transient of the system, see e.g. [Tangerman et al. (2012)], [Cantos and Veerman (2014)] and [Lunze (2013)], the locations of poles and zeros affecting the input-output behaviour described in [Briegel et al. (2011)] or [Zamani et al. (2015)], or the scaling of stability margin, see e.g. [Barooah et al. (2009)] or [Hao and Barooah (2010)].

These approaches are well suited for the analysis of overall system behaviour such as the asymptotic stability. However, they do not reveal how the disturbance, in our case the reference command, is locally and temporarily amplified by an individual agent. In other words, how the travelling wave, generated by the disturbance, changes the output of the agent before it reflects from the boundary in the system and reaches the agent again. This local-temporal-performance analysis can be carried out by the travelling-wave approach proposed in the thesis.

1.2.2 Transfer-function approach to travelling waves

The origins of control based on travelling waves lies in the 1960's in the mathematical modeling and analysis of flexible structures. [Vaughan (1968)] was one of the first treatments analysing simpler instances of flexible structures such as beams and plates. The analysis and control of more complex flexible structures from the viewpoint of travelling wave-modes was investigated in a series of papers by von Flotow and his colleagues in [Flotow (1986a)] and [Flotow (1986b)].

Recently, the concept was revisited by O'Connor in [O'Connor (2006)] and [O'Connor (2007)] for vibrationless positioning of lumped multi-link flexible mechanical systems. It was named *wave-based control* and it is based on the so-called *wave transfer function*, which describes how the traveling wave propagates in the lumped system. Parallelly with O'Connor, the wave concept was also considered for the control of continuous flexible structures by Halevi and his colleagues in [Halevi (2005)], [Halevi and Wagner-Nachshoni (2006)] and [Sirota and Halevi (2015)] under the name *absolute vibration suppression*. It relies on the transfer function as well,

though, in this case, the time delay plays a key role. Surprisingly, it was shown by [Peled et al. (2012)] that both the wave-based control and the absolute vibration suppression are a feedback version of the input shaping control. It was also shown that the wave-based control can be generalized even for continuous flexible systems, e.g., a steel rod, and then it coincides with the absolute vibration suppression. A more thorough comparison by [Martinec et al. (2015c)] revealed that the wave-based control and Multi-Mode Zero-Vibration input shaping concept, developed by ([Vyhlídal et al. (2013)]), can be combined, which has an advantage of both an appropriate initial excitation of the system by the input shaper and the increased robustness due to the wave-based feedback architecture.

The description of the travelling waves is based on the assumption of the spatial causality, that is, the boundary condition does not affect the wave travelling towards it. This assumption applied to the description of infinite number of agents in the multi-agent system results in the description by irrational transfer functions. The analysis of irrational and rational transfer functions differ in several aspects, see [Curtain and Morris (2009)] for a thorough overview. For instance, despite many examples of the inverse Laplace transform of irrational transfer functions, see [Bateman and Erdélyi (1954)], it is difficult to find an exact impulse response for many of them. We note that the travelling wave approach can be used to describe even a system with a finite number of agents by considering the boundary conditions.

The key idea of the wave-based control is to generate a wave at the actuated front-end of the interconnected system and let it propagate to the opposite end of the system, where it reflects and returns back to the front-end actuator. When it reaches the front again, it is absorbed by the front-end actuator by means of the wave transfer function. An interesting but troublesome property of the wave transfer function is the presence of the square root function. This makes its implementation in the time domain very challenging. To be able to run numerical simulations, the author of the thesis therefore introduced a convergent recursive algorithm that approximates the wave transfer function for an arbitrary dynamics

of the local system.

There are other viewpoints on wave-based control. One was introduced by [Ojima et al. (2001)] in terms of the characteristic impedance for a mass-spring system. Alternative viewpoint was introduced by [Nagase et al. (2005)] for the wave-based control of ladder electric networks. The impedance matching in power networks is also closely related to the wave-based control, e.g., [Thorp et al. (1998)] or [Lesieutre (2002)].

Although it seems to be complicated to use the wave concept in practice due to the irrationality of the controllers, there are several implementation of the wave absorbers in practice, see for instance [Saigo et al. (2004)], [Kreuzer and Steidl (2011)] or [O'Connor et al. (2008)]. The wave-based control is not limited only to the one-dimensional systems, that means the systems with a path-graph topology, but it can also be applied to two-dimensional systems as shown in [Mei (2011)] or [Sirota and Halevi (2014)], and possibly to nonlinear systems [O'Connor et al. (2008)].

1.2.3   Fractional order systems

It might seem that the irrational transfer function is closely related to the fractional order systems, see for instance [Ortigueira (2008)] and [Elwakil (2010)] for tutorials, where the square root of the Laplace variable s appears. The fractional order systems is an interesting field of research with a rich history, see the introduction of [Das (2011)]. The systems are well analyzed [Petras (2008)] and even supported by Matlab Crone toolbox [Oustaloup et al. (2000)].

The fractional order systems are based on fractional derivatives, hence, they consider fractional orders of s, for instance $1/(s^{0.5} + 1)$. Unfortunately, the methods developed for the analysis of these systems cannot be used for irrational transfer functions such as $1/\sqrt{s+1}$. Yet, we can still use some of their methods [Vinagre et al. (2000)] for approximating the wave transfer function, for instance the continued fraction method and the Carlson's method.

1.3   Aim of the Thesis

The thesis is motivated by the results of O'Connor and his colleagues ([O'Connor (2006)], [O'Connor (2007)] and [O'Connor et al. (2008)]) about the wave transfer function and its use for the suppression of vibration in mass-spring model. The main goal of the thesis is to tailor these results in the field of distributed control. In other words, we aim to describe a wave-like behaviour of a multi-agent system. We demonstrate the main idea on the following simple examples.
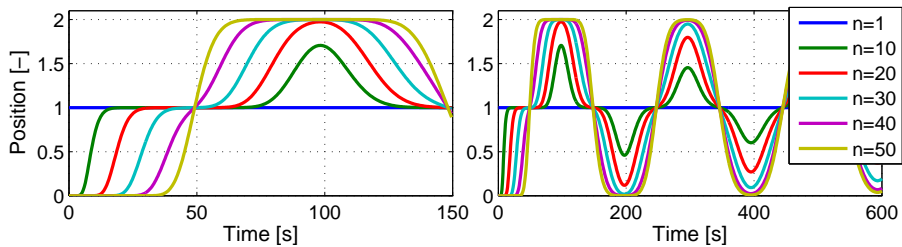
Figure 1.1: Step response of a multi-agent system with 50 identical agents driven by the symmetric bidirectional control law. The 1st agent (blue) line is the reference input to the system.

A demonstration of the wave-like behaviour is shown in Fig. 1.1 and Fig. 1.2. The figures show the response of 50 identical agents with a path-graph topology. Comparing top-left and top-right panels in Fig. 1.2, we can see a wave-like response of the agents. The wave travels from the left (1st agent) to the right. The agents with higher indexes successively change their position from 0 to 1. The wave reaches the last agent at time $t = 60\,s$ (middle-left panel), reflects and travels back to the left (middle-right panel), which for instance, makes the 30th agent to move to position 2. The wave continues travelling to the 1st, reflects back, and travels to the right again. In this manner, the wave keeps reflecting back and forth, which generates the standing wave pattern in Fig. 1.1. These reflections also causes that the settling time of the system is very long.

If it were possible to prevent the reflection of the wave from one of the ends, then the settling time would significantly be shorter see Fig. 1.3.
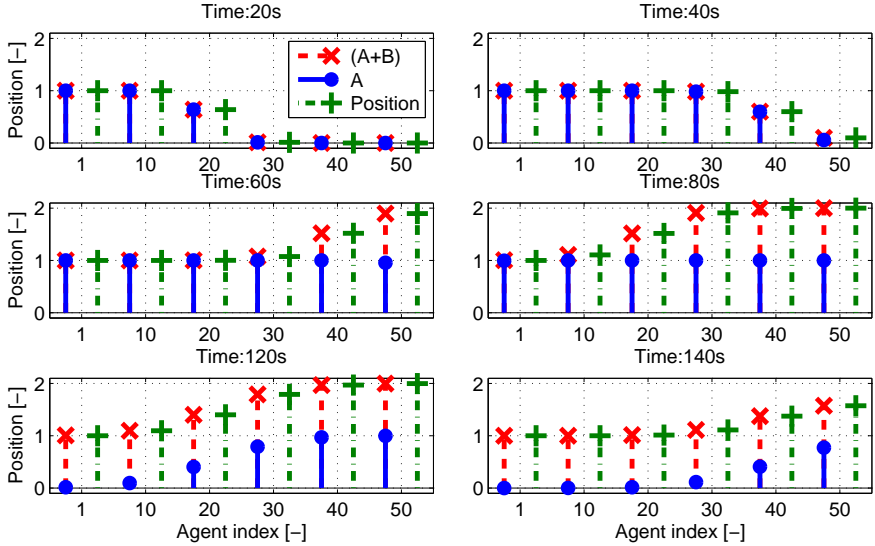
Figure 1.2: The response of individual agents at several time instances. The A and B (blue and red lines) are the waves that propagate in the system in the forward and backward directions, respectively, which will be explained in details later.

This motivates the questions: How to describe the propagation of the wave? How to absorb the wave on the ends of the system?
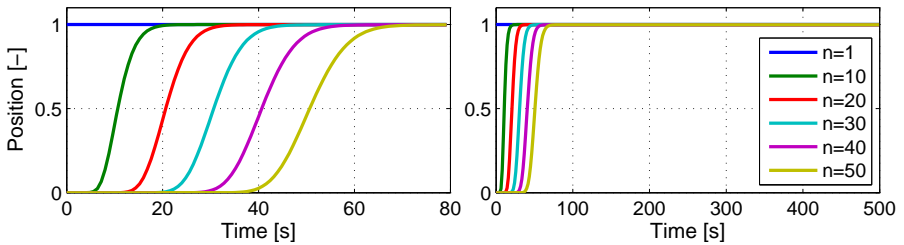
Figure 1.3: The response of the system from Fig. 1.1 with the wave-absorbing control law implemented on the last agent. The wave-absorbing control law prevents reflection of the wave at the last agent.

A natural extension of the above example is to consider a system where the agents are not identical. For instance, let us consider a system of 25

cars followed by 25 trucks. The response of such a system is shown in
Fig. 1.4. Similarly as in previous case, we can see that the wave travels
from the first to the last agent. But as the wave reaches the last car (25th
agent), it looks like that it reaches a virtual boundary and is partially
reflected back. For instance, we can see in the left panel for the first
50 seconds that the 10th agent travels to position 1 at first, but at time
$t = 30\,s$ it moves to position 0.7, while the 30th agent does not travel
to 1 but only to 0.7. This introduces the following problems. How to
describe the reflection at the boundary between cars and trucks? How
is the reflection related to the dynamics of the agents? Is it possible to
suppress it?
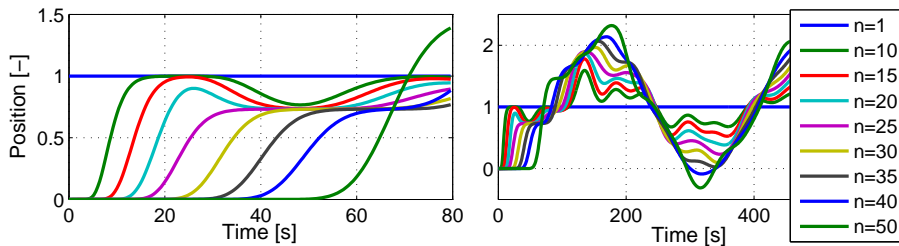
Figure 1.4: The response of the multi-agent system with 25 cars and 25
trucks.

The above examples illustrate that there is a wave phenomenon in a multi-
agent system with the path-graph topology. Does a similar phenomenon
also occur in a system with general-graph topology, that is in a system
where the agents have more than two neighbours? The numerical simula-
tions shown in Figs. 1.5 and 1.6 confirm it. We can see that the responses
of the agents are identical in all systems for about first 18 seconds. This
example raises yet another question. Why are the responses at the begin-
ning of the simulation identical?

Answering the aforementioned questions is the aim of this thesis.
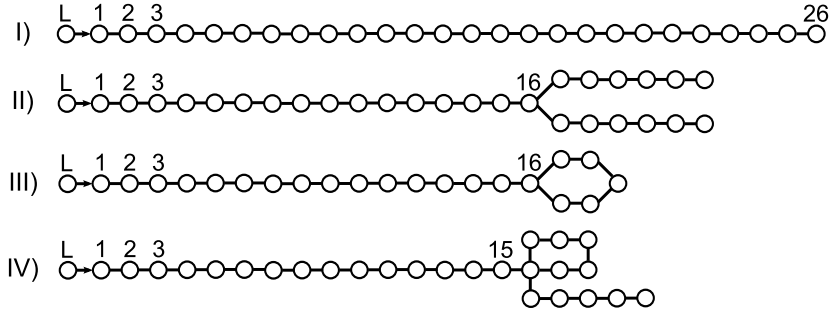
Figure 1.5: The topologies of the distributed systems.

1.4   Organization of the Thesis

The thesis is organized as follows. The second chapter introduces the travelling waves in a multi-agent system with path-graph topology, which is based on the work by [Martinec et al. (2014b)]. It focuses on the case where the agents are identical and have the symmetric bidirectional controller, which is generalized in the third chapter for the case where the agents are not identical. The third chapter is mainly based on [Martinec et al. (2014c)]. The fourth chapter, presented in [Martinec et al. (2015a)], analyzes how the wave propagates in system with the path-graph topology of identical agents but asymmetric bidirectional controller. A part of the fifth chapter has been presented in [Martinec et al. (2015b)]. This chapter also generalizes the travelling wave concept from the path graph to general graph topology.
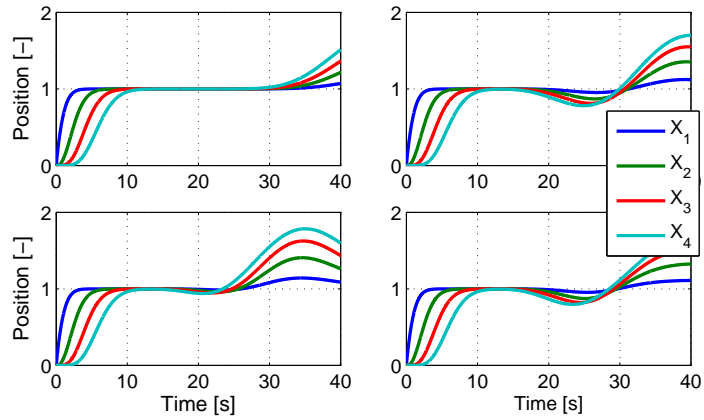
Figure 1.6: The comparison of the responses of the systems with four different interaction topologies. The topologies are given in Fig. 1.5 and they are related to this figures as follows: top-left panel - topology I); top-right panel - topology II); bottom-left panel - topology III); bottom-right panel - topology IV).

2 Path-graph topology and the waves

In this chapter, a finite one-dimensional platoon of vehicles moving along a highway lane is considered. Each individual vehicle in the platoon is locally controlled by a bidirectional controller, which represents a string-damper connection in mechanical structures and hence enables a wave to propagate back and forth along the line. One or both of the platoon ends are controlled by the *wave-absorbing controller* allowing active absorption of the traveling wave.

The key objective of the chapter is to generalize the principle of the wave-based control for vehicular platoons in such a way that the distances between vehicles are additionally considered. In this regard, the presented concept offers a symmetric version of bidirectional control enhanced by the feedback control of one or both platoon ends. Thus, it significantly decreases long transient oscillations during platoon manoeuvres such as acceleration/deceleration or changing the distances between vehicles. In addition, the chapter contributes to the following a) It generalizes the wave transfer function description for arbitrary dynamics of the local system, b) it offers a convergent recursive algorithm for the approximation of the wave transfer function, c) it presents an alternative way of deriving the wave transfer function using a continued fraction approach, and d) it provides the mathematical derivation of the transfer functions describing reflections at the platoon ends.

2.1   Local control of the platoon vehicles

A vehicle in a platoon indexed by n is modelled in the Laplace domain as

$$X_n(s) = P(s)U_n(s), \tag{2.1}$$

where s is the Laplace variable, $X_n(s)$ is a position of the nth vehicle in the Laplace domain, $P(s)$ represents the transfer function of the system dynamics and $U_n(s)$ is the system input which is generated by the local controller of the vehicle specified in the following.

Except for the leader, indexed $n = 0$, and the rear-end vehicle, each vehicle in the platoon is equipped with a symmetric bidirectional controller $C(s)$ with the task of equalizing the distances to its immediate predecessor and successor, giving

$$U_n(s) = C(s)(D_{n-1}(s) - D_n(s)), \tag{2.2}$$

where $D_n(s)$ is the distance between vehicles indexed by n and $n+1$, hence $D_n(s) = X_n(s) - X_{n+1}(s)$ and $D_{n-1}(s) = X_{n-1}(s) - X_n(s)$. Substituting (2.2) into (2.1) yields the resulting model of the in-platoon vehicle with the bidirectional control for the inter-vehicle distances,

$$X_n(s) = P(s)C(s)(X_{n-1}(s) - 2X_n(s) + X_{n+1}(s)). \tag{2.3}$$

Using the notation,

$$\alpha(s) = \frac{1}{P(s)C(s)} + 2, \tag{2.4}$$

equation (2.3) is rewritten as

$$X_n(s) = \frac{1}{\alpha(s)}(X_{n-1} + X_{n+1}). \tag{2.5}$$

The vehicle at the rear end of the platoon is driven by the predecessor following algorithm and is supposed to equalize the distance to its immediate

predecessor and reference distance D_{ref},

$$X_N(s) = \frac{1}{\alpha(s) - 1}(X_{N-1}(s) - D_{\text{ref}}(s)), \tag{2.6}$$

where $X_N(s)$ is the position of the vehicle at the rear end of the platoon.

To carry out numerical simulations, we will use the model that is often used in associated theoretical studies. The vehicle is described by a double integrator model with a simple (linear) model of friction, ξ, and is controlled by a PI controller. Hence, $P(s) = 1/(s^2 + \xi s)$ and $C(s) = (k_{\text{p}}s + k_{\text{i}})/(s)$, where k_{p} and k_{i} are proportional and integral gains of the PI controller, respectively. Such a model was also used in the experimental studies presented in [Martinec et al. (2012)].

2.1.1 Analyzed properties

The DC gain describing the steady-state amplification of a system and L_2 string stability describing the amplification of disturbance in a system with the path-graph topology are important analytical tools of system performance analysis. They are defined as follows.

Definition 1. *The DC gain κ_{G} of the transfer function $G(s)$ is defined as $\kappa_{\text{G}} = \lim_{s \to 0} G(s)$.*

Definition 2. *(From [Eyre et al. (1998)]) A system is called L_2 string stable if there is an upper bound on the L_2-induced system norm of $T_{0,n}$ that does not depend on the number of agents, where $T_{0,n}$ is the transfer function from $X_{\text{ref}}(s)$, that is the reference position of the leader, to $X_n(s)$.*

2.2 Wave Transfer Function

The bidirectional property of locally controlled systems causes that a change in the movement of the leading vehicle propagates through the platoon as a *wave*. To describe this wave, we need to find out how a change in the position of a vehicle is influenced by a change in the posi-

tion of its immediate neighbours. For a moment, let us assume that the length of the platoon is infinite, so that there is no platoon end where the wave can reflect. A generalization for a platoon with one platoon end, i.e., a semi-infinite platoon, is done in the next section.

2.2.1 Mathematical model of the wave transfer function

In accordance with the standard arguments for the *wave equation* as found, for instance, in [Asmar (2004)], the solution to the wave equation can be decomposed into two components: $A_n(s)$ and $B_n(s)$ (also called *wave variables* in the literature), which represent two waves propagating along a platoon in the forward and backward directions, respectively.

To find a transfer function describing the wave propagation, we are searching for two linearly independent recurrence relations that satisfy (2.5). We first recursively apply (2.5) and (2.6) with $D_{\text{ref}}(s) = 0$ for a platoon with an increasing number of vehicles. The transfer function for a platoon with two vehicles is $A_1/A_0 = (\alpha - 1)^{-1}$, for a platoon with three vehicles $A_1/A_0 = \left(\alpha - (\alpha - 1)^{-1}\right)^{-1}$, for a platoon with four vehicles $A_1/A_0 = \left(\alpha - \left(\alpha - (\alpha - 1)^{-1}\right)^{-1}\right)^{-1}$ and so on. Continuing recursively, A_1/A_0 is expressed by the continued fraction

$$\frac{A_1}{A_0} = \cfrac{1}{\alpha - \cfrac{1}{\alpha - \cfrac{1}{\alpha - \cfrac{1}{\ddots}}}}. \tag{2.7}$$

On the other hand, the continued-fraction expansion of a square root is given by [Jones and Thron (1984)]

$$\sqrt{z^2 + y} = z + \cfrac{y}{2z + \cfrac{y}{2z + \cfrac{y}{2z + \cfrac{y}{\ddots}}}}. \tag{2.8}$$

Letting the number of vehicles approach infinity, the right-hand sides of (2.7) and (2.8) are equal, provided that $y = -1$ and $z = \alpha/2$. Hence,

$$\frac{A_1}{A_0} = \frac{\alpha}{2} - \frac{1}{2}\sqrt{\alpha^2 - 4}. \tag{2.9}$$

Likewise, the transfer function A_2/A_1 can be derived from (2.5) and (2.6) for $n = 2$ as

$$\alpha A_1 = A_0 + A_2. \tag{2.10}$$

Substituting for A_0 from the previous recursive step (2.9) gives

$$\alpha A_1 = A_1 \left(\frac{\alpha}{2} + \frac{1}{2}\sqrt{\alpha^2 - 4} \right) + A_2, \tag{2.11}$$

which provides

$$\frac{A_2}{A_1} = \frac{\alpha}{2} - \frac{1}{2}\sqrt{\alpha^2 - 4}. \tag{2.12}$$

Continuing recursively, we can find that the transfer function A_{n+1}/A_n is again equal to (2.9) or (2.12). We can conclude that the transfer function from the nth to $(n+1)$th vehicle is the same for each vehicle, and is equal to

$$G_1(s) = \frac{\alpha(s)}{2} - \frac{1}{2}\sqrt{\alpha^2(s) - 4}. \tag{2.13}$$

Analogously, the second linearly independent recurrence relation of (2.5) and (2.6) is searched for by their recursive application with a decreasing index of vehicles. After similar algebraic manipulations as for A_n, we find

$$\frac{B_n}{B_{n-1}} = \alpha - \cfrac{1}{\alpha - \cfrac{1}{\alpha - \cfrac{1}{\alpha - \cfrac{1}{\ddots}}}}. \tag{2.14}$$

17

Letting the number of vehicles approach infinity, the right-hand sides of (2.14) and (2.8) are equal provided that $y = -1$ and $z = \alpha/2$. Hence,

$$\frac{B_n}{B_{n-1}} = \frac{\alpha}{2} + \frac{1}{2}\sqrt{\alpha^2 - 4}. \tag{2.15}$$

The transfer function from nth to $(n-1)$th vehicle is again the same for each vehicle, and is equal to

$$G_2(s) = \frac{\alpha(s)}{2} + \frac{1}{2}\sqrt{\alpha^2(s) - 4}. \tag{2.16}$$

The resulting model of the vehicular platoon with an infinite number of vehicles is therefore described as follows

$$X_n(s) = A_n(s) + B_n(s), \tag{2.17}$$
$$A_{n+1}(s) = G_1(s)A_n(s), \tag{2.18}$$
$$B_n(s) = G_2(s)B_{n-1}(s), \tag{2.19}$$
$$G_1(s) = G_2^{-1}(s), \tag{2.20}$$

where (2.20) follows from the multiplication of (2.13) and (2.16). Equations (2.18)-(2.19) express the *rheological property* of the platoon, that is, they define the form of how these two components propagate through the platoon. Equation (2.20) expresses the *principle of reciprocity*, that is, if $A(s)$ propagates with the help of $G_1(s)$ to higher indexes of vehicles, then $B(s)$ propagates with the help of $G_1(s)$ to lower indexes of vehicles.

It should be noted that if there is a boundary in the system, e.g., if the length of the platoon is finite, where the rheology property for wave propagation changes abruptly, the principles must be supplemented by boundary conditions. We discuss this case in the following section.

The resulting model is summarized in the following Theorem.

Theorem 1. *The model of the vehicular platoon with an infinite number*

of vehicles is

$$X_n(s) = A_n(s) + B_n(s), \tag{2.21}$$

$$A_{n+1}(s) = G(s)A_n(s), \tag{2.22}$$

$$B_n(s) = G(s)B_{n+1}(s), \tag{2.23}$$

where $G(s) = G_1(s)$ is the Wave Transfer Function and $G_2(s) = G^{-1}(s) = 1/G(s)$,

$$G(s) = \frac{1}{2}\alpha(s) - \frac{1}{2}\sqrt{\alpha^2(s) - 4}, \tag{2.24}$$

$$G^{-1}(s) = \frac{1}{2}\alpha(s) + \frac{1}{2}\sqrt{\alpha^2(s) - 4}, \tag{2.25}$$

with $\alpha(s) = 2 + 1/M(s)$, or, alternatively, $\alpha(s) = G(s) + G^{-1}(s)$.

Remark. *We can see that the Wave Transfer Function is linear and irrational. The irrationality of the function comes from the separation of the output, $X_n(s)$, into two travelling waves, $A_n(s)$ and $B_n(s)$, that are independent of each other as they travel in the system with infinite number of vehicles. However, every system with a finite number of identical vehicles and path-graph topology has the leader and the rear-end vehicle, which represent boundaries and cause reflections of the travelling waves. In this case, A_n and B_n are no longer independent. Therefore, to find the wave transfer functions, we have to consider a system with infinite number of vehicles. Infinite dimensionality of the system then makes the transfer functions to be irrational.*

In basic wave physics, the boundary is assumed to satisfy the spatial causality, that is, the boundary condition does not affect the wave travelling towards it. In other words, (2.21)-(2.23) hold regardless of the topological distance and dynamics of the rear-end vehicle. Therefore, we can apply (2.21)-(2.23) to describe the travelling waves even in a system with a finite number of vehicles, although, these relations are valid only for the vehicles that are not placed on the boundary. The boundary vehicle that causes the reflection of the waves must be treated separately, see Section 2.3. In general, any vehicle that is not described by (2.3) represents a boundary for

19

the travelling wave. This can be generalized even for vehicles (or agents) that have more than two neighbours. This is shown in Chapter 5. Therefore, the travelling-wave decomposition, (2.21)-(2.25) is valid even for a path graph that is part of a more complex graph.

In view of the Wave Transfer Function, the term 'travelling wave' can be defined as follows.

Definition 3. *The* travelling wave *is a disturbance that travels in the system in the forward direction from $A_n(s)$ to $A_{n+1}(s)$ and in the backward direction from $B_{n+1}(s)$ to $B_n(s)$.*

2.2.2   Verification of the wave transfer function

We now outline an alternative way to derive the wave transfer function. Let the model of the vehicular platoon (2.21)-(2.23) hold and now search for the transfer functions $G_1(s)$ and $G_2(s)$ that satisfy these three equations. Substituting (2.21) into (2.5) yields

$$\alpha(A_n + B_n) = A_{n-1} + B_{n-1} + A_{n+1} + B_{n+1}, \tag{2.26}$$

which, in view of (2.22) and (2.23), is

$$\alpha(s) = G_1(s) + G_2(s). \tag{2.27}$$

We can substitute either for $G_1(s)$ or $G_2(s)$ from (2.20). Either possibility leads to the same quadratic equation $(m = 1, 2)$,

$$G_m^2(s) - \alpha(s)G_m(s) + 1 = 0, \tag{2.28}$$

with two linearly independent solutions,

$$G_m(s) = \frac{\alpha}{2} \mp \frac{1}{2}\sqrt{\alpha^2 - 4}. \tag{2.29}$$

Let $G_1(s)$ be chosen as the solution with the negative sign in front of the square root. Then (2.20) only allows $G_2(s)$ to be the solution with

the positive sign in front of the square root. Hence, $G_1(s)$ and $G_2(s)$ are identical to those derived in the previous section. The quadratic equation (2.28) can be employed as a starting model for the positioning of multi-link flexible mechanical systems [O'Connor (2006)].

2.2.3 Approximation of the wave transfer function

It will be shown later that to be able to implement the wave-absorbing controller, we need to find the impulse response of the wave transfer function, i.e., the inverse Laplace transform of $G(s)$. Due to the presence of the square root in $G(s)$, it is very challenging to find an exact impulse response of $G(s)$. However, we can approximate the impulse response with a finite impulse response (FIR) filter. Therefore, we first approximate the wave transfer function in the Laplace domain, then transform this approximate form to the time domain and finally truncate and sample the approximate impulse response to obtain FIR filter coefficients.

The square root function in (2.29) can be approximated by various ways, e.g., Newton's method, the binomial theorem, or continued fraction expansion (2.7). We employ the last option since it guarantees the convergence of iterative approximations and is applicable to an arbitrary dynamics of the local system with generalized parameter $\alpha(s)$ as in (2.4). The recursive formula (2.7) immediately provides the iterative approximation of $G(s)$,

$$G^l(s) = \frac{1}{\alpha(s) - G^{l-1}(s)}, \tag{2.30}$$

where $l = 1, 2, \ldots$, and the initial value $G^0(s) = 1$. The approximate $G^l(s)$ can be transformed to the time domain by Matlab or Mathematica. Our experience with the inverse Laplace solvers for the Fractional Calculus *Crone* [Malti et al. (2012)], *invlap* [de Hoog et al. (1982)], *weeks* [Weeks (1966)] and *nilt* [Brancik (1999)] in Matlab is that, while they are not capable of performing the inverse Laplace transform of (2.29) due to the square root function, they carry out the inverse Laplace transform of $G^l(s)$

(a) Bode characteristics - magnitude.   (b) The impulse responses.
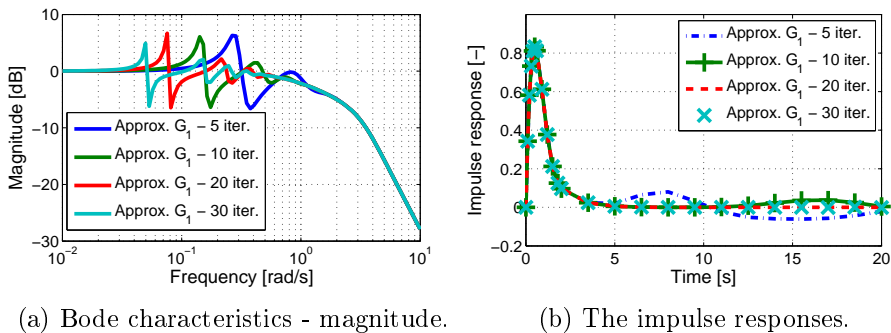
Figure 2.1: Characteristics of the approximate $G(s)$ after several iterations by (2.30) for $k_\mathrm{p} = k_\mathrm{i} = \xi = 4$.

without complications since (2.30) is a rational function.

The approximate $G^l(s)$ can be interpreted as follows. Equation (2.30) represents the transfer function from the position of the leader to the position of the first follower in a platoon of l vehicles. Increasing the number of iterations (2.30) means that the length of a platoon grows and the effect of the rear-end vehicle on $G(s)$ weakens. The approximation of $G(s)$ therefore successively improves. Fig. 2.1 show the Bode characteristics $G^l(s)$ and the associated impulse responses for various numbers of iterations, respectively. Increasing the numbers of iterations makes the peak in the Bode characteristic sharper, more localized and moves it towards lower frequencies, eventually disappearing entirely. The basic characteristic of the impulse response is adjusted after a few iterations while small differences occur at longer times. To obtain the FIR filter coefficients, we truncate the approximate impulse response at a few seconds and sample it with an appropriate frequency. In our numerical simulations it is sufficient to stop the iterative procedure after 20 iterations, to truncate the impulse response at 15 to 25 seconds and sample it at the frequency of $100\,\mathrm{Hz}$. The error caused by the truncation is shown in Fig. 2.2.

(a) Frequency response - magnitude (b) Frequency response - phase

Figure 2.2: Continued fraction approximation. Compared 'full' and 'truncated-in-time' approximations. The approximation was constructed in 25 recursive steps, truncated at time 25 s and sampled with frequency 200 Hz. The oscillations in the phase near frequency 100 Hz are caused by numerical instabilities.

2.3 Reflection of the wave at platoon ends

To be able to design a wave-absorbing controller for the platoon end, we first need to mathematically describe the wave reflection. In contrast to the previous section where an infinite platoon is considered, we now consider a semi-infinite platoon having one end that is either controlled externally (forced end) or allowed to move freely (free end). When a wave propagates along a platoon and reaches its free end, it is reflected with the same polarity, i.e., the same sign of amplitude, but with the opposite polarity at the fixed/forced end. This phenomenon, known from basic wave physics [French (2003)], is discussed in the following in terms of the wave transfer function.

2.3.1 The forced-end boundary

A vehicle that is externally controlled and is not linked with the other vehicles is called the forced-end boundary. However, the neighbouring vehicle is one-directionally linked with this forced boundary. The platoon

leader therefore represents the forced-end boundary. The reflection at the
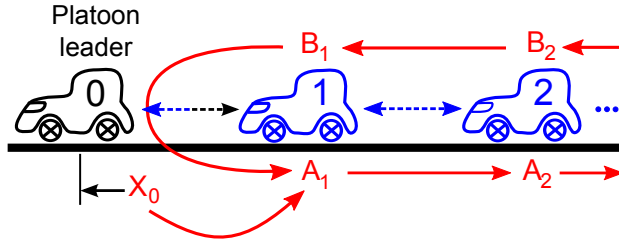
Figure 2.3: Scheme of the wave reflection at the leader, i.e., the reflection at the forced-end boundary, described by (2.31).

forced-end boundary is sketched in Fig. 2.3. A change in the position of the forced end, X_0, generates the outgoing wave as a first contribution to A_1. Moreover, the incoming wave (B_1) is reflected at the forced end and transformed to the outgoing wave as the second contribution to A_1.

Lemma 1. *The reflection at the forced-end boundary is described by*

$$A_1(s) = G(s)X_0(s) - G(s)^2 B_1(s). \tag{2.31}$$

Proof. We first combine (2.21)-(2.23) to obtain

$$X_{n+1}(s) = G(s)A_n(s) + G^{-1}(s)B_n(s), \tag{2.32}$$

$$X_{n-1}(s) = G^{-1}(s)A_n(s) + G(s)B_n(s). \tag{2.33}$$

Equation (2.5), specified for the first vehicle behind the platoon leader, is

$$\alpha(s)X_1(s) = X_0(s) + X_2(s). \tag{2.34}$$

Substituting (2.21) for $X_1(s)$ and (2.32) for $X_2(s)$ yields

$$\alpha(s)(A_1(s) + B_1(s)) = X_0(s) + G(s)A_1(s) + G^{-1}(s)B_1(s), \tag{2.35}$$

which can be rewritten for $A_1(s)$ as

$$A_1(s) = \frac{1}{\alpha(s) - G(s)} X_0(s) + \frac{G^{-1}(s) - \alpha(s)}{\alpha(s) - G(s)} B_1(s). \tag{2.36}$$

The term in front of $B_1(s)$ can be arranged as

$$\frac{G^{-1}(s) - \alpha(s)}{\alpha(s) - G(s)} = \frac{-\frac{\alpha(s)}{2} + \frac{1}{2}\sqrt{\alpha^2(s) - 4}}{\frac{\alpha(s)}{2} + \frac{1}{2}\sqrt{\alpha^2(s) - 4}} = -\frac{G(s)}{G^{-1}(s)} = -G^2(s), \tag{2.37}$$

Similarly, the term in front of $X_0(s)$ is expressed as

$$\frac{1}{\alpha(s) - G(s)} = \frac{1}{\frac{\alpha(s)}{2} + \frac{1}{2}\sqrt{\alpha^2(s) - 4}} = \frac{1}{G^{-1}(s)} = G(s). \tag{2.38}$$

Finally, we have

$$A_1(s) = G(s)X_0(s) - G^2(s)B_1(s). \tag{2.39}$$

$\square$

Eq.(2.31) first shows that changing the position of the forced end is translated to A_1 through G. Second, since the DC gain of G is equal to plus one (see Fig. 2.2), the minus sign in front of G^2 causes the wave to be reflected with the opposite sign.

2.3.2 The free-end boundary

A free-end boundary is a boundary where a vehicle is two-directionally linked with one neighbour only and, additionally, it is aware of the reference distance. The rear-end vehicle described by (2.6) represents the free-end boundary.

The reflection at the free-end boundary is outlined in Fig. 2.4. The wave travelling from the free-end boundary (B_N) is composed of two parts, the
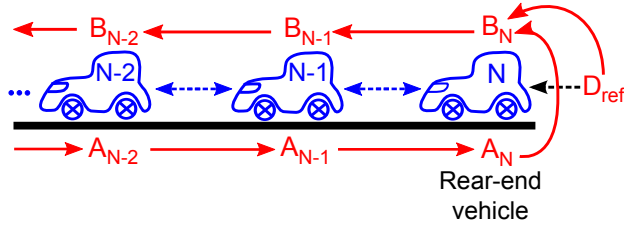
Figure 2.4: Scheme of the wave reflection at the rear-end vehicle, i.e., the reflection at the free-end boundary, described by (2.40).

incoming wave (A_N) which is reflected back and the component due to adjusting the reference distance D_{ref}.

Lemma 2. *The reflection at the free-end boundary is described by*

$$B_N(s) = G(s)A_N(s) + \frac{G(s) - 1}{\alpha(s) - 2}D_{\text{ref}}(s). \tag{2.40}$$

Proof. Substituting (2.21) and (2.33) into (2.6) yields

$$(A_N(s) + B_N(s))(\alpha(s) - 1) = G^{-1}(s)A_N(s) + G(s)B_N(s) - D_{\text{ref}}(s), \tag{2.41}$$

which, after rearranging, gives

$$B_N(s) = \frac{G^{-1}(s) - \alpha(s) + 1}{\alpha(s) - 1 - G(s)}A_N(s) - \frac{1}{\alpha(s) - 1 - G(s)}D_{\text{ref}}(s), \tag{2.42}$$

where

$$\frac{G^{-1}(s) - \alpha(s) + 1}{\alpha(s) - 1 - G(s)} = \frac{1 - \frac{\alpha(s)}{2} + \frac{1}{2}\sqrt{\alpha^2(s) - 4}}{-1 + \frac{\alpha(s)}{2} + \frac{1}{2}\sqrt{\alpha^2(s) - 4}} =$$

$$\frac{\alpha(s) - \frac{\alpha^2(s)}{2} - \sqrt{\alpha^2(s) - 4} + \frac{\alpha(s)}{2}\sqrt{\alpha^2(s) - 4}}{2 - \alpha(s)} = \frac{2 - \alpha(s)}{2 - \alpha(s)}G(s) = G(s). \tag{2.43}$$

Similarly,

$$
\begin{aligned}
\frac{1}{\alpha(s) - 1 - G(s)} &= G(s) \frac{1}{G^{-1}(s) - \alpha(s) + 1} = \\
\left(\frac{\alpha(s)}{2} - \frac{1}{2} \sqrt{\alpha^2(s) - 4} \right) &\frac{1 - \frac{\alpha(s)}{2} + \frac{1}{2} \sqrt{\alpha^2(s) - 4}}{\left(1 - \frac{\alpha(s)}{2} \right)^2 - \frac{1}{4}(\alpha^2(s) - 4)} = \frac{G(s) - 1}{2 - \alpha(s)}.
\end{aligned}
\tag{2.44}
$$

Hence, (2.42) is

$$
B_N(s) = G(s) A_N(s) + \frac{G(s) - 1}{\alpha(s) - 2} D_{\text{ref}}(s).
\tag{2.45}
$$

$\square$

The reflection from the free-end boundary does not change the sign which is expressed by the plus sign in front of $G(s) A_N(s)$. Moreover, the signal reflected from the free-end is delayed as a linear function of $G(s)$, while as a quadratic function when it is reflected from the forced-end boundary, as shown by (2.31).

It should be noted that the verification of the above wave-based model was done in [O'Connor (2007)]. The transfer function

$$
\frac{X_N(s)}{X_0(s)} = G^N(s) \frac{1 + G(s)}{1 + G^{2N+1}(s)},
\tag{2.46}
$$

where N is the index of the last vehicle, was shown to be identical to the transfer function derived by the state space description. This result is valid not only for a double integrator with P controller, but also for an arbitrary dynamics of the local system.

2.4 Wave-absorbing controller

The three main control requirements are: i) to have the platoon travelling with the reference velocity v_{ref}, ii) to keep inter-vehicle distances d_{ref} and

iii) to actively absorb the wave travelling towards the platoon's end.

This section introduces three possible configurations of the platoon with the wave-absorbing controller. First, we will describe the configuration where the wave-absorbing controller is implemented at the platoon leader.

2.4.1   Front-sided wave-absorbing controller

Absorption of the wave

To absorb the incoming wave at the platoon front, the transfer function from B_1 to A_1 in (2.31) has to be equal to zero, where B_1 is the amplitude of the wave travelling from the rear-end vehicle and observed at the vehicle indexed as 1, while A_1 is the amplitude of the wave travelling from the leader and observed at the vehicle indexed as 1. In other words, we are searching for X_0 (a commanded position for the leader) to satisfy the equation $GX_0/B_1 - G^2 = 0$. The only solution is

$$X_0(s) = G(s)B_1(s). \tag{2.47}$$

To be consistent with the model (2.21)-(2.20), we denote $B_0 = GB_1$ and $A_0 = X_0 - B_0$. Then (2.31) is expressed as $A_1 = GX_0 - GB_0 = GA_0$. Summarizing, the wave components of the leader are

$$B_0(s) = G(s)X_1(s) - G^2(s)A_0(s), \tag{2.48}$$
$$A_0(s) = X_0(s) - B_0(s). \tag{2.49}$$

This means that, if one component of the position of the leader is equal to B_0, then the leader absorbs the incoming wave. We can imagine it as the leader is pushed/pulled by its followers and it manoeuvres like one of the in-platoon vehicles.

Acceleration to the reference velocity

The previous algorithm actively absorbs the incoming wave to the platoon leader. To change the platoon velocity and inter-vehicle distances are other tasks to be solved.

To accelerate the platoon, we need to add an external/reference input, X_{ref}, to the leader, which causes the change of (2.47) to $X_0 = B_0 + X_{\mathrm{ref}}$. The rear-end vehicle represents the free-end boundary, therefore, B_0 is expressed by the combination of (2.22), (2.23), (2.31) and (2.48) as $B_0 = G^{2N+1} X_{\mathrm{ref}}$. The resulting transfer function from X_{ref} to X_0 is

$$\frac{X_0(s)}{X_{\mathrm{ref}}(s)} = 1 + G^{2N+1}(s). \tag{2.50}$$

Fig. 2.2 showed that the DC gain of G is equal to one, therefore, the DC gain of $(1 + G^{2N+1}(s))$ is equal to two. This means that to accelerate the platoon to reference velocity v_{ref}, the leader must be commanded to accelerate to a velocity $v_{\mathrm{ref}}/2$ at the beginning of the manoeuver, as shown in Fig. 2.5.

Fig. 2.5 additionally shows an independent validation of the wave transfer function approach. The derivation of the sum of $A + B$ velocity components (red crosses) of the wave travelling through the platoon are compared against the velocities simulated by the Matlab Simulink (green plus signs). We can see an excellent agreement between the wave-transfer-function-derived and independently-simulated velocities.

Changing of the inter-vehicle distances

Increasing the inter-vehicle distances poses a more difficult task than merely accelerating the platoon. The reason is that the rear-end vehicle reacts to the change of reference distance d_{ref} by acceleration/deceleration. This creates a velocity wave propagating towards the leader who absorbs it by changing its velocity. This means, however, that when all vehicles reach the desired inter-vehicle distance d_{ref}, the whole platoon
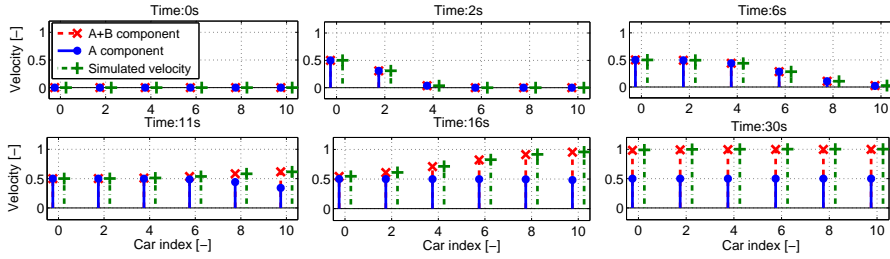
Figure 2.5: Simulation of the velocity wave propagating through the platoon with the Front-sided wave-absorbing controller at several time instances. At the beginning, $t = 0\,\mathrm{s}$, all platoon vehicles are standing except for the leader which accelerates to a velocity $0.5\,\mathrm{ms}^{-1}$. At intermediate times, the wave travels to the rear vehicle, where it is reflected and travels back to the leader to be completely absorbed. By propagating, it forces platoon vehicles to accelerate by another $0.5\,\mathrm{ms}^{-1}$ to a velocity $1\,\mathrm{ms}^{-1}$. At the final stage, $t = 30\,\mathrm{s}$, the leader is the last one reaching the velocity $1\,\mathrm{ms}^{-1}$ and the whole platoon moves with $1\,\mathrm{ms}^{-1}$. The red crosses represent the derivation of $A + B$ positional components computed by the wave transfer function approach, the green plus signs are the velocities simulated by the Matlab Simulink.

travels with a new velocity different from the original. Only by an additional action by the leader, see the next paragraph, the original velocity can be reestablished.

Although the platoon has a finite number of vehicles, it behaves like a semi-infinite platoon because no wave reflects from the platoon leader, who is equipped with the wave absorber. Since (2.40) holds for a semi-infinite platoon, it can be now used to determine the transfer function from D_{ref} to the velocity of the leader, $V_0(s)$, that is

$$\frac{V_0(s)}{D_{\mathrm{ref}}(s)} = G^N(s)\frac{s(G(s) - 1)}{\alpha(s) - 2}. \tag{2.51}$$

The DC gain of (2.51) reads as

$$\kappa_{\mathrm{f}} = \lim_{s \to 0}\left(G^N(s)\frac{s(G(s) - 1)}{\alpha(s) - 2}\right). \tag{2.52}$$

In the case where the reference distance is changed and the leader does not accelerate, the velocity of the platoon changes by $\kappa_\mathrm{f} d_\mathrm{ref}$. This means that the platoon slows down or even moves backwards. To compensate this undesirable velocity change, the leader is commanded to accelerate to the velocity $(-\kappa_\mathrm{f} d_\mathrm{ref})/2$. The platoon will consequently travel with the original velocity, hence compensating for the acceleration/deceleration of the rear-end vehicle. This leads to the DC gain of (2.51) for the PI controller to be $(-\sqrt{k_\mathrm{i}/\xi})$.

Overall control of the leader

Let us now assume that the leader has a positional controller with input $X_\mathrm{f}(s)$. Summarizing preceding subsections yields the resulting control law of the leader in the following theorem.

Theorem 2. *The wave-absorbing control law of the leader is*

$$X_\mathrm{f}(s) = X_\mathrm{ref}(s) + B_0(s) = (1 - G^2(s))X_\mathrm{ref}(s) + G(s)X_1(s). \quad (2.53)$$

From the above discussion, $X_\mathrm{ref}(s)$ must be represented by a ramp signal with slope w_0,

$$w_0 = \frac{1}{2}\left(v_\mathrm{ref} - \kappa_\mathrm{f} d_\mathrm{ref}\right), \quad (2.54)$$

to ensure that the platoon travels with a reference velocity v_ref and inter-vehicle distances d_ref. In case of the PI controller, $w_0 = \left(v_\mathrm{ref} + \sqrt{k_\mathrm{i}/\xi} d_\mathrm{ref}\right)/2$. The Front-sided wave-absorbing controller is summarized in Fig. 2.6.

2.4.2   Rear-sided wave-absorbing controller

Instead of placing the wave-absorbing controller at the platoon front, it can be placed at the platoon rear. In this case, the platoon has one leader in the front and one wave-absorbing controller at the rear. However, the absence of the predecessor follower in the platoon has an important consequence. Any velocity change by the leader, $V_0(s)$, causes a change in
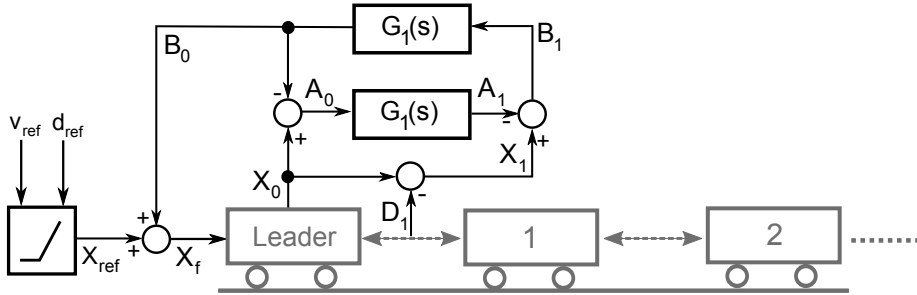
Figure 2.6: Scheme of the Front-sided wave-absorbing vehicular platoon controller.

the distance to the first follower, $D_1(s)$, as shows the following corollary. Consequently, all other distances between vehicles are changed.

Corollary 1. *The wave-absorbing controller implemented on the leader changes the transfer function $D_1(s)/V_0(s)$, where $V_0(s)$ is the velocity of the leader and $D_1(s) = X_0(s) - X_1(s)$ is the distance between the leader and the first follower, as follows*

$$\frac{D_1(s)}{V_0(s)} = \frac{1}{s}(1 - G(s)). \tag{2.55}$$

Proof. Assuming a semi-infinite platoon, equation (2.9) gives $X_1(s) = G(s)X_0(s)$. Hence,

$$D_1(s) = X_0(s) - G(s)X_0(s) = \frac{1}{s}(1 - G(s))V_0(s). \tag{2.56}$$

$\square$

This negative effect is to be compensated by an acceleration/deceleration of the rear-end vehicle. We denote κ_r to be the DC gain of the transfer function from $V_0(s)$ to $D_1(s)$. Having specified the DC gain, a certain reference signal needs to be sent to the platoon end to set up a desired inter-vehicle distance d_{ref}. The input to the positional controller of the

rear-end vehicle, $X_\mathrm{r}(s)$, is expressed, analogous to (2.53), as

$$X_\mathrm{r}(s) = X_\mathrm{ref,rear}(s) + G(s)A_{N-1}(s), \tag{2.57}$$

where $G(s)A_{N-1}(s) = G(s)X_{N-1}(s) - (G(s))^2 X_\mathrm{ref,rear}(s)$ is the transfer function of the wave absorber and $X_\mathrm{ref,rear}(s)$ is a reference ramp signal with slope w_r,

$$w_r = \frac{1}{2}\left(v_\mathrm{ref} - \kappa_\mathrm{r}d_\mathrm{ref}\right). \tag{2.58}$$

In other words, the platoon leader drives the platoon to travel with velocity v_ref, while the rear-end vehicle makes the platoon travel with inter-vehicle distances d_ref. For the PI controller case, $\kappa_\mathrm{r} = k_\mathrm{i}/\xi$.

It should be stressed that, for this type of control, the last vehicle must know the reference velocity of the whole platoon. This may be undesirable, since only the leader is usually aware of the reference velocity. It may, however, be useful in situations, for instance, when the leader is not able to measure the distance to its immediate follower, or when the leader has no access to the reference distance.

2.4.3 Two-sided wave-absorbing controller

The Front-sided and Rear-sided wave-absorbing controllers can be combined by implementing wave absorbers to both the platoon leader and the rear-end vehicle. In this case, no wave is reflected back from neither of the platoon ends.

The input to the positional controller of the leader is given by (2.53) with the ramp signal (2.54), while the input to the positional controller of the rear-end vehicle is (2.57) with the ramp signal (2.58). In this way, each platoon end generates a velocity wave propagating towards the opposite end. Likewise, as for the Front-sided and Rear-sided wave-absorbing controllers (Section 2.4.1 and 2.4.2), the amplitudes of the two waves are summed up to v_ref, meaning that the platoon travels with velocity v_ref

and inter-vehicle distances d_{ref}.

2.4.4   Asymptotic and string stability

First, we prove the important lemma on the H_∞ norm of the Wave transfer function.

Lemma 3. *The H_∞ norm of the Wave transfer function is limited as follows*

$$\|G(s)\|_\infty \leq 1. \tag{2.59}$$

Proof. We will show that $\|G^{-1}(s)\|_\infty \geq 1$. Then it implies that $\|G(s)\|_\infty \leq 1$. To inspect the amplification and phase shift on frequency ω, we substitute $\jmath\omega$ for s in the definition of $G^{-1}(s)$ in (2.25), where $\jmath$ is the imaginary unit, and obtain the complex number z_2 in the polar form,

$$z_2 = r_2 \exp(\jmath\varphi_2). \tag{2.60}$$

Similarly as in (2.16), we can separate z_2 into two parts,

$$z_2 = \frac{1}{2}z + \frac{1}{2}\sqrt{z_s}, \tag{2.61}$$

where

$$\begin{aligned} z &= \alpha(\jmath\omega) = r\exp(\jmath\varphi), \\ z_s &= z^2 - 4 = r_s \exp(\jmath\varphi_s). \end{aligned} \tag{2.62}$$

The magnitude r_s is given by

$$r_s = (r^2\cos(2\varphi) - 4)^2 + (r^2\sin(2\varphi))^2 = r^4 + 8r^2 + 16 - 16r^2\cos^2\varphi. \tag{2.63}$$

with magnitude r_2 then expressed as

$$r_2 = \left[\frac{1}{4}\left(r^2 + r_s + 2r\sqrt{r_s}\left(\cos\frac{\varphi_s}{2}\cos\varphi + \sin\frac{\varphi_s}{2}\sin\varphi\right)\right)\right]^{\frac{1}{2}}$$
$$= \left[\frac{1}{4}\left(r^2 + r_s + 2r\sqrt{r_s}\cos\left(\varphi - \frac{\varphi_s}{2}\right)\right)\right]^{\frac{1}{2}}. \tag{2.64}$$

The minimum of r_s over all possible phases is for $\varphi = k\pi$, $k \in \mathbb{Z}$, and is equal to

$$\min(r_{\mathrm{s}}) = \sqrt{r^4 - 8r^2 + 16} = |r^2 - 4| = \begin{cases} 4 - r^2 & \text{if } 0 \le r \le 2 \\ r^2 - 4 & \text{if } r > 2 \end{cases} \tag{2.65}$$

Therefore,

$$\frac{1}{4}(r^2 + r_s) \ge 1. \tag{2.66}$$

In the next step, we will show that $|\varphi - \varphi_s/2| \le \pi/2$, which means that $\cos(\varphi - \varphi_s/2)$ is nonnegative. It is a known fact that the sum of two complex numbers with phases δ_1 and δ_2, where $\delta_1 \le \delta_2$ and $\delta_1, \delta_2 \in [-\pi, \pi)$, yields a complex number with the phase $\delta \in [-\pi, \pi)$, that is

$$\delta \in [\delta_1, \delta_2] \text{ if } |\delta_1 - \delta_2| < \pi, \tag{2.67}$$
$$\delta \in [\delta_2, \delta_1] \text{ if } |\delta_1 - \delta_2| > \pi, \tag{2.68}$$
$$\delta = \delta_1 \text{ or } \delta = \delta_2 \text{ if } |\delta_1 - \delta_2| = \pi. \tag{2.69}$$

This implies that

$$|\delta - \delta_2| \le \pi \wedge |\delta_1 - \delta| \le \pi. \tag{2.70}$$

The phase φ_s calculated from (2.62) is $\varphi_s = 2\varphi - \theta$, where $|\theta| \le \pi$

according to (2.70). Then,

$$\left| \varphi - \frac{\varphi_s}{2} \right| = \left| \varphi - \varphi + \frac{1}{2}\theta \right| = \frac{1}{2}|\theta| \leq \frac{1}{2}\pi. \tag{2.71}$$

Therefore,

$$\cos\left(\varphi - \frac{\varphi_s}{2} \right) \geq 0 \tag{2.72}$$

and (2.64) gives,

$$r_2 \geq 1. \tag{2.73}$$

This means that the amplification of $G^{-1}(s)$ for all frequencies is greater or equal to one, or the amplification of $G(s)$ for all frequencies is less than or equal to one, hence $||G(s)||_\infty \leq 1$. □

Lemma 4. *If $M(s)$ is proper and has no CRHP (closed-right half plane) zeros and no CRHP poles, except for poles at the origin, and if*

$$1 + 4M(\jmath\omega) \tag{2.74}$$

does not intersect the non-positive real axis for $\omega \in (0, \infty)$, where $M(s) = P(s)C(s)$, then the wave transfer function $G(s)$ is asymptotically stable.

Proof. The proof is based on [Curtain and Morris (2009)] (Theorem A.2), which states: *A linear system is stable if and only if its transfer function $T(s)$ is analytic in the right-half plane and $||T||_\infty < \infty$, where $||T||_\infty = \sup_{Re(s)>0} |T(s)|$.*

It was proved in Lemma 3 that the WTF defined by (2.24) satisfies $||G||_\infty \leq 1$. Hence, it remains to derive the condition, when the WTF is analytic in the right-half plane.

First, we treat the square root function in (2.24). In the complex function analysis, for instance p. 99-100 in [Stein and Shakarchi (2010)], it is shown that the square root function $f(z) = \sqrt{z}$ is analytic everywhere,

except for the non-positive real axis. Therefore, $f_2(\alpha) = \sqrt{\alpha^2 - 4}$ in (2.24) is analytic everywhere, except for $\alpha \in \langle -2, 2 \rangle$ on the real axis. Since $\alpha(s) = 2 + 1/M(s)$, we can say that $f_2(\alpha)$ is analytic everywhere, except for the interval $(-\infty, -1/4\rangle$. Due to the Maximum modulus principle (Theorem 4.5 [Stein and Shakarchi (2010)]), we can assess the analyticity by the Nyquist plot of $M(s)$. This means that, if $M(\jmath\omega)$ does not intersect interval $(-\infty, -1/4\rangle$ for $\omega \in (0, \infty)$, then the WTF is stable.

The first part of the WTF, $1 + 0.5/M$, is a rational transfer function. A rational function is analytic in the CRHP if and only if it has no singularities in this plane. The only possible singularities of $1 + 0.5/M$ are CRHP zeros of $M(s)$. Therefore, if $M(s)$ has no CRHP zero, then $1 + 0.5/M$ is analytic. Since the difference of two analytic functions is again analytic, then the WTF is analytic and asymptotically stable under the above conditions.

□

We follow the L_2 string stability definition from Definition 2. In the case of the platoon with the Front-sided wave-absorbing controller, the position of the nth vehicle is described by

$$X_n(s) = (G^n(s) + G^{2N+1-n}(s))X_0(s). \tag{2.75}$$

Due to the triangle inequality and the fact that $||G||_\infty \leq 1$, which is shown in Lemma 3, we obtain

$$||G^n(s) + G^{2N+1-n}(s)||_\infty \leq ||G^n(s)||_\infty + ||G^{2N+1-n}(s)||_\infty \leq 2. \tag{2.76}$$

This means that the magnitude of the maximum peak in the frequency response of the transfer function from the position of the leader to the position of the nth vehicle is less than or equal to 2. Since the L_2-induced norm and H_∞ coincide, we can state that the platoon with the Front-sided wave-absorbing controller is L_2 string stable.

The position of the nth vehicle with the absorber placed at the rear-end

vehicle is

$$X_n(s) = G^n(s)X_0(s) + (G^{N-n}(s) - G^{N+n}(s))X_N(s). \qquad (2.77)$$

We apply the same idea and state that the H_∞ norm of both $G^n(s)$ and $(G^{N-n}(s) - G^{N+n}(s))$ are bounded regardless of the number of vehicles. Therefore, the platoon with the Rear-sided wave-absorbing control is L_2 string stable.

The position of the nth vehicle in a platoon with absorbers on both ends is expressed as

$$X_n(s) = G^n(s)X_0(s) + G^{N-n}(s)X_N(s), \qquad (2.78)$$

which immediately shows that the platoon with the Two-sided wave-absorbing controller is also L_2 string stable.

The results of this section can be summarized in the following lemma.

Lemma 5. *The platoon bidirectional controller and the wave-absorbing controller implemented on the leader and/or on the rear-end vehicle is L_2 string stable.*

2.5   Numerical simulations

We consider the linear friction of our system from Section 2.1 to be $\xi = 4$ and search for the parameters of the PI controller such that oscillations of the impulse response of $G(s)$ are minimized. The parameters $k_\mathrm{p} = k_\mathrm{i} = 4$ satisfy this requirement. All numerical simulations are run for the platoon of 50 vehicles to demonstrate that the wave-absorbing controllers are capable of controlling large platoons.

To demonstrate the advantages of the wave-absorbing controllers, we will compare their performance against a simple bidirectional control without any wave-absorbing controller. This means that the leader travels with a constant velocity v_ref for the whole time of the simulation. Fig. 2.7

shows the outcome of a numerical simulation when the leader without wave-absorbing controller increases its velocity. We can see significant limitations in the bidirectional control, where the oscillatory behaviour in the movement of the platoon is caused by numerous wave reflections from both platoon ends. Eventually, the platoon settles to the desired velocity after many velocity oscillations. These oscillations not only significantly prolong the settling time, but they could lead to accidents inside the platoon.
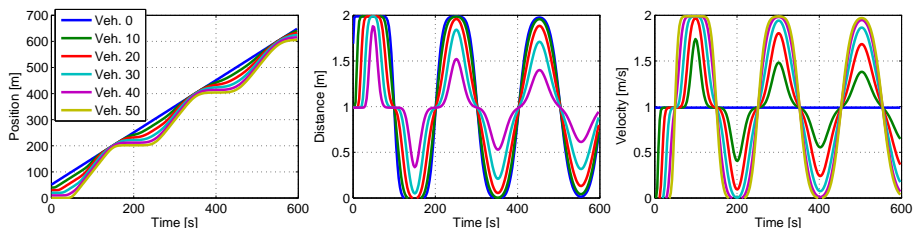
Figure 2.7: Simulation of the platoon without the wave-absorbing controller when the leader accelerates to a velocity $v_{\mathrm{ref}} = 1\,\mathrm{ms}^{-1}$. The reference distance is kept fixed, $d_{\mathrm{ref}} = 1\,\mathrm{m}$, for the whole time.

The performance of the Front-sided wave-absorbing controller during two platoon manoeuvrers is shown in Fig. 2.8. In the first 150 s manoeuver, the platoon accelerates to reach a desired velocity. In comparison with the simple bidirectional control, see Fig. 2.7, the settling time is now significantly shorter. Moreover, under some circumstances, it can be guaranteed that vehicles do not crash into each other during the platoon acceleration. In fact, the distances between vehicles are increased at the beginning of the acceleration as suggested by (2.55) and shown in the middle panel of Fig. 2.8. However, the distances may undershoot the initial inter-vehicles distances in the second part of the acceleration manoeuver. If the impulse response of the wave transfer function is tuned such that it does not undershoot the zero value, then the distances between vehicles can not become less than the initial inter-vehicle distances. In the opposite case (not shown here), where the platoon travels with a constant velocity and starts to decelerate, the distances between vehicles are temporarily decreased and a collision may occur.
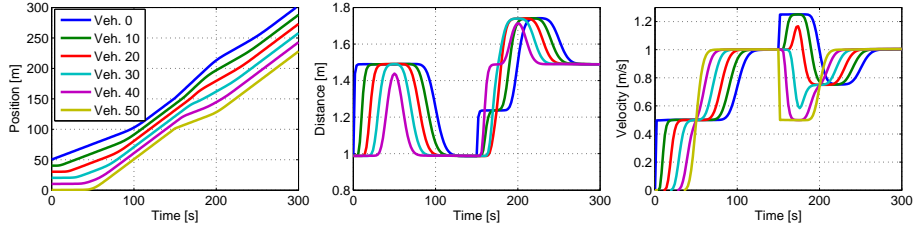
Figure 2.8: Simulation of two platoon manoeuvrers with the Front-sided wave-absorbing controller. At the beginning, the vehicles are standing still separated by one meter. For the first manoeuver, the platoon is commanded to accelerate to $v_{ref} = 1\,\mathrm{ms}^{-1}$ with $d_{ref} = 1\,\mathrm{m}$ starting at time $t = 0\,\mathrm{s}$. At time $t = 150\,\mathrm{s}$, the platoon is commanded to perform the second manoeuver such that the reference distance is increased to $d_{ref} = 1.5\,\mathrm{m}$ without changing the reference velocity.

At time $t = 150\,\mathrm{s}$ in Fig. 2.8, the platoon is commanded to perform the second manoeuver such that the reference distance is increased, but the reference velocity is kept unchanged. The rear-end vehicle reacts to this command at the same time as the leader since it is controlled by the reference distance that is now changing. However, the end vehicles differ in action; the leader accelerates, while the rear-end vehicle decelerates. This behaviour creates an undesirable overshoot in distances.

A numerical simulation of the two manoeuvrers for the platoon controlled by the Rear-sided wave-absorbing controller is shown in Fig. 2.9. During the acceleration manoeuver the inter-vehicle distances between vehicles closer to the rear end are temporarily decreased while those for vehicles near the leader are temporarily increased. During the changing-distance manoeuver, on the other hand, no overshoot in distances occurs.

In Fig. 2.10, the acceleration and changing-distance manoeuvrers carried out for the one-sided wave-absorbing controllers are now performed for the two-sided wave-absorbing controller. Since both platoon ends are fully controlled, the settling time is only half of that for the one-sided wave-absorbing controllers. The middle panel in Fig. 2.10 shows that there is no overshoot in distances during the second manoeuver. On the
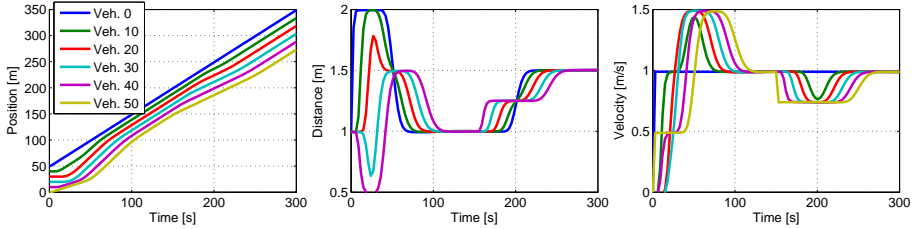
Figure 2.9: As in Fig. 2.8 but for the Rear-sided wave-absorbing controller.

other hand, there is no guarantee that the vehicles will not collide during the acceleration manoeuver.
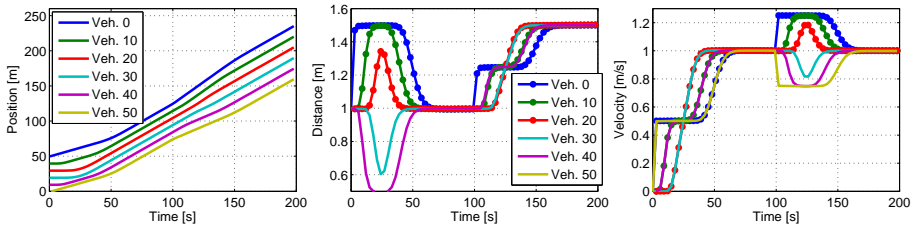
Figure 2.10: As in Fig. 2.8 but for the Two-sided wave-absorbing controller. The second command to increase d_{ref} comes at $t = 100\,\mathrm{s}$.

2.5.1 Asymmetric bidirectional controller

The so-called asymmetric bidirectional controller, introduced in [Barooah et al. (2009)], is another approach to improve the performance of the bidirectional controller. The idea is to implement two local controllers with different parameters for each vehicle, the 'front' controller and the 'rear' controller. The 'front' controller keeps the reference distance to the predecessor, while the 'rear' controller keeps the reference distance to the follower. In our numerical simulations, we choose the same parameters for the 'front' PI controller $k_{\mathrm{p}}^{\mathrm{f}} = k_{\mathrm{i}}^{\mathrm{f}} = 4$, but different parameters for the 'rear' PI controller $k_{\mathrm{p}}^{\mathrm{r}} = k_{\mathrm{i}}^{\mathrm{r}} = 3.6$. The parameter of the linear friction remains the same, i.e. $\xi = 4$.

41

Numerical simulations of the asymmetric bidirectional controller are shown in Fig. 2.11. The settling time is shorter than for the symmetric bidirectional controller (in agreement with [Barooah et al. (2009)]) but at the cost of higher overshoots, which corresponds to the fact that H_∞ norm grows exponentially with the number of vehicles in the platoon, [Herman et al. (2014a)]. Fig. 2.11 also reveals that the performance of the asymmetric bidirectional controller is worse, in terms of the settling time and the overshoots, than the performance of a platoon with a wave absorber.
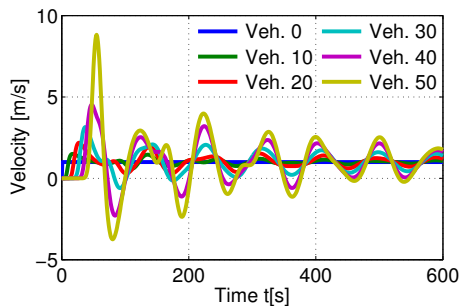
Figure 2.11: Numerical simulation of the platoon with the asymmetric bidirectional controller accelerating to $v_{\mathrm{ref}} = 1\,\mathrm{ms}^{-1}$.

2.5.2   Evaluation of the performance

We now numerically evaluate the performance of the acceleration manoeuver described in the previous section with the help of the mean squared error (MSE) criterion,

$$\mathrm{MSE} = \frac{1}{N+1} \sum_{n=0}^{N} \frac{1}{T} \sum_{t=0}^{T} (v_{\mathrm{ref}}(t) - v_n(t))^2, \qquad (2.79)$$

where T is the simulation time (in our case $T = 500\,\mathrm{s}$), $v_{\mathrm{ref}}(t)$ is the reference velocity of the platoon at time t and $v_n(t)$ is the actual velocity of the nth vehicle at time t.

The comparison in performance of the five controllers for various platoon lengths is depicted in Fig. 2.12. We can see that the MSE increases

linearly for all wave-absorbing controllers, but quadratically for the simple symmetric bidirectional control and exponentially for the asymmetric bidirectional control. Moreover, a linear increase in MSE for the Two-sided controller is only about half of that for the Front-sided controller. The linear increase of MSE for the Rear-sided controller lies between these two cases. Evidently, the wave-absorbing controller qualitatively improves the performance of the bidirectional control.
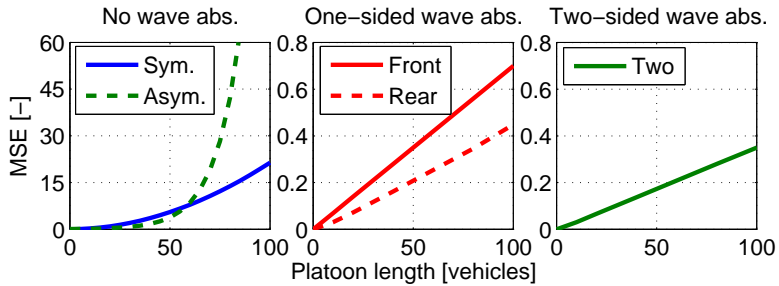
Figure 2.12: MSE performance evaluation of the acceleration manoeuver from Figs. 2.7, 2.8 and 2.10. The five controllers are evaluated; simple symmetric bidirectional and asymmetric bidirectional (left panel), Front-sided wave-absorbing controller (solid line in the middle panel), Rear-sided wave-absorbing controller (dashed line in the middle panel) and Two-sided wave-absorbing controller (right panel) for various platoon lengths according to (2.79).

The settling time of the acceleration manoeuver arising from the all five types of controllers are compared in Fig. 2.13. We can see that the settling time increases quadratically with platoon length for a platoon with simple symmetric bidirectional controller with no wave absorber, as was shown in [Hao and Barooah (2012b)], but approximately linearly for a platoon with wave-absorbing controllers. The qualitative improvement of the settling time is caused by the fact that the wave absorber changes the structure of a platoon to a multiple identical system connected in series, for instance, the transfer function of the Two-sided wave-absorbing architecture is G^N. In fact, the settling time of such a system grows nearly linearly, as analytically outlined in 2.7.1.
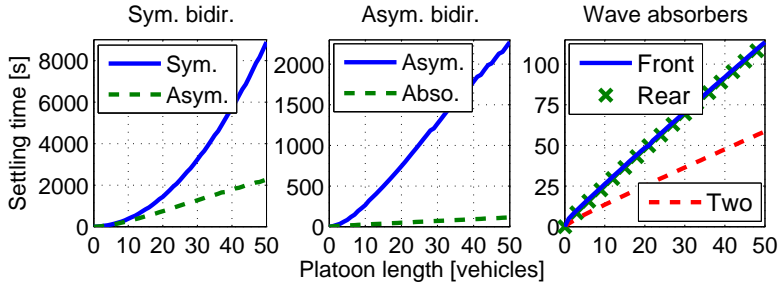
Figure 2.13: The time required for platoons of various lengths to accelerate and stay within a range of 5% of v_{ref}. The left panel shows comparison of the asymmetric bidirectional architecture with the symmetric bidirectional controller with no wave absorber. The middle panel compares the asymmetric bidirectional architecture with the Front-sided wave absorber. The settling time of all the wave-absorbing architectures is compared in the right panel.

2.5.3   Effect of noise in the platoon

This subsection examines the performance of the five controllers when noise is present in the system. The reference commands for a platoon of 20 vehicles are $v_{\text{ref}} = 0\,\text{ms}^{-1}$ and $d_{\text{ref}} = 0\,\text{m}$, that is, the platoon is commanded not to move. A normally distributed noise is simulated for 2000 seconds and added to distance measurements of each vehicle, except for the leader. Different realizations of the normally distributed noise with the mean value $\mu = 0$ and variance $\sigma^2 = 1$ are applied to each vehicle.

Table 2.1 assesses quantitatively the effect of noise on the performance of the five controllers. The mean squared error of positions, MSE_{pos}, and the arithmetic mean of positions, Mean_{pos}, show that the platoon without any absorber and with the Rear-sided wave-absorbing controller perform significantly better than with the other two controllers. This is due to the fact that at least one of the platoon ends is anchored at position 0, meaning that the platoon does not drift away from position 0, which is not the case for the Front-sided and Two-sided wave-absorbing controllers. Despite the disturbances by noise, all wave-absorbing controllers are better at maintaining the coherence of the platoon than the simple bidirectional

controller, as indicated by the mean squared error of inter-vehicle distances, MSE_{dist}, and the maximum distance between the leader and the rear end, MAX_{dist}.

Table 2.1: Performance of the five controllers when considering the normally distributed noise affecting distance measurement of vehicles. Four criterions used for the evaluation are introduced in the text.

	MSE_{pos}	Mean_{pos}	MSE_{dist}	MAX_{dist}
Sym. (no abs.)	2.7×10^7	2×10^{-3}	1.9×10^5	5.75
Asym. (no abs.)	1.1×10^7	22×10^{-3}	1.7×10^5	5.6
Front-sided wave abs.	8.4×10^7	-3.9	2.4×10^4	1.37
Rear-sided wave abs.	7.1×10^5	3.2×10^{-3}	2.5×10^4	1.15
Two-sided wave abs.	1.3×10^8	-3.1	1.8×10^4	0.64

2.5.4 Oscillatory bidirectional controller

It should be pointed out that the wave-absorbing controller is conceptualized as an extension of the symmetric bidirectional controller. It is not capable of attenuating the wave travelling inside the platoon, but only at the platoon ends. If the bidirectional control scheme is not properly designed, then the wave may be amplified before it reaches one of the ends. In such a case, the bidirectional controller needs to be redesigned to resolve the amplification problem. A rule of thumb is to design a bidirectional controller such that the impulse response of $G(s)$ does not undershoot the zero value.

Numerical simulations of a poorly designed bidirectional controller are shown in Fig. 2.14, where the PI coefficients are the same as in the previous section, $k_{\text{p}} = 4$, $k_{\text{i}} = 4$, but the linear friction is significantly smaller, $\xi = 1.03$ (compared with $\xi = 4$ previously). We can see that the behaviour of the whole platoon is oscillatory and that the wave is amplified as it travels inside the platoon. When the wave reaches the rear-end vehicle, it is absorbed with the Rear-sided wave-absorbing controller.
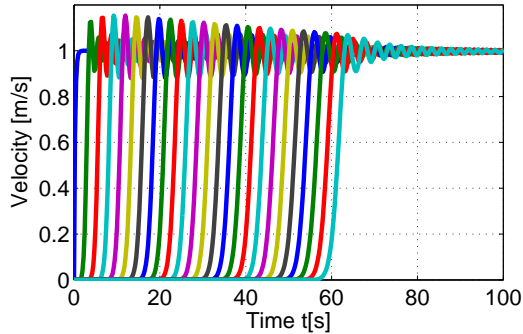
Figure 2.14: Numerical simulation of the platoon accelerating to $v_{\mathrm{ref}} = 1\,\mathrm{ms}^{-1}$ with a poorly designed bidirectional controller. The vehicles are indexed from left to right by 0, 5, 10, 15, ..., 120. The rear-end vehicle is equipped with the wave-absorbing controller.

2.6   Conclusions

This chapter introduces novel concepts for the control of a vehicular platoon, which significantly improve the popular bidirectional control. The main idea is to control the front or both ends of a platoon to actively damp the waves of positional changes arriving from the opposite platoon end. The absorbing-end vehicle is assumed to i) measure the distance to its neighbour, ii) know its own position and iii) represent the dynamics of a vehicle in terms of the wave transfer function.

The new schemes allow us to control the platoon velocity and the inter-vehicle distances without long-lasting transient and oscillatory behaviour. The velocity errors during the platoon manoeuvres with the traditional bidirectional control grows quadratically with the number of vehicles in the platoon, while errors grow only linearly for the bidirectional control enhanced with the wave-absorbing controller. Moreover, the platoon with the wave-absorbing controller is string stable.

Additionally, the wave-absorbing controller preserves the advantages of bidirectional control such as: i) The lack of a need for vehicle-to-vehicle communication, ii) none of the vehicles needs to know the number of

vehicles in the platoon, iii) an in-platoon vehicle does not need to know its index relative position in the platoon, and iv) an in-platoon vehicle does not need to know the reference velocity and the reference distance of the platoon.

However, a considerable mathematical difficulty in the wave-absorbing control lies in finding the impulse response of the wave transfer function. Here, we proposed the iterative approach of constructing an approximation of the wave transfer function that is based on a continued fraction representation. Even for a small number of iterative steps, when the wave transfer function is rather roughly approximated, the wave-absorbing control still performs efficiently to damp oscillations in the platoon's characteristics (i.e., velocity, inter-vehicle distances).

It should be noted that the absorbing-end vehicle is assumed to be equipped with the positional controller since the differences in positions between vehicles are controlled. Alternatively, when the absorbing-end vehicle is equipped with a velocity controller, the commanded position of the vehicle derived using (2.53) or (2.57) can be numerically differentiated to obtain the velocity commanded to the absorbing-end vehicle.

Undesirable overshoots in the velocities or inter-vehicle distances of the wave-absorbing control can be eliminated by introducing time delays in the reference signal applied to one of the platoon ends. An appropriate value of this time delay is dependent upon the platoon length and thus it requires the extension of the wave-absorbing control. This topic warrants further investigation.

2.7 Appendix to the chapter

2.7.1 Settling time of systems in series

We aim to show that the settling time of the identical systems connected in a series grows nearly linearly with the number of vehicles. The key idea is to find an appropriate first-order system with an envelope that contains

the impulse response of the given individual system, therefore, it gives an upper-limit estimate of the settling time. It is important to stress that this 'proof' considers the settling time of the impulse response.

Let us assume an asymptotically stable linear system of an arbitrary order, $T(s)$, and a linear first-order system $T_e(s) = \lambda/(s + \epsilon)$. We denote the settling times of $(T(s))^K$ and $(T_e(s))^K$ as τ_K and $\tau_{e,K}$, respectively. The parameters λ and ϵ are chosen such that: a) $\tau_{e,1} > \tau_1$ and b) the impulse response of $T(s)$ is bounded by the envelope of the impulse response of $T_e(s)$, which implies that $\tau_{e,K} > \tau_K$ for $K \in \mathbb{N}$. This means that $\tau_{e,K}$ gives an upper limit of the settling time τ_K. We define $\tau_{e,1}$ as the time elapsed until the impulse response of $T_e(s)$ enters (and does not leave it afterwards) a deviation band $\pm\eta$. In other words, $\tau_{e,1}$ is a solution of the equation

$$\lambda \exp\left(-\epsilon\tau_{e,1}\right) = \eta, \tag{2.80}$$

that is

$$\tau_{e,1} = -\frac{1}{\epsilon}\ln\left(\frac{\eta}{\lambda}\right). \tag{2.81}$$

Inverse Laplace transform of $(T_e(s))^K$ is

$$g_K(t) = \lambda^K \frac{1}{(K-1)!}t^{K-1}\exp\left(-\epsilon t\right). \tag{2.82}$$

Therefore, the settling time $\tau_{e,K}$ is a solution of the equation

$$\lambda^K \frac{1}{(K-1)!}\tau_{e,K}^{K-1}\exp\left(-\epsilon\tau_{e,K}\right) = \eta. \tag{2.83}$$

It may happen that there are more than two solutions of (2.83). In that case, we take the largest real solution. In this regard, the settling time $\tau_{e,K}$ is expressed as

$$\tau_{e,K} = -(K-1)\frac{1}{\epsilon}W_{-1}\left(-(K-1)^{-1}\epsilon\lambda^{-N/(N-1)}\sqrt[K-1]{\eta(K-1)!}\right),$$
$$K > 1, \tag{2.84}$$

where W_{-1} is the lower branch of the Lambert-W function, see [Corless et al. (1996)]. Finally, substituting (2.80) into (2.84) gives

$$\tau_{\text{e},K} = -(K-1)\frac{1}{\epsilon}W_{-1}\left(-(K-1)^{-1}\epsilon\lambda^{-1}\exp\left(\frac{-\epsilon\tau_{e,1}}{(K-1)}\right)\right.$$
$$\left.\sqrt[K-1]{(K-1)!}\right), \quad K > 1. \tag{2.85}$$

The settling time described in (2.85) grows almost linearly with the increasing number of vehicles as shown in Fig. 2.15.
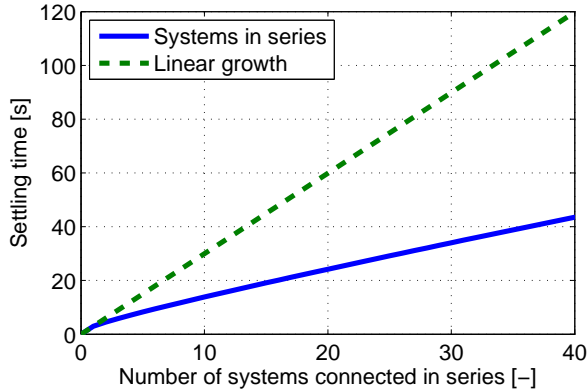
Figure 2.15: The settling time of the identical systems connected in a series evaluated according to (2.81) and (2.84) compared with a linear growth of the settling time. Parameters of the system are: $\epsilon = 1$, $\lambda = 1$ and $\eta = 0.05$.

2.7.2 Approximation of the Wave transfer function using Newton's method

Newton's method is an iterative process of finding the roots of a function. The iterative process is defined as

$$x_{n+1} = x_n - \frac{f(x_n)}{f'(x_n)}, \tag{2.86}$$

49

where x_n is the nth approximation of the root of the function. The applicability of Newton's method to complex quadratic polynomials was already studied by A. Cayley in 1879 [Cayley (1879)]. Later, by work of P. Fatou and G. Julia, the method was generalized for polynomials of higher orders. It turned out that the basin of attraction of complex polynomials, especially of higher order polynomials is very complex and needs to be revised very carefully. Every root of the complex polynomial has its own basin of attraction, a *Fatou set*, which is separated from the basin of other roots by the *Julia set*. The set of complex numbers from the Julia set do not converge to any root. Interestingly enough, the Julia set has usually fractal structure.

Carlson and Halijak in 1963 [Carlson and Halijak (1964)] were the first to show that the Newton's method can be applied even for the approximation of irrational functions, such as $\left(\dfrac{1}{s}\right)^{\frac{1}{n}}$. Here, the method will be used to approximate $G(s)$ by a rational transfer function based on the quadratic function

$$f(G(s)) = G^2(s) - \alpha(s)G(s) + 1, \tag{2.87}$$

which comes from (2.28). The first derivative of f

$$f'(G(s)) = \frac{dF(G(s))}{dG(s)} = 2G(s) - \alpha(s). \tag{2.88}$$

Newton's recursive formula (2.86) is then

$$\begin{aligned}
G(s)_{n+1} &= G(s)_n - \frac{f(G_n(s))}{f'(G_n(s))} \\
&= G(s)_n - \frac{G^2(s)_n - \alpha(s)G(s)_n + 1}{2G(s)_n - \alpha(s)} = \frac{G^2(s)_n - 1}{2G(s)_n - \alpha(s)}.
\end{aligned} \tag{2.89}$$

The higher number of iteration means the better approximation but also the higher order of the approximate system. It was also proven that Newton's method converges quadratically for the roots of a single multiplicity.

Therefore, only a few iterations are usually sufficient to get a satisfactory approximation.

How to choose the initial guess, $G(s)_0$, is a difficult question to answer. We expect that the Julia set is connected and that there are two basins of attractions i.e. two Fatou sets, since we have two different roots. We can immediately see that the initial guess $G(s)_0 = \frac{1}{2}\alpha(s)$ is problematic. Newton's method also fails to converge, if the initial guess is equal to one of the roots, i.e. $G(s)_0 = G(s)$ and $G(s)_0 = 1/G(s)$.

We experimentally found out that the relative order of $G(s)_0$ plays a crucial role. Specifically, $G(s)_0$ converges to $G(s)$ only if $G(s)_0$ satisfies

$$r_{\mathrm{G0}} < r_\alpha, \tag{2.90}$$

where r_{G0} and r_α are the relative degree of $G(s)_0$ and $\alpha(s)$, respectively. For example, $r_\alpha = 2$ for $\alpha(s) = \dfrac{s^3 + \xi s^2 + 2k_p s + 2k_i}{k_p s + k_i}$, therefore, choosing $G(s)_0 = \dfrac{s^2}{s+1}$, the iteration converge to $G(s)$ but for $G(s)_0 = \dfrac{s^3}{s+1}$ or $G(s)_0 = s^2$ the iteration converge to $1/G(s)$ etc. The results of the approximations are shown in Fig. 2.16. We can see that 3 iteration steps give a very similar result as 20 steps of the Continued Fraction approximation.

It is convenient to use the approximation of the Wave transfer function in the time domain. Therefore, we carry out the inverse Laplace transform of the approximate $G(s)_n$ and truncate it in time, similarly as for the Continued-fraction approximation. The result is shown in Fig. 2.17.

Different equation used for approximation

We can also use a different equation for Newton's approximation. In the platoon of two vehicles, that means one leader and one follower ($N = 1$),
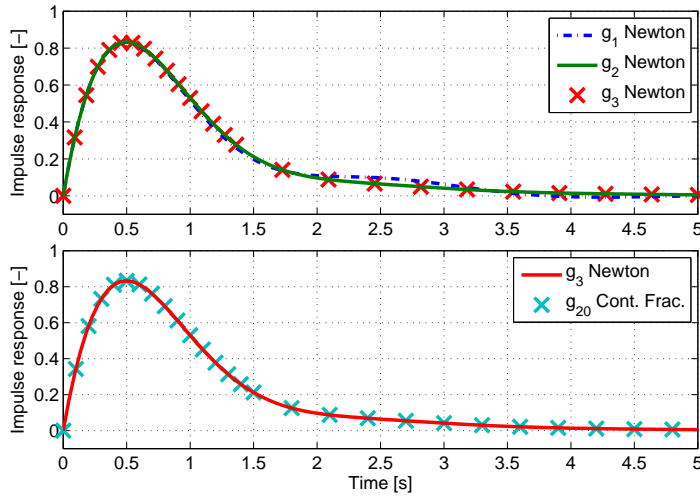
Figure 2.16: Comparison of Newton's and Continued fraction approximations for system with $k_p = k_i = \xi = 4$. The index at g shows the number of iteration steps.

the transfer function between their positions is

$$\frac{X_1(s)}{X_0(s)} = \frac{1}{\alpha(s) - 1} = \frac{P(s)C(s)}{1 + P(s)C(s)}. \tag{2.91}$$

With the knowledge of the forced and free boundary reflections, we can express this transfer function as

$$\frac{X_1(s)}{X_0(s)} = \frac{G(s)(1 + G(s))}{1 + G^3(s)}. \tag{2.92}$$

Therefore,

$$f_2(G(s)) = \frac{G(s)(1 + G(s))}{1 + G^3(s)} - \frac{1}{\alpha(s) - 1} = 0 \tag{2.93}$$

and

$$f_2'(G(s)) = \frac{dF_2(G(s))}{dG(s)} = \frac{1 - G^2(s)}{(G^2(s) - G(s) + 1)^2}. \tag{2.94}$$

52

(a) Bode characteristics - magnitude.   (b) Bode characteristics - phase.
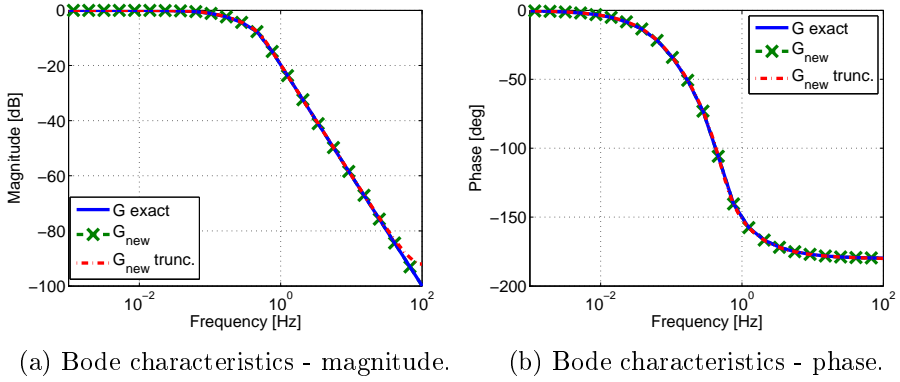
Figure 2.17: Comparison of 'full' and 'truncated-in-time' Newton's approximations. The approximation was constructed in 3 iteration steps, truncated at time 50 s and sampled with frequency 200 Hz.

The resulting approximation formula is then

$$G(s)_{n+1} = G(s)_n - \frac{f_2(G_n(s))}{f_2'(G_n(s))}. \tag{2.95}$$

Although this approximation works, it is less numerically stable than the quadratic-equation approximation in (2.89) because of higher order of the approximation.

It should be noted that other iterative root-finding algorithms, such as e.g. Halley's, Whittaker's, Chebyshev's etc., see [Amat et al. (2004)], may also be used to approximate the Wave transfer function in the Laplace domain.

2.7.3 Approximation of the Wave transfer function using binomial theorem

Another type of approximation is based on the binomial theorem

$$(1 + x)^k = \sum_{k=0}^{\infty} \binom{n}{k} x^k, \tag{2.96}$$

where

$$\binom{n}{k} = \prod_{l=1}^{k} \frac{n-l+1}{l}.$$ (2.97)

We carry out the binomial approximation for the system used in simulations, where $\alpha(s) = \dfrac{s^3 + \xi s^2 + 2k_p s + 2k_i}{k_p s + k_i}$ and the Wave transfer function

$$
\begin{aligned}
G(s) =& \frac{s^3 + \xi s^2 + 2k_p s + 2k_i}{2(k_i + k_p s)} \\
& - \frac{s\sqrt{s^4 + 2\xi s^3 + \xi^2 s^2 + 4k_p s^2 + 4k_p \xi s + 4k_i s + 4k_i \xi}}{2(k_i + k_p s)}.
\end{aligned}
$$ (2.98)

The binomial approximation has three steps. In the first step show that the binomial expansion of the square root polynomial cancels out the non-square root polynomial in the numerator of (2.98) and thus this transfer function proper. In the second step we show how to expand the square root using the binomial theorem. In the last step we find the impulse response of (2.98).

First step — The transfer function is proper

Let us define ϵ implicitly by

$$s\sqrt{\xi^2 s^2 + 2\xi s^3 + 4k_p \xi s + 4k_i \xi + s^4 + 4k_p s^2 + 4k_i s} = s^3 \sqrt{1 + \epsilon}.$$ (2.99)

This gives

$$\epsilon = \frac{2\xi}{s} + \frac{4k_p + \xi^2}{s^2} + \frac{4k_p \xi + 4k_i}{s^3} + \frac{4k_i \xi}{s^4}.$$ (2.100)

By the binomial theorem, we have

$$\sqrt{1+\epsilon} = 1 + \frac{1}{2}\epsilon - \frac{1}{8}\epsilon^2 + \frac{1}{16}\epsilon^3 + ... = \sum_{n=0}^{\infty} \binom{0.5}{n} \epsilon^n. \tag{2.101}$$

The approximation is then given as

$$\sqrt{1+\epsilon} \approx \sum_{n=0}^{n_{max}} \binom{0.5}{n} \epsilon^n, \tag{2.102}$$

where n_{max} is the maximum number of iterations.

Now, we focus on the numerator of (2.98). Setting $n_{max} = 1$ yields

$$\text{num}_1 = s^3 + \xi s^2 + 2k_p s + 2k_i - s^3(1+0.5\epsilon) = -\frac{\xi^2}{2}s - 2k_p\xi - \frac{2k_i\xi}{s}. \tag{2.103}$$

Increasing the number of iterations to $n_{max} = 3$ yields

$$\begin{aligned}
\text{num}_3 &= s^3 + \xi s^2 + 2k_p s + 2k_i - s^3\left(1+0.5\epsilon - \frac{1}{8}\epsilon^2 + \frac{1}{16}\epsilon^3\right) \\
&= -\frac{\xi^2}{2}s - 2k_p\xi - \frac{2k_i\xi}{s} + \frac{s^3}{8}\epsilon^2 - \frac{s^3}{16}\epsilon^3 \\
&= \frac{1}{s}\left(2k_p^2 + \frac{5\xi^4}{8}\right) + \frac{1}{s^2}(...) + \frac{1}{s^3}(...) + \frac{1}{s^4}(...) + ...
\end{aligned} \tag{2.104}$$

In other words, the largest power of s in the numerator is -1 after 3 iterations. The higher iterations do not change this power. This shows that the binomial approximation of (2.98) is proper.

Second step — Expansion of the square root

By the binomial theorem, we have

$$(x+y)^\beta = \sum_{\alpha=0}^{\beta} \binom{\beta}{\alpha} x^\alpha y^{(\beta-\alpha)} = \sum_{\alpha=0}^{\beta} \binom{\beta}{\alpha} (x_1+x_2)^\alpha (y_1+y_2)^{(\beta-\alpha)}$$

$$= \sum_{\alpha=0}^{\beta} \binom{\beta}{\alpha} \sum_{\gamma=0}^{\alpha} x_1^\gamma x_2^{(\alpha-\gamma)} \sum_{\delta=0}^{\beta-\alpha} \binom{\beta-\alpha}{\delta} y_1^\delta y_2^{(\beta-\alpha-\delta)}$$

$$= \sum_{\alpha=0}^{\beta} \sum_{\gamma=0}^{\alpha} \sum_{\delta=0}^{(\beta-\alpha)} \binom{\beta}{\alpha}\binom{\alpha}{\gamma}\binom{\beta-\alpha}{\delta} x_1^\gamma x_2^{(\alpha-\gamma)} y_1^\delta y_2^{(\beta-\alpha-\delta)}.$$

$$(2.105)$$

By (2.100), the nth power of ϵ is

$$\epsilon^n = \left(\frac{2\xi}{s} + \frac{4k_p + \xi^2}{s^2} + \frac{4k_p\xi + 4k_i}{s^3} + \frac{4k_i a}{s^4} \right)^n$$

$$= \left(\frac{A}{s} + \frac{B}{s^2} + \frac{C}{s^3} + \frac{D}{s^4} \right)^n, \qquad (2.106)$$

where $A = 2\xi$, $B = 4k_p + \xi^2$, $C = 4k_p\xi + 4k_i$ and $D = 4k_i\xi$. Applying the expansion (2.105) yields

$$\epsilon^n = \sum_{k=0}^{n} \sum_{l=0}^{k} \sum_{h=0}^{(n-k)} \binom{n}{k}\binom{k}{l}\binom{n-k}{h} \frac{A^l B^{(k-l)} C^h D^{(n-k-h)}}{s^{(4n-2k-l-h)}}. \quad (2.107)$$

Last step — Inverse Laplace transform

It is now possible, yet very laboriously, to find inverse Laplace transform of (2.98). Let us split the transfer function into two polynomials

$$G(s) = P_1(s) + P_2(s) \qquad (2.108)$$

where

$$P_1(s) = \frac{s^3 + \xi s^2 + 2k_p s + 2k_i - s^3(1 + 0.5\epsilon - \frac{1}{8}\epsilon^2 + \frac{1}{16}\epsilon^3)}{2(k_p s + k_i)} \quad (2.109)$$

which was shown to be proper and

$$P_2(s) \approx s^3 \frac{\sum_{n=4}^{n_{max}} \binom{0.5}{n} \epsilon^n}{2(k_p s + k_i)}. \quad (2.110)$$

It can be shown that

$$\frac{1}{s^n(s+\lambda)} = \mathcal{L}\left\{ (-1)^n \frac{e^{-\lambda t}}{\lambda^n} + \sum_{k=0}^{n-1} (-1)^{(n-k+1)} \frac{t^k}{k!\lambda^{n-k}} \right\}, \quad (2.111)$$

where $\mathcal{L}$ symbolizes the Laplace transform. This formula can be used to find the inverse Laplace transform of both $P_1(s)$ and $P_2(s)$. Rather than finding it by hand, we use Matlab or Mathematica.

Fig. 2.18 shows the comparison of the Binomial approximations for several values of n_{max} and Newton's approximation. We can see that we need a large number of iteration steps of the Binomial method, which is a significant drawback of the method.

2.7.4 Wave transfer function - double integrator model

We validate the three approximating methods by carrying out the Laplace transform analytically for a simple example of a double-integrator system. In such a system $\alpha = s^2 + 2$ and

$$G(s) = 1 + \frac{s^2}{2} - \frac{s}{2}\sqrt{s^2 + 4}. \quad (2.112)$$

We will show that the inverse Laplace transform leads to the Bessel func-
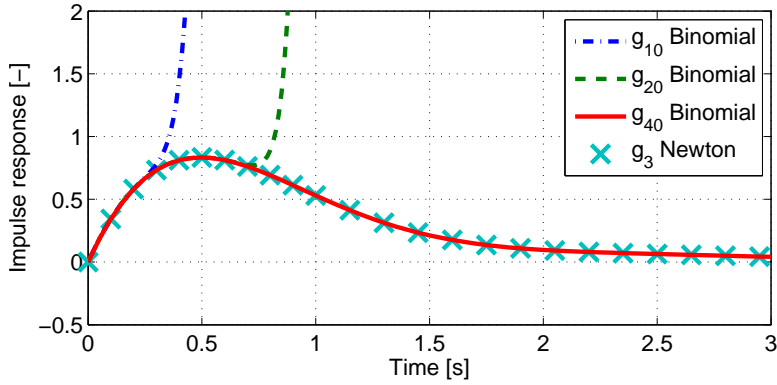
Figure 2.18: Comparison of the Binomial and Newton's approximations for the system with $k_p = k_i = \xi = 4$. The index at g shows the number of iteration steps.

tions. We use the following properties of the Bessel functions

$$\mathcal{L}\{J_0(2t)\} = \frac{1}{\sqrt{s^2 + 4}}, \tag{2.113}$$

$$(J_0(2t))' = -2J_1(2t), \tag{2.114}$$

$$(J_1(2t))' = 2J_0(2t) - \frac{J_1(2t)}{t}, \tag{2.115}$$

where $J_0(t)$ is the Bessel function of the first kind and zero order.

We differentiate the square root term in (2.112) with respect to s

$$\frac{dG}{ds} = s - \frac{s^3 + 2s}{\sqrt{s^4 + 4s^2}} = s - \frac{s^2 + 2}{\sqrt{s^2 + 4}}, \tag{2.116}$$

Using (2.113) and the following rules for the Inverse Laplace transform

$$f''(t) = \mathcal{L}^{-1}\left\{s^2 F(s) - sf(0) - f'(0)\right\} \tag{2.117}$$

$$\frac{1}{t}f(t) = \mathcal{L}^{-1}\left\{\int_s^\infty F(\sigma)d\sigma\right\}, \tag{2.118}$$

we find

$$g(t) = \frac{1}{t} \left(J_0(2t) \right)'' + 2J_0(2t), \qquad (2.119)$$

where

$$\left(J_0(2t) \right)'' = \left(-2J_1(2t) \right)' = \frac{2}{t} J_1(2t) - 4J_0(2t). \qquad (2.120)$$

We note that the 's' in (2.116) corresponds to the initial condition of the Bessel functions from $\left(J_0(2t) \right)''$ as

$$s \left(J_0(2t) \right)_{t=0} + \left(-2J_1(2t) \right)_{t=0} = s. \qquad (2.121)$$

Therefore

$$g(t) = \frac{2}{t^2} J_1(2t) - \frac{2}{t} J_0(2t). \qquad (2.122)$$

We can see in Fig. 2.19 that Newton's and the Continued fraction methods give identical approximation of the Wave transfer function.

2.7.5   Overview of some Wave transfer functions

The overview of the Wave transfer functions is shown in Figs. 2.20 and 2.21. All the step responses converge to one due to at least one integrator in the agent's model. The Wave transfer functions for the systems with three integrators (bottom panels) are asymptotically stable, despite the fact that the multi-agent system with the path-graph topology is asymptotically unstable (see Table 7.1, p. 156).
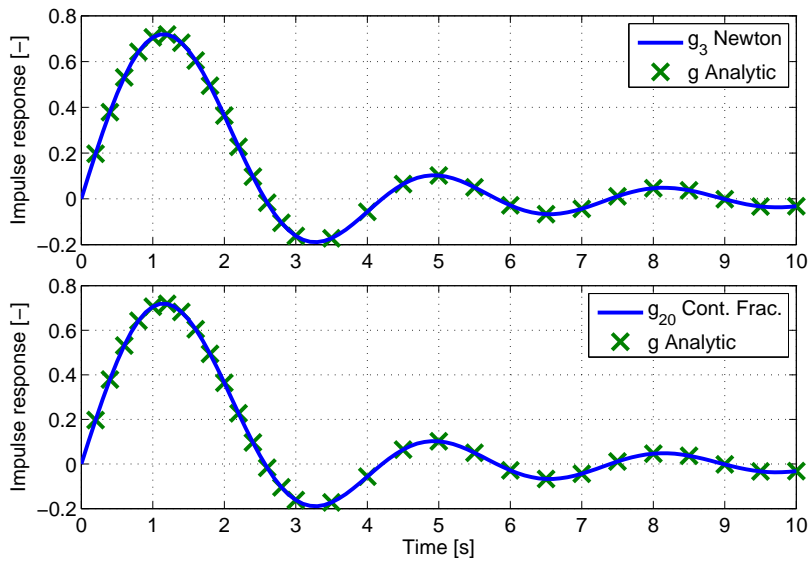
Figure 2.19: Comparison of Newton's and the Continued fraction approximations with the analytic derivation of the impulse response from (2.122) of the Wave transfer functions in (2.112). The index at g shows the number of iteration steps.
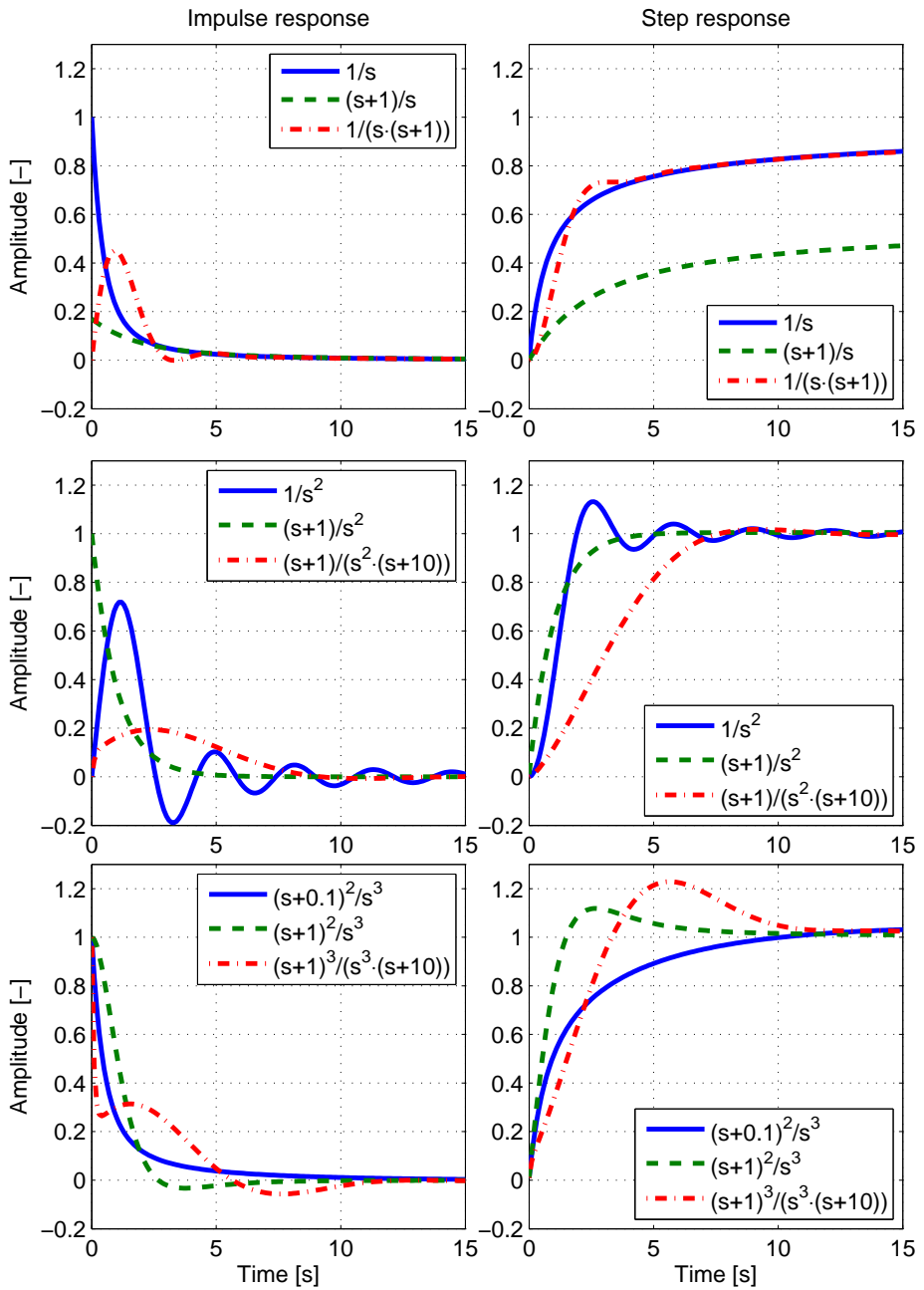
Figure 2.20: The comparison of the impulse and step responses of the Wave transfer function for various agent models.
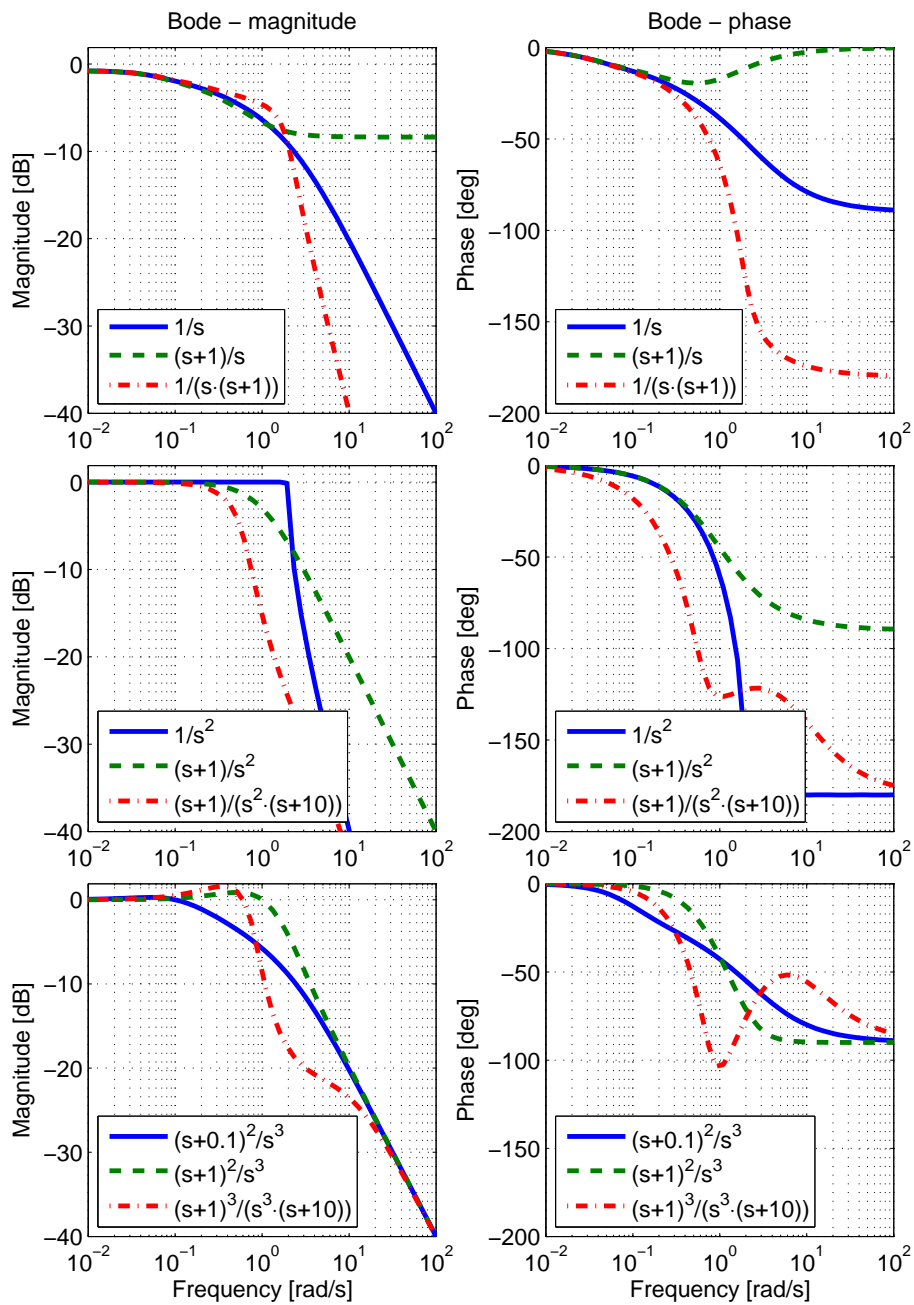
Figure 2.21: The comparison of the Bode frequency response of the Wave transfer function for various agent models.

3 Heterogeneous agents and the waves

The previous chapter shows that the interaction between the vehicles, or generally– agents, causes that a change in the output (e.g. position) of even a remote agent affects all the other agents. If we study their responses from the local point-of-view, we can notice that the change is propagated as a wave. For instance, if the first agent changes its output, it initiates a wave that travels along the system to the last agent, where it is reflected and travels back. When it reaches the first agent, it reflects back again. These two reflections at the system boundaries significantly prolong the settling time.

The same phenomenon is occurs if the agents are non-identical, for instance, if the agents have different dynamics, or different controllers. In fact, the travelling wave is partially reflected at non-identical agents inside the multi-agent system. We can imagine this behaviour as the reflection of the wave at a boundary between two media of different properties, see for instance [French (2003)]. A wave reflection is usually an undesired effect since it prolongs the settling time. One way to avoid the reflections inside the system is to force the agents to be identical, which is usually impractical, or even impossible. On the other hand, a wave description allows us to design a feedback controller that compensates the different dynamics of the agents, which shortens the settling time.

In this chapter, we aim to provide the mathematical description of the travelling waves propagating along a multi-agent system with non-identical agents and path-graph topology. The underlying questions are: How do

the different dynamics of the agents affect the travelling wave? How to mathematically describe this effect? How to compensate it?

The main contributions of the chapter are: i) mathematical description of the travelling waves in a multi-agent system with non-identical agents and a path-graph topology (Theorems 3 and 4), ii) a local performance analysis of the multi-agent system by the analysis of the wave amplification determined by the DC gains (Lemma 7), and iii) a design of a controller that prevents a reflection of the travelling wave, which shortens the transient of the system (Theorems 5 and 6).

3.1   Mathematical preliminaries

3.1.1   Local control law

We consider a multi-agent system with a path-graph interaction topology. The dynamics of agents is described by a linear single-input-single-output model with the transfer function $P_n(s)$, where n is index of the agent. The output, $X_n(s)$, is given as

$$X_n(s) = P_n(s)U_n(s), \tag{3.1}$$

where $U_n(s)$ is the input to the agent generated by a local control law of the agent. This law aims to equalize agent output with the outputs of the two neighbouring agents. It is modelled as

$$U_n(s) = C_{\mathrm{f},n}(s)(X_{n-1}(s) - X_n(s)) + C_{\mathrm{r},n}(s)(X_{n+1}(s) - X_n(s)) \\ + C_{\mathrm{f},n}(s)W_{\mathrm{f},n}(s) + C_{\mathrm{r},n}(s)W_{\mathrm{r},n}(s), \tag{3.2}$$

where $C_{\mathrm{f},n}(s)$ and $C_{\mathrm{r},n}(s)$ are transfer functions of the controllers of the front and rear agents, respectively, $W_{\mathrm{f},n}(s)$ and $W_{\mathrm{r},n}(s)$ are the inputs to the agent. We assume that the inputs are equal to zero unless we specify them otherwise. We consider that each agent may have a different dynamical model as well as a different set of controllers and denote the front agent transfer function (ATF) and rear ATF by $M_{\mathrm{f},n}(s) = P_n(s)C_{\mathrm{f},n}(s)$

and $M_{r,n}(s) = P_n(s)C_{r,n}(s)$, respectively. The resulting model of the nth agent, assuming zero initial conditions, is shown in Fig. 3.1 and is described as

$$X_n(s) = M_{f,n}(s)(X_{n-1}(s) - X_n(s)) + M_{r,n}(s)(X_{n+1}(s) - X_n(s))$$
$$+ M_{f,n}(s)W_{f,n}(s) + M_{r,n}(s)W_{r,n}(s). \tag{3.3}$$

Figure 3.1: The model of nth agent.

The first agent is described as

$$X_1(s) = M_{f,1}(s)(W_{f,1}(s) - X_1(s)) + M_{r,1}(s)(X_2(s) - X_1(s)), \quad (3.4)$$

where $W_{f,1}(s) = X_{\text{ref}}(s)$ is the external input to the multi-agent system, which represents the reference output of the multi-agent system. The last agent, i.e. the rear-end agent $(n = N)$ of the system, is described as

$$X_N(s) = M_{f,N}(s)(X_{N-1}(s) - X_N(s)). \tag{3.5}$$

3.1.2 The wave generated by an input to the agent

We generalize (2.21) for the case with a non-zero input. For now, we consider only the input $W_{\mathrm{r},n}$ while $W_{\mathrm{f},n} = 0$. Hence, the model (3.3) of the nth agent is

$$
\begin{aligned}
X_n(s) = M_{\mathrm{f},n}(s)(X_{n-1}(s) - X_n(s)) + M_{\mathrm{r},n}(s)(X_{n+1}(s) - X_n(s)) \\
+ M_{\mathrm{r},n}(s)W_{\mathrm{r},n}(s).
\end{aligned} \tag{3.6}
$$

In this case, the input $W_{\mathrm{r},n}(s)$ generates a wave that propagates in the multi-agent system in the same manner as described by (2.22) and (2.23). However, (2.21) is changed as follows

$$
X_n(s) = G(s)A_{n-1}(s) + G(s)B_{n+1}(s) + T_{\mathrm{r},n}(s)W_{\mathrm{r},n}(s), \tag{3.7}
$$

where $T_{\mathrm{r},n}(s) = X_n(s)/W_{\mathrm{r},n}(s)$ for $N \to \infty$. We are interested in finding $T_{\mathrm{r},n}(s)$, hence, we substitute (2.22) and (2.23) into (3.6) and get

$$
\begin{aligned}
T_{\mathrm{r},n}W_{\mathrm{r},n} = M_{\mathrm{f},n}(GT_{\mathrm{r},n}W_{\mathrm{r},n} - T_{\mathrm{r},n}W_{\mathrm{r},n}) \\
+ M_{\mathrm{r},n}(GT_{\mathrm{r},n}W_{\mathrm{r},n} - T_{\mathrm{r},n}W_{\mathrm{r},n}) + M_{\mathrm{r},n}W_{\mathrm{r},n}.
\end{aligned} \tag{3.8}
$$

Rearranging results in

$$
T_{\mathrm{r},n}(s) = \frac{M_{\mathrm{r},n}(s)}{1 + M_{\mathrm{f},n}(s) + M_{\mathrm{r},n}(s) - M_{\mathrm{f},n}(s)G(s) - M_{\mathrm{r},n}(s)G(s)}. \tag{3.9}
$$

The transfer function $T_{\mathrm{f},n}(s) = X_n(s)/W_{\mathrm{f},n}$ for a non-zero input $W_{\mathrm{f},n}$ can be arranged in a similar way as $T_{\mathrm{r},n}(s)$.

3.2 Soft and hard boundaries

3.2.1 Mathematical definition of the boundaries

We consider that the multi-agent system consists of non-identical agents. In general, we can distinguish between three cases: i) $M_{\mathrm{r},n} \neq M_{\mathrm{f},n+1}$, ii)

$M_{\mathrm{f},n} \neq M_{\mathrm{r},n}$, and iii) a combination of i) and ii). All three cases causes a partial reflection of the travelling wave. Therefore, we can consider them as boundaries for the wave. First, let us focus on the boundaries caused by i) and ii).

Definition 4. *The* soft boundary *is a virtual boundary between two agents, indexed s and $s+1$, with the following property*

$$M_{\mathrm{r},s}(s) \neq M_{\mathrm{f},s+1}(s), \tag{3.10}$$

where $M_{\mathrm{r},s}(s)$ and $M_{\mathrm{f},s+1}(s)$ defines the model of an agent in (3.3).

The soft boundary is, for instance, located in a platoon of non-identical vehicles governed by the same symmetric bidirectional control law, see [Martinec et al. (2014d)], or in a mass-spring model with identical springs but non-identical masses.

The second type of boundary is defined as follows.

Definition 5. *The* hard boundary *is a virtual boundary located at the hth agent with the property*

$$M_{\mathrm{f},h}(s) \neq M_{\mathrm{r},h}(s), \tag{3.11}$$

where $M_{\mathrm{f},h}(s)$ and $M_{\mathrm{r},h}(s)$ defines the model of an agent in (3.3).

The hard boundary is, for instance, located in a platoon of identical vehicles governed by the asymmetric bidirectional control, or in a mass-spring model with identical masses but different springs, see Fig. 3.2.

The adjective 'hard' emphasizes the fact that the hard boundary is located at an agent, in contrast to the soft boundary, located between two agents. To distinguish between the incident, transmitted and reflected waves at the hard boundary, we decompose X_h to the hard-boundary wave components as

$$X_h(s) = A_{h,\mathrm{L}}(s) + B_{h,\mathrm{L}}(s) = A_{h,\mathrm{R}}(s) + B_{h,\mathrm{R}}(s), \tag{3.12}$$

67
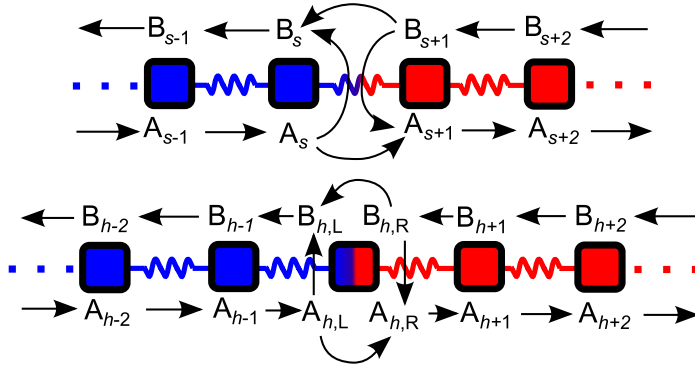
Figure 3.2: Scheme of a multi-agent system with the soft (top panel) and hard (bottom panel) boundaries, respectively. The blue and red squares are agents with the WTFs of $G(s)$ and $H(s)$, respectively, defined later. The virtual connections between the agents are illustrated by springs. The blue-red spring is the soft boundary and the blue-red square is the hard boundary.

where the indexes L and R denote the wave components that are next to the left and right sides of the boundary, respectively. Changing the output of the agent with the hard boundary initiates two waves propagating in opposite directions with different dynamics. This is treated in following technical lemma.

Lemma 6. *If there is no other boundary next to the hard-boundary agent, then*

$$A_{h,\mathrm{L}}(s) = G(s)A_{h-1}(s), \quad B_{h,\mathrm{L}}(s) = G^{-1}(s)B_{h-1}(s), \tag{3.13}$$

$$A_{h,\mathrm{R}}(s) = H^{-1}(s)A_{h+1}(s), \quad B_{h,\mathrm{R}}(s) = H(s)B_{h+1}(s), \tag{3.14}$$

where

$$G(s) = \frac{1}{2}\alpha_1 - \frac{1}{2}\sqrt{\alpha_1^2 - 4}, \quad H(s) = \frac{1}{2}\alpha_2 - \sqrt{\alpha_2^2 - 4}, \tag{3.15}$$

$\alpha_1 = 2 + 1/M_{\mathrm{f},h}(s)$ *and* $\alpha_2 = 2 + 1/M_{\mathrm{r},h}(s)$.

Proof. The proof is the same as the proof of Theorem 1 in Section 2.2.1.

In this case, two different sets of continued fractions can be found, one converges to G and G^{-1}, and the other one to H and H^{-1}. □

The third case introduced at the beginning of this section, that is the combination of the soft and hard boundaries, can be treated by generalization of Lemma 6 given in Section 3.5.

3.2.2 Mathematical description of the boundaries

Theorem 3. *A soft boundary is described in the Laplace domain by the following four boundary-transfer functions (BTFs),*

$$T_{\text{aa}} = \frac{A_{s+1}}{A_s} = \frac{H - HG^2}{1 - HG}, \quad T_{\text{ba}} = \frac{A_{s+1}}{B_{s+1}} = \frac{HG - H^2}{1 - HG}, \tag{3.16}$$

$$T_{\text{bb}} = \frac{B_s}{B_{s+1}} = \frac{G - H^2G}{1 - HG}, \quad T_{\text{ab}} = \frac{B_s}{A_s} = \frac{HG - G^2}{1 - HG}, \tag{3.17}$$

where

$$G(s) = \frac{1}{2}\alpha_1 - \frac{1}{2}\sqrt{\alpha_1^2 - 4}, \quad H(s) = \frac{1}{2}\alpha_2 - \sqrt{\alpha_2^2 - 4}, \tag{3.18}$$

$\alpha_1 = 2 + 1/M_{\text{r},s}(s)$ *and* $\alpha_2 = 2 + 1/M_{\text{f},s+1}(s)$.

Proof. This technical result follows the mathematical derivation of reflection at a forced boundary derived in Lemma 1. The model of a forced boundary was shown to be $A_1 = GX_0 - G^2B_1$. We can use this result and describe the soft boundary as

$$A_{s+1} = -H^2 B_{s+1} + HX_s, \tag{3.19}$$

$$B_s = -G^2 A_s + GX_{s+1}. \tag{3.20}$$

Substituting (2.21) for X_s and (3.20) for B_s yields

$$A_{s+1} = -H^2 B_{s+1} + H(A_s - G^2 A_s + G(A_{s+1} + B_{s+1})). \tag{3.21}$$

Separating A_{s+1} gives the final result

$$A_{s+1} = A_s \frac{H - HG^2}{1 - HG} + B_{s+1} \frac{HG - H^2}{1 - HG}. \tag{3.22}$$

Similarly, substituting (2.21) for X_s and (3.19) for A_{s+1} gives

$$B_s = -G^2 A_s + G(-H^2 B_{s+1} + H(A_s + B_s) + B_{s+1}). \tag{3.23}$$

Finally, separating B_n yields

$$B_s = B_{s+1} \frac{G - GH^2}{1 - HG} + A_s \frac{HG - G^2}{1 - HG} \tag{3.24}$$

$\square$

The interpretation of the theorem is as follows. If there is a wave travelling to the soft boundary from the left-hand side, then it is partially reflected from the boundary (described by T_{ab}) and partially transmitted through the boundary (described by T_{aa}). Likewise, if the wave travels from the opposite side, then the transfer functions T_{ba} and T_{bb} represent the respective waves. Mathematically,

$$X_s(s) = G(s)(1 + T_{\mathrm{ab}}(s))A_{s-1}(s) + T_{\mathrm{bb}}(s)B_{s+1}(s), \tag{3.25}$$
$$X_{s+1}(s) = H(s)(1 + T_{\mathrm{ba}}(s))B_{s+2}(s) + T_{\mathrm{aa}}(s)A_s(s). \tag{3.26}$$

The forced-end boundary is an example of the soft boundary. Substituting $G = 0$ into (3.16) and (3.17) gives $T_{\mathrm{aa}} = H$, $T_{\mathrm{ba}} = -H^2$ and $T_{\mathrm{bb}} = T_{\mathrm{ab}} = 0$.

Theorem 4. *The BTFs describing the hard boundary in the Laplace domain are*

$$T_{\mathrm{AA}} = \frac{A_{h,\mathrm{R}}}{A_{h,\mathrm{L}}} = \frac{(1 + G)(1 - H)}{1 - HG}, \quad T_{\mathrm{BA}} = \frac{A_{h,\mathrm{R}}}{B_{h,\mathrm{R}}} = \frac{H - G}{1 - HG}, \tag{3.27}$$
$$T_{\mathrm{BB}} = \frac{B_{h,\mathrm{L}}}{B_{h,\mathrm{R}}} = \frac{(1 + H)(1 - G)}{1 - HG}, \quad T_{\mathrm{AB}} = \frac{B_{h,\mathrm{L}}}{A_{h,\mathrm{L}}} = \frac{G - H}{1 - HG}, \tag{3.28}$$

where G and H are given by (3.15).

Proof. From (3.3), the output of the agent can be rewritten as

$$X_h(s) = T_{\mathrm{L}}(s)X_{h-1}(s) + T_{\mathrm{R}}(s)X_{h+1}(s), \tag{3.29}$$

where $T_{\mathrm{L}} = M_{\mathrm{f},h}/(1 + M_{\mathrm{f},h} + M_{\mathrm{r},h})$ and $T_{\mathrm{R}} = M_{\mathrm{r},h}/(1 + M_{\mathrm{f},h} + M_{\mathrm{r},h})$. We combine (2.21), (3.13) and (3.14), and obtain

$$X_{h-1} = A_{h-1} + B_{h-1} = G^{-1}A_{h,\mathrm{L}} + GB_{h,\mathrm{L}}, \tag{3.30}$$
$$X_{h+1} = A_{h+1} + B_{h+1} = HA_{h,\mathrm{R}} + H^{-1}B_{h,\mathrm{R}}. \tag{3.31}$$

Substituting (3.30) and (3.31) into (3.29) and using (3.12) for X_h, we have

$$A_{h,\mathrm{L}} + B_{h,\mathrm{L}} = T_{\mathrm{L}}(G^{-1}A_{h,\mathrm{L}} + GB_{h,\mathrm{L}}) + T_{\mathrm{R}}(HA_{h,\mathrm{R}} + H^{-1}B_{h,\mathrm{R}}). \tag{3.32}$$

Rearranging (3.32) with respect to the hard-boundary wave components gives

$$A_{h,\mathrm{L}}(1 - T_{\mathrm{L}}G^{-1}) + B_{h,\mathrm{L}}(1 - T_{\mathrm{L}}G) = B_{h,\mathrm{R}}(T_{\mathrm{R}}H^{-1}) + A_{h,\mathrm{R}}T_{\mathrm{R}}H. \tag{3.33}$$

The four wave components are now reduced to three components by substituting $A_{h,\mathrm{R}} = A_{h,\mathrm{L}} + B_{h,\mathrm{L}} - B_{h,\mathrm{R}}$ into (3.33),

$$B_{h,\mathrm{L}} = B_{h,\mathrm{R}}\frac{T_{\mathrm{R}}H - T_{\mathrm{R}}H^{-1}}{T_{\mathrm{L}}G + T_{\mathrm{R}}H - 1} + A_{h,\mathrm{L}}\frac{1 - T_{\mathrm{L}}G^{-1} - T_{\mathrm{R}}H}{T_{\mathrm{L}}G + T_{\mathrm{R}}H - 1}, \tag{3.34}$$

or, alternatively, by substituting $B_{h,\mathrm{L}} = A_{h,\mathrm{R}} + B_{h,\mathrm{R}} - A_{h,\mathrm{L}}$,

$$A_{h,\mathrm{R}} = A_{h,\mathrm{L}}\frac{T_{\mathrm{L}}G - T_{\mathrm{L}}G^{-1}}{T_{\mathrm{L}}G + T_{\mathrm{R}}H - 1} + B_{h,\mathrm{R}}\frac{1 - T_{\mathrm{L}}G - T_{\mathrm{R}}H^{-1}}{T_{\mathrm{L}}G + T_{\mathrm{R}}H - 1}. \tag{3.35}$$

These formulas can further be simplified by expressing T_{L} and T_{R} in terms of G and H. Specifically, $M_{\mathrm{f},h} = \left(G + G^{-1} - 2\right)^{-1}$ and $M_{\mathrm{r},h} =$

$\left(H + H^{-1} - 2\right)^{-1}$. Substituting them into (3.34) and (3.35) yields

$$B_{h,\mathrm{L}} = B_{h,\mathrm{R}}\frac{(1+H)(1-G)}{1-HG} + A_{h,\mathrm{L}}\frac{G-H}{1-HG}, \tag{3.36}$$

$$A_{h,\mathrm{R}} = A_{h,\mathrm{L}}\frac{(1+G)(1-H)}{1-HG} + B_{h,\mathrm{R}}\frac{H-G}{1-HG}, \tag{3.37}$$

which proves the Theorem. $\qquad\square$

The interpretation of the theorem is as follows. A wave incident from the left side of the hard boundary (described by $A_{h,\mathrm{L}}$) is partially reflected from the boundary (described by T_{AB}) and partially transmitted through the boundary (described by T_{AA}). For the wave incidenting from the opposite side (described by $B_{h,\mathrm{R}}$), the transfer functions are T_{BA} and T_{BB}, respectively. The output of the hard-boundary agent can be expressed in two equivalent ways,

$$X_h = G(1 + T_{\mathrm{AB}})A_{h-1} + HT_{\mathrm{BB}}B_{h+1}, \tag{3.38}$$

$$X_h = GT_{\mathrm{AA}}A_{h-1} + H(1 + T_{\mathrm{BA}})B_{h+1}. \tag{3.39}$$

The free-end boundary from Section 2.3.2 is an example of the soft boundary. In this case $H = 0$, which gives $T_{\mathrm{AA}} = T_{\mathrm{BB}} = G$ and $T_{\mathrm{AB}} = T_{\mathrm{BA}} = 0$.

For the case of identical agents, that is, when $G = H$, Theorems 3 and 4 yield $T_{\mathrm{aa}} = T_{\mathrm{bb}} = G$, $T_{\mathrm{ab}} = T_{\mathrm{ba}} = T_{\mathrm{AB}} = T_{\mathrm{BA}} = 0$ and $T_{\mathrm{AA}} = T_{\mathrm{BB}} = 1$, which is in agreement with (2.21)-(2.23).

3.2.3   Properties of the boundaries

Although the above definitions and physical interpretations of the boundaries are different, they have some common features. For instance, they have bounded DC gains, or there is an inverse-reciprocity relation indicating that T_{aa} is closely related to T_{BB} rather than to T_{AA}, while T_{ab} is related to T_{BA}, and so on. More specifications are as follows.

Corollary 2. *The soft and hard BTFs are related as follows,*

$$T_{\mathrm{aa}}(s) = T_{\mathrm{BB}}(s) + G(s) - 1, \quad T_{\mathrm{ba}}(s) = H(s)T_{\mathrm{AB}}(s), \qquad (3.40)$$
$$T_{\mathrm{bb}}(s) = T_{\mathrm{AA}}(s) + H(s) - 1, \quad T_{\mathrm{ab}}(s) = G(s)T_{\mathrm{BA}}(s), \qquad (3.41)$$
$$T_{\mathrm{AA}}(s) = 1 + T_{\mathrm{AB}}(s), \qquad T_{\mathrm{BB}}(s) = 1 + T_{\mathrm{BA}}(s), \qquad (3.42)$$
$$T_{\mathrm{AA}}(s) + T_{\mathrm{BB}}(s) = 2, \qquad T_{\mathrm{AB}}(s) + T_{\mathrm{BA}}(s) = 0. \qquad (3.43)$$

Proof. By straightforward application of Theorem 3 and Theorem 4. □

The amplitude of the wave that is reflected at or transmitted through the boundary can be approximated by the DC gain of the BTFs. Usually, there is at least one integrator both in the front and rear ATFs allowing the agent to follow the ramp of X_{ref}, which can, for instance, represent that a vehicular platoon travelling with constant velocity. In this case, it holds.

Corollary 3. *If there is at least one integrator in the front ATF and at least one integrator in the rear ATF, then the DC gains of the BTFs are related as follows*

$$\kappa_{\mathrm{aa}} + \kappa_{\mathrm{bb}} = 2, \quad \kappa_{\mathrm{ab}} + \kappa_{\mathrm{ba}} = 0, \qquad (3.44)$$
$$\kappa_{\mathrm{aa}} - \kappa_{\mathrm{ab}} = 1, \quad \kappa_{\mathrm{bb}} - \kappa_{\mathrm{ba}} = 1, \qquad (3.45)$$
$$\kappa_{\mathrm{aa}} = \kappa_{\mathrm{BB}}, \quad \kappa_{\mathrm{ba}} = \kappa_{\mathrm{AB}}, \quad \kappa_{\mathrm{bb}} = \kappa_{\mathrm{AA}}, \quad \kappa_{\mathrm{ab}} = \kappa_{\mathrm{BA}}, \qquad (3.46)$$

where κ_{aa} is the DC gain of T_{aa}, κ_{ab} is the DC gain of T_{ab} etc.

Proof. Under the above assumptions, the DC gain of a WTF is equal to one, i.e. $\lim G(s)_{s \to 0} = 1$ and $\lim H(s)_{s \to 0} = 1$. Then, the proof is a straightforward application of Corollary 2. □

The particular values of κ_{aa} and κ_{bb} are given by the following lemma.

Lemma 7. *Let both $M_{\mathrm{r},n}$ and $M_{\mathrm{f},n+1}$ have at least one integrator. If $M_{\mathrm{r},n}$ and $M_{\mathrm{f},n+1}$ have the same number of integrators, then the DC gains of the*

soft BTFs are

$$\kappa_{\text{aa}} = \frac{2}{\sqrt{\dfrac{n_{1,0}d_{2,0}}{n_{2,0}d_{1,0}}} + 1}, \quad \kappa_{\text{bb}} = \frac{2}{\sqrt{\dfrac{n_{2,0}d_{1,0}}{n_{1,0}d_{2,0}}} + 1}, \tag{3.47}$$

where $n_{1,0}/d_{1,0} = \lim_{s\to0} s^{k_1} M_{\text{r},n}$, $n_{2,0}/d_{2,0} = \lim_{s\to0} s^{k_2} M_{\text{f},n+1}$, *and* k_1 *and* k_2 *is the number of integrators in* $M_{\text{r},n}$ *and* $M_{\text{f},n+1}$, *respectively. If* $M_{\text{r},n}$ *has more integrators than* $M_{\text{f},n+1}$, *then*

$$\kappa_{\text{aa}} = 0, \quad \kappa_{\text{bb}} = 2. \tag{3.48}$$

If $M_{\text{f},n+1}$ *has more integrators than* $M_{\text{r},n}$, *then*

$$\kappa_{\text{aa}} = 2, \quad \kappa_{\text{bb}} = 0. \tag{3.49}$$

Proof. Let us denote $\alpha_1 = 2 + 1/M_{\text{r},n} = 2 + d_1/n_1$ and $\alpha_2 = 2 + 1/M_{\text{f},n+1} = 2 + d_2/n_2$. We will begin with deriving the DC gain κ_{aa} of the T_{aa} transfer function,

$$\kappa_{\text{aa}} = \lim_{s\to0} T_{\text{aa}} = \lim_{s\to0} \frac{H - HG^2}{1 - HG} = \lim_{s\to0} \frac{1 - G^2}{H^{-1} - G} = \frac{0}{0}, \tag{3.50}$$

since $\lim_{s\to0} G = \lim_{s\to0} H = 1$ for at least one integrator in $M_{\text{r},n}$ and $M_{\text{f},n+1}$. Applying l'Hopital's rule to (3.50) gives

$$\kappa_{\text{aa}} = \lim_{s\to0} \frac{2G}{H^{-2}H'(G')^{-1} + 1} = \lim_{s\to0} \frac{2}{H'(G')^{-1} + 1}, \tag{3.51}$$

where the symbol $'$ denotes the differentiation with respect to variable s. First, the differentiation of (3.18) yields

$$G' = \frac{1}{2}\alpha_1' - \frac{1}{2}\frac{\alpha_1\alpha_1'}{\sqrt{\alpha_1^2 - 4}}. \tag{3.52}$$

The individual contributions to $\lim_{s \to 0} G'$ are

$$\lim_{s \to 0} \alpha_1' = \lim_{s \to 0} \frac{d_1' n_1 - d_1 n_1'}{n_1^2} = \begin{cases} \in \mathbb{R}, & \text{if } k_1 = 1, \\ 0, & \text{if } k_1 > 1, \end{cases} \tag{3.53}$$

and

$$\lim_{s \to 0} \frac{\alpha_1'}{\sqrt{\alpha_1^2 - 4}} = \lim_{s \to 0} \frac{d_1' n_1 - d_1 n_1'}{n_1 \sqrt{d_1^2 + 4 d_1 n_1}}$$
$$= \lim_{s \to 0} \frac{s^{(k_1/2)} \left(s^{(k_1/2)-1} k_1 d_{1,0} n_1 - s^{(k_1/2)} d_{1,0} n_1' \right)}{s^{(k_1/2)} n_1 \sqrt{s^{k_1} d_{1,0}^2 + 4 d_{1,0} n_1}}$$
$$= \lim_{s \to 0} \frac{\left(s^{(k_1/2)-1} k_1 d_{1,0} n_1 \right)}{n_1 \sqrt{4 d_{1,0} n_1}} = \lim_{s \to 0} k_1 s^{(k_1/2)-1} \frac{1}{2} \sqrt{\frac{d_{1,0}}{n_{1,0}}}, \tag{3.54}$$

where $d_{1,0} = \lim_{s \to 0} s^{-k_1} d_1$ and $n_{1,0} = \lim_{s \to 0} n_1$. Moreover $\lim_{s \to 0} \alpha_1 = 2$. Similarly, $\lim_{s \to 0} H'$ can be evaluated. Then

$$\lim_{s \to 0} \frac{H'}{G'} = \lim_{s \to 0} s^{(k_2 - k_1)/2} \frac{k_2}{k_1} \sqrt{\frac{n_{1,0} d_{2,0}}{n_{2,0} d_{1,0}}}, \tag{3.55}$$

where $d_{2,0} = \lim_{s \to 0} s^{-k_2} d_2$ and $n_{2,0} = \lim_{s \to 0} n_2$. Finally, substituting (3.55) into (3.51) yields

$$\kappa_{\mathrm{aa}} = \lim_{s \to 0} \frac{2}{s^{(k_2 - k_1)/2} \dfrac{k_2}{k_1} \sqrt{\dfrac{n_{1,0} d_{2,0}}{n_{2,0} d_{1,0}}} + 1}. \tag{3.56}$$

Therefore, if $M_{\mathrm{r},n}$ and $M_{\mathrm{f},n+1}$ have the same number of integrators ($k_1 = k_2$), then (3.56) simplifies to (3.47). If $k_2 > k_1$, i.e., $M_{\mathrm{f},n+1}$ have more integrators than $M_{\mathrm{r},n}$, then (3.55) converges to zero and $\kappa_{\mathrm{aa}} = 2$. In the opposite case, (3.55) diverges and $\kappa_{\mathrm{aa}} = 0$. The DC gain $\kappa_{\mathrm{bb}} = 2 - \kappa_{\mathrm{aa}}$ is from (3.44). $\qquad \square$

Corollary 4. *If there is at least one integrator in the front ATF and at least one integrator in the rear ATF, then the DC gains of the BTFs are*

bounded as

$$-1 \leq \kappa_{\mathrm{ab}}, \kappa_{\mathrm{ba}}, \kappa_{\mathrm{AB}}, \kappa_{\mathrm{BA}} \leq 1, \tag{3.57}$$

$$0 \leq \kappa_{\mathrm{aa}}, \kappa_{\mathrm{bb}}, \kappa_{\mathrm{AA}}, \kappa_{\mathrm{BB}} \leq 2. \tag{3.58}$$

Proof. The soft-boundary DC gains are treated by Lemma 7 and Corollary 3. The hard-boundary DC gains can be calculated using Corollary 3. □

3.3 Controllers for the boundaries

We now design a feedback controller compensating the fact that the agents are not identical. The motivation is to prevent the undesired reflection of waves and thus to shorten the settling time.

3.3.1 The soft boundary controller

A soft-boundary controller can be designed for various purposes, for instance, to prevent or modify wave's transmission through the boundary. We now design an absorbing controller that prevents the reflection of a wave from the soft boundary. The derivation will be presented only for the left side of the boundary since the derivation for its right side is analogous.

First, we add input $W_{\mathrm{r},s}$ to the sth agent. By the combination of (3.25) and (3.9), we get

$$X_s = (1 + T_{\mathrm{ab}})A_s + T_{\mathrm{bb}}B_{s+1} + T_{\mathrm{r},n}(1 + T_{\mathrm{ab}})W_{\mathrm{r},s}. \tag{3.59}$$

We want to design a controller that prevents the reflection of the wave travelling to the soft boundary from the left, which is described by term $T_{\mathrm{ab}}A_s$. Therefore, we set $W_{\mathrm{r},s}(s) = F_{\mathrm{f},\mathrm{S}}(s)A_s(s)$, where $F_{\mathrm{f},\mathrm{S}}(s)$ is a transfer function of a controller that prevents the reflection of the wave. To

prevent the reflection, we eliminate term $T_{\mathrm{ab}}A_s$ by requiring

$$T_{\mathrm{ab}}(s)A_s(s) + T_{\mathrm{r},n}(s)(1 + T_{\mathrm{ab}}(s))F_{\mathrm{f,S}}(s)A_s(s) = 0, \tag{3.60}$$

which is the constraint for the controller,

$$F_{\mathrm{f,S}}(s) = \frac{-T_{\mathrm{ab}}(s)}{T_{\mathrm{r},n}(s)(1 + T_{\mathrm{ab}}(s))}. \tag{3.61}$$

Substituting for $T_{\mathrm{ab}}(s)$ from (3.17) and for $T_{\mathrm{r},n}(s)$ from (3.9), the 'absorbing' transfer function has a simple form

$$F_{\mathrm{f,S}}(s) = G(s) - H(s). \tag{3.62}$$

It remains to specify A_s, which represents a wave incident on the soft boundary from the left. By (2.21), (2.22) and (2.23), we have

$$A_s(s) = G(X_{s-1} - B_{s-1}) = GX_{s-1} - G^2(X_s - A_s), \tag{3.63}$$

which leads to

$$A_s(s) = \frac{G(s)}{1 - G^2(s)}X_{s-1}(s) - \frac{G^2(s)}{1 - G^2(s)}X_s(s). \tag{3.64}$$

Therefore, the left-side-absorbing control law $C_{\mathrm{L,S}}$ is described by the consequential application of the above equations as

$$
\begin{aligned}
C_{\mathrm{L,S}} &= M_{\mathrm{r},s}W_{\mathrm{r},s} = M_{\mathrm{r},s}F_{\mathrm{f,S}}A_s \\
&= M_{\mathrm{r},s}\,(G - H)\,\frac{G}{1 - G^2}\,(X_{s-1} - GX_s)\,.
\end{aligned} \tag{3.65}
$$

The model of sth agent with implemented left-side absorbing controller is shown in Fig. 3.3.

By modifying (3.59), the output of the sth agent with the left- and right-
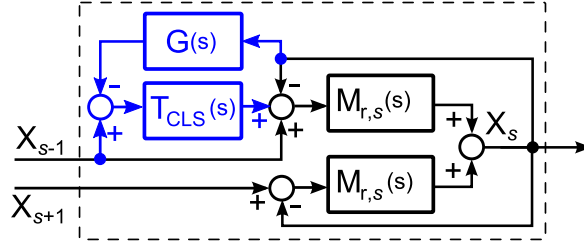
Figure 3.3: The model of sth agent with the left-side absorbing controller (highlighted in blue), where $T_{\mathrm{CLS}} = G(s)(G(s) - H(s))/(1 - G^2(s))$ from (3.65). The front and rear ATFs are identical since, for now we assume only one soft boundary in the system as at the top of Fig. 3.2.

side absorbing controllers is

$$X_s = (1 + T_{\mathrm{ab}})A_s + T_{\mathrm{bb}}B_{s+1} + F_{\mathrm{f,S}}T_{\mathrm{r},n}(1 + T_{\mathrm{ab}})A_s$$
$$+ T_{\mathrm{bb}}F_{\mathrm{r,S}}T_{\mathrm{f},n}B_{s+1} = GA_{s-1} + GB_{s+1}, \tag{3.66}$$

where $F_{\mathrm{r,S}}(s)$ is equivalent to $F_{\mathrm{f,S}}(s)$ for the right side of the soft boundary. Likewise, the output of the $(s+1)$th agent with the absorbing controllers is

$$X_{s+1}(s) = H(s)A_s(s) + H(s)B_{s+2}(s). \tag{3.67}$$

The results can be summarized in the following theorem.

Theorem 5. *The control law preventing any wave to be reflected from the soft boundary is described in the Laplace domain as*

$$X_s = M_{\mathrm{r},s}(X_{s-1} - 2X_s + X_{s+1}) + C_{\mathrm{L,S}}, \tag{3.68}$$
$$X_{s+1} = M_{\mathrm{f},s+1}(X_s - 2X_{s+1} + X_{s+2}) + C_{\mathrm{R,S}}, \tag{3.69}$$

where

$$C_{\mathrm{L,S}} = M_{\mathrm{r},s}\frac{G(G-H)}{1-G^2}\left(X_{s-1}-GX_s\right), \tag{3.70}$$

$$C_{\mathrm{R,S}} = M_{\mathrm{f},s+1}\frac{H(H-G)}{1-H^2}\left(X_{s+1}-HX_s\right). \tag{3.71}$$

We note that the control law described in Theorem 5 is the only way to fully absorb a wave since term $T_{\mathrm{ab}}A_s$ in (3.59) is cancelled by the choice of $W_{\mathrm{r},s}(s) = F_{\mathrm{f,S}}(s)A_s(s)$.

3.3.2 The hard boundary controller

Controlling the hard boundary is similar to that of the soft boundary in Section 3.3.1. Here, we only provide a brief description of the absorbing-controller design.

The output of the hth agent from (3.38) controlled with additional input $W_{\mathrm{f},h}(s)$ is

$$X_h = (1+T_{\mathrm{AB}})A_{h,\mathrm{L}} + T_{\mathrm{BB}}B_{h,\mathrm{R}} + T_{\mathrm{f},n}W_{\mathrm{f},h}, \tag{3.72}$$

where $W_{\mathrm{f},h}(s) = F_{\mathrm{f,H}}(s)A_{h,\mathrm{L}}(s)$ and $F_{\mathrm{f,H}}(s)$ is a transfer function of a controller that prevents the reflection of a wave. To prevent the reflection of the wave travelling towards the hard boundary from the left, we set $T_{\mathrm{AB}}A_{h,\mathrm{L}} = -F_{\mathrm{f,H}}T_{\mathrm{f},n}W_{\mathrm{f},h}$. Hence,

$$F_{\mathrm{f,H}}(s) = -\frac{T_{\mathrm{AB}}(s)}{T_{\mathrm{f},n}(s)} = \frac{(H(s)-G(s))(1-G(s))}{G(s)(1-H(s))}. \tag{3.73}$$

The $A_{h,\mathrm{L}}$ term represents the wave travelling towards the hard boundary from the left, which is again computed by (3.64),

$$A_{h,\mathrm{L}}(s) = \frac{G(s)}{1-G^2(s)}X_{h-1}(s) - \frac{G^2(s)}{1-G^2(s)}X_h(s). \tag{3.74}$$

79

The left-side-absorbing control law is then

$$C_{\mathrm{L,H}} = M_{\mathrm{f},h} F_{\mathrm{f,H}} A_{h,\mathrm{L}} = M_{\mathrm{f},h} \frac{H - G}{(1+G)(1-H)}(X_{h-1} - GX_h). \quad (3.75)$$

The design of the right-side absorbing controller is similar. When both controllers are implemented on the hth agent, we get

$$X_h(s) = A_{h,\mathrm{L}}(s) + B_{h,\mathrm{R}}(s) = G(s)A_{h-1}(s) + H(s)B_{h+1}(s), \quad (3.76)$$

where (3.42) have been considered.

Combining (3.76) and (3.12) gives $A_{h,\mathrm{L}} = A_{h,\mathrm{R}}$ and $B_{h,\mathrm{L}} = B_{h,\mathrm{R}}$. In words, the hard boundary between the wave components indexed by L and R is removed at the hth agent and the wave transmits through the agent without being reflected.

The results can be summarized in the following theorem.

Theorem 6. *The control law that prevents any wave to be reflected from the hard boundary is described in the Laplace domain as*

$$X_h = M_{\mathrm{f},h}(X_{h-1} + X_h) + M_{\mathrm{r},h}(X_{h+1} - X_h) + C_{\mathrm{L,H}} + C_{\mathrm{R,H}}, \quad (3.77)$$

where

$$C_{\mathrm{L,H}} = M_{\mathrm{f},h}\frac{H - G}{(1+G)(1-H)}(X_{h-1} - GX_h), \qquad\qquad (3.78)$$

$$C_{\mathrm{R,H}} = M_{\mathrm{r},h}\frac{G - H}{(1+H)(1-G)}(X_{h+1} - HX_h). \qquad\qquad (3.79)$$

By comparison of Theorems 5 and 6 we can see that we need to implement the wave absorber on two agents for the soft boundary but only on one agent for the hard boundary.

3.3.3 Stability of the controllers

The stability of the proposed controllers is treated by the following theorem.

Theorem 7. *If the WTFs are asymptotically stable, then the multi-agent system with the path-graph topology and the control law from Theorem 5 or Theorem 6 is asymptotically stable. Furthermore, the control laws and the wave absorbers, located on the first or rear-end agent make the multi-agent system L_2 string stable.*

Proof. In this proof, we assume that there is only one soft boundary in a multi-agent system. However, the proof for the case with multiple soft and/or hard boundaries can be carried out analogously. We consider a multi-agent system with a path-graph topology with $M_{\mathrm{f},i} = M_{\mathrm{r},i}$, $M_{\mathrm{f},j} = M_{\mathrm{r},j}$, where $i = 1, 2, ..., m$ and $j = m+1, m+2, ..., k$. Therefore, there is a soft boundary between agents indexed by m and $m+1$.

First, we prove the theorem for the case with a wave absorber only on the first agent. If there is a wave absorber implemented on the first agent, then the combination of (2.22), (2.23) (3.66) and (3.67) gives

$$\frac{X_p(s)}{X_{\mathrm{ref}}(s)} = G^p(s) + G^{2m+1-p}(s)H^{2k}(s), \text{ if } p \leq m, \tag{3.80}$$

$$\frac{X_p(s)}{X_{\mathrm{ref}}(s)} = G^m(s)H^{p-m}(s) + G^m(s)H^{2k+1+m-p}(s), \text{ if } p > m. \tag{3.81}$$

In the alternative case of the wave absorbers implemented either on the rear-end agent, or on both the first and the rear-end agents, the output of the pth agent is described by

$$\frac{X_p(s)}{X_{\mathrm{ref}}(s)} = G^p(s), \text{ if } p \leq m, \tag{3.82}$$

$$\frac{X_p(s)}{X_{\mathrm{ref}}(s)} = G^m(s)H^{p-m}(s), \text{ if } p > m. \tag{3.83}$$

Since G and H are asymptotically stable, and $||G||_\infty \le 1$ and $||H||_\infty \le 1$, then (3.80)-(3.83) are asymptotically stable too and have the H_∞ norm limited regardless of the number of agents in the system. In view of Definition 2, we see that these two systems are L_2 string stable.

Now, we prove the theorem for the case with no wave absorber on the first or rear-end agents. First, we show a way to find the transfer function from X_{ref} to X_1 for the system with $m = 3$ and $k = 5$. In this case, $A_1 = GX_{\text{ref}} - G^7 H^{10} A_1$ and $B_1 = G^6 H^{10} X_{\text{ref}} - G^7 H^{10} B_1$, hence

$$\frac{X_1(s)}{X_{\text{ref}}(s)} = \frac{A_1(s) + B_1(s)}{X_{\text{ref}}(s)} = \frac{G(s) + G^6(s)H^{10}(s)}{1 + G^7(s)H^{10}(s)}. \tag{3.84}$$

Similarly,

$$\frac{X_2(s)}{X_{\text{ref}}(s)} = \frac{G^2(s) + G^5(s)H^{10}(s)}{1 + G^7(s)H^{10}(s)}, \tag{3.85}$$

and so on. For the pth agent, we have

$$\frac{X_p(s)}{X_{\text{ref}}(s)} = \frac{G^p(s) + G^{2m+1-p}(s)H^{2k}(s)}{1 + G^{2m+1}(s)H^{2k}(s)}, \text{ if } p \le m, \tag{3.86}$$

$$\frac{X_p(s)}{X_{\text{ref}}(s)} = \frac{G^m(s)H^{p-m}(s) + G^m(s)H^{k+2m+3-p}(s)}{1 + G^{2m+1}(s)H^{2k}(s)}, \text{ if } p > m. \tag{3.87}$$

Note that the transfer functions between two arbitrary agents can be expressed similarly.

Due to (2.24), we have $M/(1+2M) = G/(1+G^2)$. The Nyquist criterion of stability states that if $M/(1 + \lambda M)$ is stable for $\lambda \in (0, 4\rangle$, and if there are neither CRHP poles nor CRHP zeros in $M(s)$, then the Nyquist curve of $M(s)$ does not encircle the point $[-1/4, 0]$. Hence, $M(s)$ does not intersect the interval $(-\infty, -1/4\rangle$. Therefore, if (2.74) holds, then $M/(1 + 2M)$ is asymptotically stable.

In view of the Nyquist criterion of stability, we can say that, if $M/(1+2M)$ is stable, that is, if $G/(1+G^2)$ is stable, and if $||G||_\infty \le 1$ and $||H||_\infty \le 1$,

then the transfer function

$$\frac{G(s)}{1 + G^2(s)G^{q_1}(s)H^{q_2}(s)},\tag{3.88}$$

is asymptotically stable for $q_1, q_2 \in \mathbb{N}$. Furthermore, since G and H are asymptotically stable, then the transfer function

$$\frac{G(s)G^{q_3}(s)H^{q_4}(s)}{1 + G^2(s)G^{q_1}(s)H^{q_2}(s)},\tag{3.89}$$

is asymptotically stable for $q_3, q_4 \in \mathbb{N}$. Comparing (3.89) with (3.86) and (3.87), we can say that the transfer function between two arbitrary agents in a system with no wave absorber on the first or rear-end agents and with the control law given by Theorem 5 is asymptotically stable.

The proof of the control law from Theorem 6 can be carried out analogously. The only difference is in different powers of G and H in (3.80)-(3.83), (3.86) and (3.87), which does not affect neither the asymptotic nor string stability.

□

3.4 Numerical simulations of the soft boundary

The numerical simulations are carried out with *WaveBox*, which is a set of functions and examples in MATLAB that numerically approximates WTFs and BTFs. The *WaveBox* also contains a set of examples that show the effect of boundaries and absorbers. Some of the examples are presented in this section. The *WaveBox* was written by the author of the thesis and is available at [Martinec (2015)].

3.4.1   Soft boundary performance

The numerical simulations are carried out for a system with 8 agents described by

$$M_{\mathrm{f},i}(s) = M_{\mathrm{r},i}(s) = \frac{4s+4}{s^2(s+4)}, \quad i = 1,2,3,4, \tag{3.90}$$

$$M_{\mathrm{f},j}(s) = M_{\mathrm{r},j}(s) = \frac{s+1}{s^2(s+3)}, \quad j = 5,6,7,8, \tag{3.91}$$

which represents a double integrator agent with a linear model of friction controlled by a PI controller. Therefore, we consider a multi-agent system with 8 agents and a soft boundary located between the 4th and 5th agent.

The effect of the soft boundary is demonstrated in Fig. 3.4, where the wave-absorbing controllers on the first and rear-end agents are additionally implemented.

The performance of individual control strategies are shown in Fig. 3.5. Comparing the bottom-left and top-left panels, we can see that the soft-boundary absorber does not shorten the settling time if it is not combined with other absorbers on the first or rear-end agents. In the case of the absorber on the first agent (top-middle panel), the wave keeps reflecting between the soft boundary and the non-absorbing rear-end agent which prolongs the transient. The implementation of the soft-boundary absorber (bottom-middle panel) shortens the transient since it prevents the wave from being reflected back and forth. The absorbers implemented on both the first and rear-end agents (top-right panel) cause a change of the steady-state value, as predicted by Lemma 7. There are two possible ways to obtain a desired steady-state: a) overcompensate the input signal (see [Martinec et al. (2014d)]), or b) implement the soft-boundary absorber (bottom-right panel).

Fig. 3.6 shows the comparison of the inputs to the fourth agent for (i) the multi-agent system with 8 identical agents (blue solid line), where each agent is described by (3.90), (ii) the multi-agent system with non-identical agents described by (3.90)-(3.91) without the soft-boundary ab-
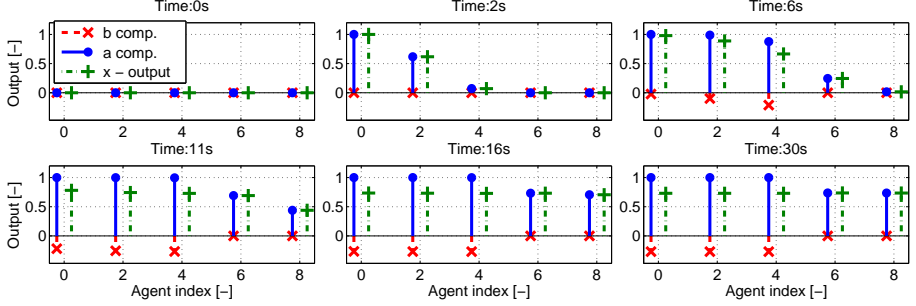
Figure 3.4: Simulation of the wave propagating in a multi-agent system with the path-graph topology defined by (3.90)-(3.91). At the beginning, $t = 0^+$ s, outputs of all agents are 0 except $x_{\mathrm{ref}}(t)$, which is changed from 0 to 1. At intermediate times, the wave travels to the soft boundary, where it is transmitted and attenuated by factor κ_{aa} and reflected by factor κ_{ab}. As the wave propagates back to the fist agent, it forces the first four agents to change their output by κ_{ab} (negative value in this case). The waves are absorbed on 1st and 8th agents by the wave-absorbing controllers. The blue circles and red crosses represent $a(t)$ and $b(t)$ components of the wave, respectively. The green plus signs stand for the outputs of the agents. The 0th agent is the input to the system from (2.53), i.e. $X_0(s) = W_{\mathrm{f},1}(s)$, $A_0(s) = X_{\mathrm{ref}}(s)$ and $B_0(s) = GB_1(s)$.

sorber (green dashed line), and (iii) the multi-agent system as in (ii) but with the soft-boundary absorber (red pluses). The input for (i) and (ii) is described by $V_{\mathrm{I}}(s) = (X_{s-1}(s) + X_{s+1}(s) - 2X_s(s))$, that means the output error. The input for (iii) is $V_{\mathrm{III}}(s) = V_{\mathrm{I}}(s) + C_{\mathrm{L,S}}(s)/M_{\mathrm{r},s}(s)$, that means the same as for (i) and (ii) plus the control law from (3.70). The wave absorbers on both the first and rear-end agents are implemented in all cases. We can see that the inputs to the fourth agent are the same for cases (i) and (iii). Therefore, the output of the wave-absorber is the difference between (ii) and (iii), which shows that the output of the controller is feasible.
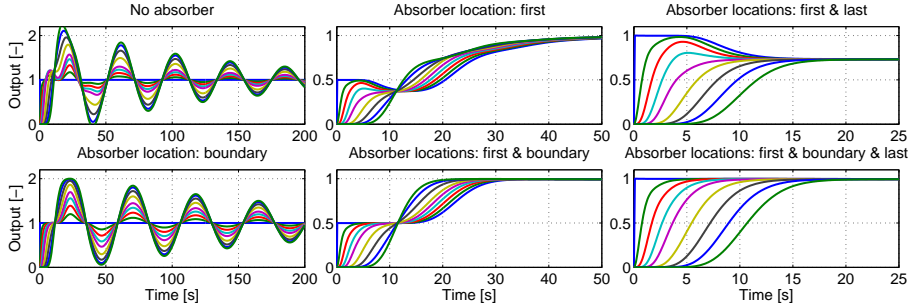
Figure 3.5: The performance comparison of individual control strategies for a multi-agent system with the soft boundary. The multi-agent system is defined by (3.90)-(3.91) with $x_{\mathrm{ref}}(0) = 1$ and $x_i(0) = 0$ for $i = 1, 2, ..., N$. The step responses of six individual control strategies are compared. The top-left: the system with no absorber; top-middle: the system with the absorber implemented on the first agent; top-right: the system with the absorbers implemented on the first and rear-end agents. In the bottom panels, the soft-boundary absorber between the agents 4 and 5 is additionally implemented.

3.4.2   Local effect of the DC gains

A local effect of the BTF DC gains is demonstrated in Fig. 3.7 for first 120 seconds of the step response of a multi-agent system with a path-graph topology described by

$$M_{\mathrm{f},i}(s) = M_{\mathrm{r},i}(s) = \frac{4s + 4}{s^2(s + 4)}, \quad i = 1, 2, ..., 40, \tag{3.92}$$

$$M_{\mathrm{f},j}(s) = M_{\mathrm{r},j}(s) = \frac{s + k_{\mathrm{p}}}{s^2(s + 3)}, \quad j = 41, 42, ..., 80. \tag{3.93}$$

Applying (2.21)-(2.23) and (3.26), the output of the 41st agent is

$$X_{41}(s) = T_{\mathrm{aa}}(s)A_{40}(s) + (1 + T_{\mathrm{ba}}(s))B_{41}(s), \tag{3.94}$$

where $B_{41}(s)$ is the wave that is transmitted through the boundary, travels from the 41st agent to the 80th agent, is reflected and travels back to the 41st agent, hence, $B_{41}(s) = T_{\mathrm{aa}}(s)H^{79}(s)A_{40}(s)$. It takes certain time for
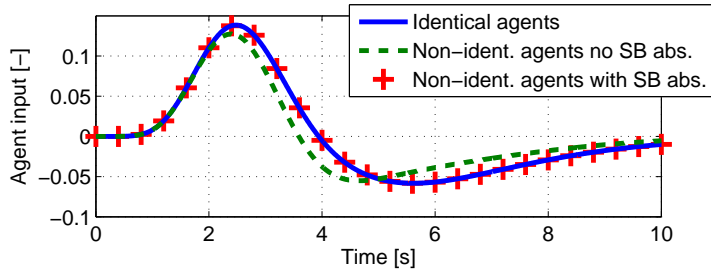
Figure 3.6: The comparison of the inputs to the fourth agent for three different multi-agent systems. The label 'SB abs.' stands for the soft-boundary absorber described by (3.65).

the wave to propagate, therefore, we can approximate the output $X_{41}(s)$ as

$$X_{41}(s) \approx T_{\mathrm{aa}}(s)A_{40}(s). \tag{3.95}$$

The approximation gives the exact results in the time-domain until the wave returns back to the 41st agent, which happens at about $t = 110\,s$.

We can see that it takes approximately 25 seconds (from $t = 30\,s$ to $t = 55\,s$) for the wave to settle. After that, the output can be approximated by the DC gain of $T_{\mathrm{aa}}(s)$ since the input is the unit-step signal of $X_{\mathrm{ref}}(s)$ and the steady-state value of the wave is not changed as it travels to the 40th agent. Hence,

$$x_{41}(t) \approx \kappa_{\mathrm{aa}}. \tag{3.96}$$

This example shows that the travelling wave approach allows us to approximate the output and how it is changed when we change the coefficients of the system, which is k_{p} in this case. The most important feature of the approximation is that it does not consider interactions among other agents. In other words, there can be an arbitrarily number of agents with an arbitrarily complex interaction topology after the 41st agent.
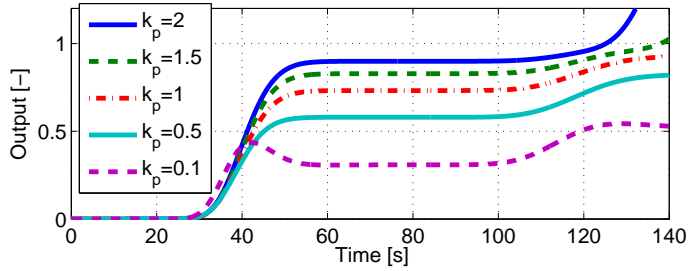
Figure 3.7: The numerical simulations of multi-agent system described by (3.92)-(3.93) for different values of k_p. The output of the 41$^\mathrm{st}$ agent is shown.

3.5   A combination of soft and hard boundaries

The soft and hard boundaries are two special cases of system boundaries. The two boundaries can be combined to form any type of complex boundary. The idea is to represent the transfer function of a complex boundary in terms of the soft- and hard-boundary BTFs. The combination of the two boundaries requires to relax the assumptions for (3.13) and (3.14), that is, there is no other boundary next to the hard or soft boundary.
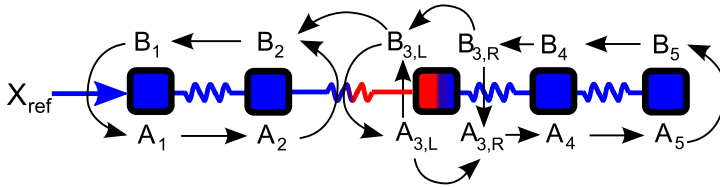
Figure 3.8: Scheme of the complex boundary between 2nd and 3rd agents composed of the soft and hard boundaries next to each other in a multi-agent system described by (3.97)-(3.98). The blue arrow in front of the first agent represents the input to the system.

The approach is demonstrated for the complex boundary in the multi-

agent system, shown in Fig. 3.8, and described by

$$M_{\mathrm{f},i}(s) = M_{\mathrm{r},i}(s) = \frac{4s+4}{s^2(s+4)}, \quad i = 1, 2, 4, 5, \tag{3.97}$$

$$M_{\mathrm{f},3}(s) = \frac{s+1}{s^2(s+3)}, \quad M_{\mathrm{r},3}(s) = \frac{4s+4}{s^2(s+4)}. \tag{3.98}$$

The boundary is formed by the combination of the soft boundary located between the agents indexed by 2 and 3 and the hard boundary located at the 3rd agent. This configuration violates the boundary conditions in (3.13) since now the wave travelling to $A_{3,\mathrm{L}}$ and the wave travelling from $B_{3,\mathrm{L}}$ transmit through the soft boundary. In view of Theorem 3, we have

$$A_{3,\mathrm{L}}(s) = T_{\mathrm{aa}}(s)A_2(s) + T_{\mathrm{ba}}(s)B_{3,\mathrm{L}}(s), \tag{3.99}$$

$$B_2(s) = T_{\mathrm{ab}}(s)A_2(s) + T_{\mathrm{bb}}(s)B_{3,\mathrm{L}}(s). \tag{3.100}$$

The second part of the complex boundary is composed of the hard boundary. Hence, by Theorem 4, we have

$$A_{3,\mathrm{R}}(s) = \overline{T_{\mathrm{AA}}}(s)A_{3,\mathrm{L}}(s) + \overline{T_{\mathrm{BA}}}(s)B_{3,\mathrm{R}}(s), \tag{3.101}$$

$$B_{3,\mathrm{L}}(s) = \overline{T_{\mathrm{AB}}}(s)A_{3,\mathrm{L}}(s) + \overline{T_{\mathrm{BB}}}(s)B_{3,\mathrm{R}}(s), \tag{3.102}$$

where the overlined transfer functions are different from those in (3.27) and (3.28). The original transfer function T_{AA} describes the wave propagating from blue to red agent, while $\overline{T_{\mathrm{AA}}}$ describes the wave propagating in the opposite direction. Due to the same reasoning, $\overline{T_{\mathrm{AA}}} = T_{\mathrm{BB}}$, $\overline{T_{\mathrm{BB}}} = T_{\mathrm{AA}}$, $\overline{T_{\mathrm{AB}}} = T_{\mathrm{BA}}$ and $\overline{T_{\mathrm{BA}}} = T_{\mathrm{AB}}$ for this complex boundary.

The same procedure can be applied to the wave-absorbing controller. They can be combined to absorb the wave reflecting from boundaries of various complexity.

The independent validation of the WTF approach is shown in Fig. 3.9, where the results of the WTF approach is compared with the simulation by the state-space approach. We can see that the two results are identical. Although the validation is based on numerical simulation, we can validate it also analytically by finding the transfer function from $X_{\mathrm{ref}}(s)$ to $(A_2(s) +$

$B_2(s)$). This transfer function is identical to the rational transfer function obtained by the state-space approach using (3.97)-(3.98).
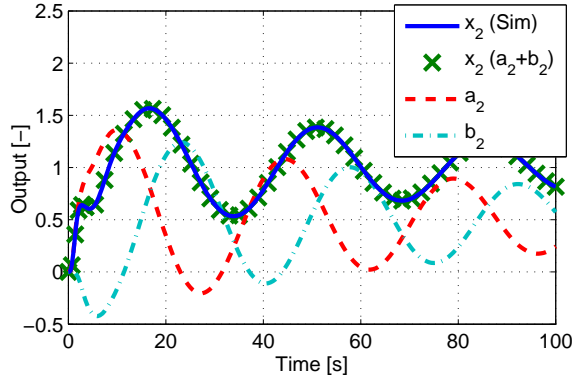

Figure 3.9: The comparison of the outputs of the 2nd agent simulated by the state-space approach using (3.97)-(3.98) (solid line) and that computed by the WTF approach using (3.99)-(3.102). The response to the step change of $x_{\mathrm{ref}}(t)$ is shown.

3.6   Conclusions

This chapter introduces a local approach to a multi-agent system with a path-graph interaction topology and non-identical agents agents. It mathematically describes two basic types of boundaries in a multi-agent system with non-identical agents and their effect on the waves travelling in the system. The wave description allows us to design a feedback controller to compensate the undesired effect of the boundaries, which shortens the settling time of the multi-agent system. Moreover, such a controller makes the multi-agent system string stable provided that the system is equipped with at least one wave absorber on the first or rear-end agents.

3.7 Appendix to the chapter

3.7.1 Approximation of the Boundary Transfer Functions

The soft and hard BTFs (3.16), (3.17), (3.27) and (3.28) are composed of two different irrational WTFs. Since to find an analytical impulse response to the irrational BTFs is usually difficult, it is convenient to construct an approximation of BTF impulse responses. There are at least two ways to do it, both are based on the approximations of $G(s)$ and $H(s)$.

First, the BTFs are approximated by a linear combination of rational approximations of $G(s)$ and $H(s)$ in the Laplace domain. To find the impulse response of a rational-function approximation is a routine procedure for the inverse-Laplace-transform solvers. However, depending on the oscillatory character of the system, only the first few seconds of the approximate impulse response are usually reliable. They are followed by numerical instabilities due to a high-order approximation of the transfer function and the limited precision of computational software.
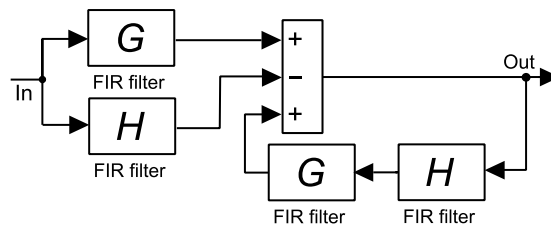

Figure 3.10: Feedback connection for approximating $T_{\mathrm{AB}}(s)$.

Second, a numerically more reliable way is to use approximated impulse responses of $G(s)$ and $H(s)$ in a feedback connection. For instance, the impulse response of $T_{\mathrm{AB}} = (G - H)/(1 - HG)$ is approximated by the feedback connection shown in Fig. 3.10.

3.7.2 Overview of the DC gains – Table 3.1

Table 3.1: The overview of the DC gains of BTFs ($\kappa_G = \lim_{s\to 0} G(s)$ and $\kappa_H = \lim_{s\to 0} H(s)$).

	A derivator in the front ATF ($\kappa_G = 0$)		No derivator nor integrator in the front ATF ($-1 < \kappa_G < 1$)		An integrator in the front ATF ($\kappa_G = 1$)	
A derivator in the rear ATF ($\kappa_H = 0$)	$\kappa_{aa}=0$ $\kappa_{AA}=1$ $\kappa_{ab}=0$ $\kappa_{AB}=0$	$\kappa_{bb}=0$ $\kappa_{BB}=1$ $\kappa_{ba}=0$ $\kappa_{BA}=0$	$\kappa_{aa}=0$ $\kappa_{AA}=1+\kappa_G$ $\kappa_{ab}=-\kappa_G^2$ $\kappa_{AB}=\kappa_G$	$\kappa_{bb}=\kappa_G$ $\kappa_{BB}=1-\kappa_G$ $\kappa_{ba}=0$ $\kappa_{BA}=-\kappa_G$	$\kappa_{aa}=0$ $\kappa_{AA}=2$ $\kappa_{ab}=-1$ $\kappa_{AB}=1$	$\kappa_{bb}=1$ $\kappa_{BB}=0$ $\kappa_{ba}=0$ $\kappa_{BA}=-1$
No derivator nor integrator in the rear ATF ($-1 < \kappa_H < 1$)	$\kappa_{aa}=\kappa_H$ $\kappa_{AA}=1-\kappa_H$ $\kappa_{ab}=0$ $\kappa_{AB}=-\kappa_H$	$\kappa_{bb}=0$ $\kappa_{BB}=1+\kappa_H$ $\kappa_{ba}=-\kappa_H^2$ $\kappa_{BA}=\kappa_H$	$-2 < \kappa_{aa},\kappa_{bb} < 2$ $0 < \kappa_{AA},\kappa_{BB} < 2$ $-1 < \kappa_{ab},\kappa_{ba} < 1$ $-1 < \kappa_{AB},\kappa_{BA} < 1$		$\kappa_{aa}=0$ $\kappa_{AA}=2$ $\kappa_{ab}=-1$ $\kappa_{AB}=1$	$\kappa_{bb}=1+\kappa_H$ $\kappa_{BB}=0$ $\kappa_{ba}=\kappa_H$ $\kappa_{BA}=-1$
An integrator in the rear ATF ($\kappa_H = 1$)	$\kappa_{aa}=1$ $\kappa_{AA}=0$ $\kappa_{ab}=0$ $\kappa_{AB}=-1$	$\kappa_{bb}=0$ $\kappa_{BB}=2$ $\kappa_{ba}=-1$ $\kappa_{BA}=1$	$\kappa_{aa}=1+\kappa_G$ $\kappa_{AA}=0$ $\kappa_{ab}=\kappa_G$ $\kappa_{AB}=-1$	$\kappa_{bb}=0$ $\kappa_{BB}=2$ $\kappa_{ba}=-1$ $\kappa_{BA}=1$	$0 \le \kappa_{aa},\kappa_{bb} \le 2$ $0 \le \kappa_{AA},\kappa_{BB} \le 2$ $-1 \le \kappa_{ab},\kappa_{ba} \le 1$ $-1 \le \kappa_{AB},\kappa_{BA} \le 1$	

4 Asymmetric control law and the waves

It was shown in the previous chapter that any type of system inhomogeneity creates a boundary and causes partial reflection of the travelling wave. The mathematical analysis of the asymmetric bidirectional connection between agents is then complicated since there are two boundaries between the neighbouring agents, see Fig. 4.1. This chapter shows that the analysis is considerably simplified by introducing the asymmetric wave transfer function (AWTF). The AWTF is derived in the same manner as the the wave transfer function presented in Section 2.2 but for a multi-agent system with identical agents and identical but asymmetric controllers.
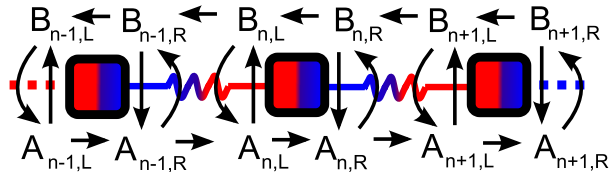

Figure 4.1: The travelling waves in system with the asymmetric bidirectional controller. There are two boundaries (one soft and one hard) between the agents, which causes multiple reflections of the wave inside the system.

Recently, papers [Hao et al. (2012)] and [Cantos and Veerman (2014)] introduce a novel type of asymmetric bidirectional control by assuming nonequal asymmetries between the output states. They showed that different couplings between the positions and velocities in the double integrator system can be beneficial for decreasing the transient and overshoots of the system response. The latter paper also suggests that the symmetry

in the positional coupling is necessary for the asymptotic and flock stabilities of an oscillator array. The reasoning of both papers were based on mathematical simulations and reasonable conjectures, which raise the following questions. Can the 'symmetry' condition be generalized for more complex agent dynamics? Is the symmetric coupling necessary for other types of graphs than a path graph? Answering these questions is the main aim of this chapter. Specifically, it shows that the symmetric coupling between the agent positions, represented by the identical DC gains of the controllers, is necessary for the string stability. This result holds for arbitrary graph and agent's model, which is a complementary result to prior findings about the string stability of asymmetric bidirectional control.

4.1 Mathematical preliminaries

We consider a formation of identical agents with a path-graph interaction topology. The goal of the formation is to drive along a line with equal distances between the agents.

The dynamics of agents is described by a linear single-input-single-output model. The output of the model is the position of the agent, $X_n(s)$, described as

$$X_n(s) = P(s)U_n(s), \tag{4.1}$$

where n denotes index of the agent, $P(s)$ is the transfer function of the model and $U_n(s)$ is the input to the agent generated by the local controllers onboard the agent. The goal of the controllers is to equalize relative distances to the immediate neighbours. Each agent has two controllers $C_\mathrm{f}(s)$ and $C_\mathrm{r}(s)$ that control the front and rear distances of the agent, respectively. We describe the controllers by transfer functions, which allows the representation of arbitrary couplings between the agents. In other words, the controllers may be of an arbitrary order and structure. We consider that each agent has the same set of controllers but the two controllers

may be different, i.e. $C_f(s) \neq C_r(s)$. Then

$$
\begin{aligned}
U_n(s) = & C_f(s)\left(X_{n-1}(s) - X_n(s)\right) \\
& + C_r(s)(X_{n+1}(s) - X_n(s)).
\end{aligned} \tag{4.2}
$$

The resulting model of the nth agent is shown in Fig. 4.2 and described by

$$
\begin{aligned}
X_n(s) = & M_f(s)(X_{n-1}(s) - X_n(s)) \\
& + M_r(s)(X_{n+1}(s) - X_n(s)),
\end{aligned} \tag{4.3}
$$

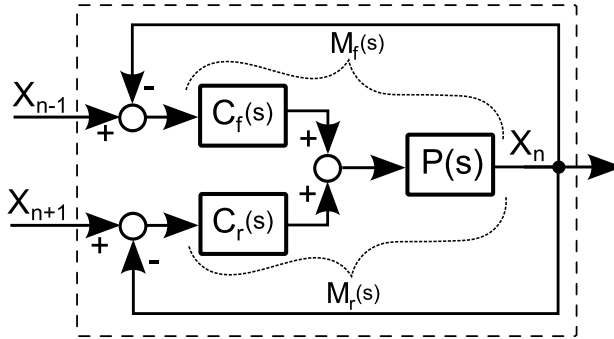where $M_f(s) = C_f(s)P(s)$ and $M_r(s) = C_r(s)P(s)$.

Figure 4.2: The model of nth agent.

The first agent $(n = 0)$, the leader, is externally controlled and serves as a reference signal for the distributed system. The rear-end agent $(n = N)$ of the path graph is described by

$$
X_N(s) = M_f(s)(X_{N-1}(s) - X_N(s)). \tag{4.4}
$$

Assumption 1. *Throughout this chapter, we assume that*

(a) $M_f(s)$ and $M_r(s)$ have the same number of p integrators.

(b) $M_f(s)$ and $M_r(s)$ are proper.

(c) $M_f(s)$ and $M_r(s)$ have no CRHP (closed-right half plane) zeros and

no CRPH poles except of p poles in the origin.

It is convenient to express $M_\mathrm{f}(s)$ and $M_\mathrm{r}(s)$ as

$$M_\mathrm{f}(s) = \frac{1}{s^p}\frac{n_\mathrm{f}(s)}{d_\mathrm{f}(s)} = \frac{1}{s^p}\frac{\sum_{k=0}^{L_\mathrm{f}} n_{\mathrm{f},k}s^k}{\sum_{k=0}^{K_\mathrm{f}} d_{\mathrm{f},k}s^k}, \tag{4.5}$$

$$M_\mathrm{r}(s) = \frac{1}{s^p}\frac{n_\mathrm{r}(s)}{d_\mathrm{r}(s)} = \frac{1}{s^p}\frac{\sum_{k=0}^{L_\mathrm{r}} n_{\mathrm{r},k}s^k}{\sum_{k=0}^{K_\mathrm{r}} d_{\mathrm{r},k}s^k}, \tag{4.6}$$

where K_f, L_f, K_r and L_r is the order of polynomial $n_\mathrm{f}(s)$, $d_\mathrm{f}(s)$, $n_\mathrm{r}(s)$ and $d_\mathrm{r}(s)$, respectively, and $n_{\mathrm{f},k}$, $d_{\mathrm{f},k}$, $n_{\mathrm{r},k}$ and $d_{\mathrm{r},k}$ are their coefficients. Without loss of generality we assume $n_{\mathrm{f},0} \neq 0$, $n_{\mathrm{r},0} \neq 0$ and $d_{\mathrm{f},0} = d_{\mathrm{r},0} = 1$.

The traditional asymmetric bidirectional control, see [Barooah et al. (2009)] or [Tangerman et al. (2012)], assumes that $M_\mathrm{f}(s) = \mu M_\mathrm{r}(s)$, where μ is a constant gain. We allow the asymmetry to be more general than scaling and focus on the relation between the kth coefficients of (4.5) and (4.6).

Definition 6. *We say that the distributed system has* symmetric positional coupling *if the open-loop model of an agent has*

$$\frac{n_{\mathrm{f},0}}{d_{\mathrm{f},0}} = \frac{n_{\mathrm{r},0}}{d_{\mathrm{r},0}}. \tag{4.7}$$

In other words, the positional coupling is symmetric if the DC gain of $M_\mathrm{f}(s)/M_\mathrm{r}(s)$ is equal to one. Similarly, the velocity coupling is symmetric if $n_{\mathrm{f},1}/d_{\mathrm{f},1} = n_{\mathrm{r},1}/d_{\mathrm{r},1}$.

4.2   Wave transfer function for asymmetric bidirectional connection

4.2.1   Introduction of the asymmetric wave approach

The bidirectional property of locally controlled agents causes that any change in the position of the leader is propagated through the distributed

system as a *wave*. When the wave reaches the rear-end agent, it reflects and propagates back to the leader, where it reflects again. This section describes the propagation of this wave.

The basic idea is to describe the position of the nth agent in a distributed system with a path graph topology by two components, $A_n(s)$ and $B_n(s)$, that represent two waves propagating along a distributed system in the forward and backward directions, respectively, similarly as in Chapter 2. However, the wave propagates differently in the directions due to the asymmetric connection. The mathematical model of such a distributed system (see Fig. 4.3) is then

$$X_n(s) = A_n(s) + B_n(s), \tag{4.8}$$

$$A_{n+1}(s) = G_+(s)A_n(s), \tag{4.9}$$

$$B_n(s) = G_-(s)B_{n+1}(s), \tag{4.10}$$

where $n \in \{1, 2, ..., N-1\}$, $G_+(s)$ and $G_-(s)$ are *asymmetric wave transfer functions* (AWTFs), which describe how the wave propagates in the system in the forward, (4.9), and backward, (4.10), directions, respectively. They are given in the following lemma.
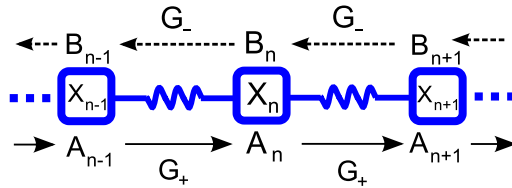

Figure 4.3: Scheme of waves travelling in a distributed system with a path graph topology. The squares stand for agents and springs illustrate the virtual connections between the agents created by the controllers. Note that all the agents are identical.

Lemma 8. *AWTFs $G_+(s)$ and $G_-(s)$ are given by*

$$G_+(s) = \frac{1}{2}\beta(s) - \frac{1}{2}\sqrt{\beta^2(s) - 4\frac{M_f(s)}{M_r(s)}}, \tag{4.11}$$

$$G_-(s) = \frac{1}{2}\alpha(s) - \frac{1}{2}\sqrt{\alpha^2(s) - 4\frac{M_r(s)}{M_f(s)}}, \tag{4.12}$$

where $M_f(s)$ and $M_r(s)$ define the system in (4.3) and

$$\alpha(s) = \frac{1 + M_f(s) + M_r(s)}{M_f(s)}, \quad \beta(s) = \frac{1 + M_f(s) + M_r(s)}{M_r(s)}. \tag{4.13}$$

Proof. **Quadratic-equation proof**

The proof is based on the same approach as in Section 2.2.2 or also in Section 3.1 of [O'Connor (2006)]. We note that the Laplace variable 's' is dropped in the following notation.

The substitution of (4.8)-(4.10) into (4.3) yields

$$A_n + B_n = M_f \left((G_+^{-1} A_n + G_- B_n) - (A_n + B_n) \right)$$
$$+ M_r \left((G_+ A_n + G_-^{-1} B_n) - (A_n + B_n) \right). \tag{4.14}$$

This equation can be decomposed into A and B parts as

$$1 = M_f G_+^{-1} - M_f + M_r G_+ - M_r, \tag{4.15}$$
$$1 = M_f G_- - M_f + M_r G_-^{-1} - M_r. \tag{4.16}$$

We rearrange it and get

$$G_+^2 - \beta G_+ + \frac{M_f}{M_r} = 0, \tag{4.17}$$

$$G_-^2 - \alpha G_- + \frac{M_r}{M_f} = 0, \tag{4.18}$$

where α and β are from (4.13). The solutions of the quadratic equations

are given by

$$G_+(s)_{1,2} = \frac{1}{2}\beta(s) \pm \frac{1}{2}\sqrt{\beta^2(s) - 4\frac{M_{\mathrm{f}}(s)}{M_{\mathrm{r}}(s)}}, \tag{4.19}$$

$$G_-(s)_{1,2} = \frac{1}{2}\alpha(s) \pm \frac{1}{2}\sqrt{\alpha^2(s) - 4\frac{M_{\mathrm{r}}(s)}{M_{\mathrm{f}}(s)}}. \tag{4.20}$$

We have specified that $G_+(s)$ describes the wave propagating along the system in the forward direction, i.e. from nth to $(n+1)$th agent. The propagation of the wave is causal, therefore, the transfer function describing this phenomenon must be either proper or strictly proper. We will show that the transfer functions $G_+(s)$ with a plus sign in front of the second term in (4.19) is not proper.

The definition of a proper irrational transfer function is given in Definition B.1 of [Curtain and Morris (2009)], which states: *The function G is proper if, for sufficiently large ρ, it holds*

$$\sup_{Re\ s \geq 0 \cap |s| > \rho} |G(s)| < \infty. \tag{4.21}$$

Due to Assumption 1, the norm of (4.19) can be unbounded only for $s \to \infty$. In addition, also $\lim_{s\to\infty} \beta(s) = \infty$, $\lim_{s\to\infty} \sqrt{\beta^2 - 4M_{\mathrm{f}}/M_{\mathrm{r}}} = \lim_{s\to\infty} \beta$. Therefore

$$\lim_{s\to\infty}\left(\frac{1}{2}\beta(s) + \frac{1}{2}\sqrt{\beta^2(s) - 4\frac{M_{\mathrm{f}}(s)}{M_{\mathrm{r}}(s)}}\right) = \infty, \tag{4.22}$$

$$\lim_{s\to\infty}\left(\frac{1}{2}\beta(s) - \frac{1}{2}\sqrt{\beta^2(s) - 4\frac{M_{\mathrm{f}}(s)}{M_{\mathrm{r}}(s)}}\right) = 0. \tag{4.23}$$

Analogous arguments apply to $G_-(s)$. We choose the proper solutions of

(4.17) and (4.18), hence,

$$G_+(s) = \frac{1}{2}\beta(s) - \frac{1}{2}\sqrt{\beta^2(s) - 4\frac{M_f(s)}{M_r(s)}}, \tag{4.24}$$

$$G_-(s) = \frac{1}{2}\alpha(s) - \frac{1}{2}\sqrt{\alpha^2(s) - 4\frac{M_r(s)}{M_f(s)}}. \tag{4.25}$$

Continued-fraction-expansion proof

We also present the alternative proof based on the continued-fraction expansion. First, we find the transfer function describing the propagation in the forward direction, $G_+(s)$. The transfer function from $X_0(s)$ to $X_1(s)$ in a system with one leader and one follower is $X_1/X_0 = M_f/(1 + M_f)$. For two followers is $X_1/X_0 = (M_f/M_r)(\beta - M_f/(1 + M_f))^{-1}$. Continuing recursively for $N \to \infty$, X_1/X_0 is expressed by the continued fraction as

$$\frac{X_1(s)}{X_0(s)} = \cfrac{M_f(s)/M_r(s)}{\beta(s) - \cfrac{M_f(s)/M_r(s)}{\beta(s) - \ddots}}. \tag{4.26}$$

Representing a square root function as the continued fraction, see [Jones and Thron (1984)],

$$\sqrt{z^2 + y} = z + \cfrac{y}{2z + \cfrac{y}{2z + \ddots}}, \tag{4.27}$$

we have

$$\frac{X_1(s)}{X_0(s)} = \frac{1}{2}\beta(s) - \frac{1}{2}\sqrt{\beta^2(s) - 4\frac{M_f(s)}{M_r(s)}}. \tag{4.28}$$

Similarly, we can find that

$$\frac{X_n(s)}{X_{n-1}(s)} = \frac{1}{2}\beta(s) - \frac{1}{2}\sqrt{\beta^2(s) - 4\frac{M_{\mathrm{f}}(s)}{M_{\mathrm{r}}(s)}}. \tag{4.29}$$

The transfer function $G_-(s)$ describing the propagation in the opposite direction can be found analogously. Namely, let the leader be placed at the opposite end of the system. Then the transfer function from $X_0(s)$ to $X_{-1}(s)$ is

$$\frac{X_{-1}(s)}{X_0(s)} = \cfrac{M_{\mathrm{r}}(s)/M_{\mathrm{f}}(s)}{\alpha(s) - \cfrac{M_{\mathrm{r}}(s)/M_{\mathrm{f}}(s)}{\alpha(s) - \ddots}} = \frac{1}{2}\alpha(s) - \frac{1}{2}\sqrt{\alpha^2(s) - 4\frac{M_{\mathrm{r}}(s)}{M_{\mathrm{f}}(s)}}. \tag{4.30}$$

$\square$

We note that the reflections of the wave from the leader and the rear-end agent described by the following lemma are not used in the derivation of the main result of this chapter. However, we feel obliged to derive them to fully cover the issue of waves in asymmetric bidirectional control. Moreover, we use the reflections for numerical verification of the proposed AWTF approach.

Lemma 9. *The reflection from the leader and the rear-end agent in the path graph is described by the transfer function $T_1(s) = A_1(s)/B_1(s)$ and $T_N(s) = B_N(s)/A_N(s)$, respectively. The transfer functions are given by*

$$T_1(s) = \frac{A_1(s)}{B_1(s)} = -G_+(s)G_-(s), \tag{4.31}$$

$$T_N(s) = \frac{B_N(s)}{A_N(s)} = G_-(s)\frac{G_+(s) - 1}{G_-(s) - 1}, \tag{4.32}$$

respectively.

Proof. The position $X_1(s)$ in (4.3) can be rewritten using (4.13) as

$$X_1 = \frac{1}{\alpha}X_0 + \frac{1}{\beta}X_2. \tag{4.33}$$

Substituting for $X_1 = A_1 + B_1$ and $X_2 = G_+ A_1 + G_-^{-1} B_1$ from (4.9) and (4.10) yields

$$A_1 = \frac{1}{\alpha}\frac{1}{1 - \frac{1}{\beta}G_+}X_0 + \frac{1}{\beta}\frac{\alpha}{\alpha}\frac{G_-^{-1} - \beta}{1 - \frac{1}{\beta}G_+}B_1. \tag{4.34}$$

The last expression can be further simplified by the following arrangements. First, from (4.13) we have

$$\frac{\beta}{\alpha} = \frac{M_{\mathrm{f}}}{M_{\mathrm{r}}}. \tag{4.35}$$

Further, by (4.11) and (4.35), it can be shown that

$$\begin{aligned} G_+^{-1} &= \frac{M_{\mathrm{r}}}{M_{\mathrm{f}}}\left(\frac{1}{2}\beta + \frac{1}{2}\sqrt{\beta^2 - 4\frac{M_{\mathrm{f}}}{M_{\mathrm{r}}}}\right) \\ &= \frac{\alpha}{\beta}(\beta - G_+) = \alpha\left(1 - \frac{1}{\beta}G_+\right). \end{aligned} \tag{4.36}$$

Likewise,

$$G_-^{-1} = \frac{\beta}{\alpha}(\alpha - G_-). \tag{4.37}$$

By rearranging (4.37), it gives

$$G_- = \alpha - \frac{\alpha}{\beta}G_-^{-1}. \tag{4.38}$$

Substituting (4.35), (4.36) and (4.38) into (4.34) gives

$$A_1 = G_+ X_0 - G_+ G_- B_1 = G_+ X_0 + T_1 B_1. \tag{4.39}$$

Now, we derive the reflection relation for the rear-end agent. Substituting (4.9), (4.10) and (4.8) into (4.4) gives

$$A_N + B_N = M_{\mathrm{f}}(G_+^{-1}A_N + G_-B_N - A_N - B_N). \tag{4.40}$$

By rearranging, it gives

$$B_N = \frac{1 + M_{\mathrm{f}} - M_{\mathrm{f}}G_+^{-1}}{M_{\mathrm{f}}G_- - M_{\mathrm{f}} - 1}A_N. \tag{4.41}$$

By (4.36) and (4.38), we have $M_{\mathrm{f}}G_+^{-1} = -M_{\mathrm{r}}G_+ + (M_{\mathrm{r}} + M_{\mathrm{f}} + 1)$ and $M_{\mathrm{f}}G_- = -M_{\mathrm{r}}G_-^{-1} + (M_{\mathrm{r}} + M_{\mathrm{f}} + 1)$. Substituting these into (4.41) results in

$$B_N = \frac{M_{\mathrm{r}}(G_+ - 1)}{M_{\mathrm{r}}(1 - G_-^{-1})}A_N = G_-\frac{G_+ - 1}{G_- - 1}A_N. \tag{4.42}$$

$\square$

4.2.2 Verification of the asymmetric wave approach

An independent validation of the AWTF approach is shown in Fig. 4.4. The numerical simulation shows the response of 20 agents with the path-graph topology, where

$$M_{\mathrm{f}}(s) = \frac{1}{3}\frac{4s + 4}{s^2(s/3 + 1)}, \quad M_{\mathrm{r}}(s) = \frac{1}{3}\frac{2.5s + 4}{s^2(s/3 + 1)}. \tag{4.43}$$

We can see excellent agreement between the state-space approach based on (4.3) and the AWTF approach. The waves A_{10} and B_{10} are computed as

$$A_{10} = G_+^{10}X_0 + T_N G_+^{19}T_1 G_-^{19}A_{10}, \tag{4.44}$$

$$B_{10} = G_-^{10}T_N G_+^{20}X_0 + T_N G_+^{19}T_1 G_-^{19}B_{10}. \tag{4.45}$$

The first term on the right-hand side describes the wave traveling to the agent due to a change of $X_0(s)$. The second term describes the wave

returning back to the agent due to the reflections at the leader and the rear-end agent. The wave X_{10} is a sum of A_{10} and B_{10}.

We can also see that the approximation $x_{10}(t) \approx a_{10}(t)$ holds in the time-domain for the first 20 seconds, then the wave returns back to the 10th agent which causes an increase of B_{10}.
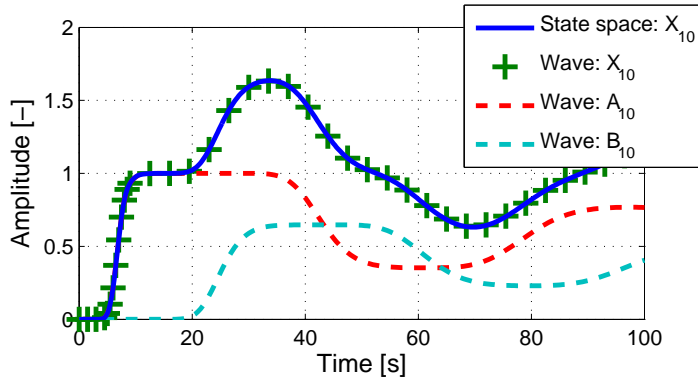

Figure 4.4: The comparison of the positions of the 10th agent in the system defined by (4.43) simulated by the state-space approach using (4.3) (blue solid line) and by the AWTF's approach using (4.9), (4.10) and Lemmas 8 and 9 (green crosses). The two components A_{10} and B_{10} from (4.8) are shown with the dashed red and blue lines, respectively. The response on the step change of X_0 is shown.

4.2.3 Properties of AWTFs

To be able to track the leader travelling at a constant velocity with the zero steady-state error we require two integrators to be present in the model of each agent. The DC gains of the AWTFs in this case are limited to one as the following lemma describes.

Lemma 10. *If there is at least one integrator in $M_f(s)$ and $M_r(s)$, defined by (4.5) and (4.6), then the DC gains of the AWTFs given by (4.11) and*

(4.12) are

$$\lim_{s \to 0} G_+(s) = \kappa, \quad \lim_{s \to 0} G_-(s) = 1, \qquad \text{if } 0 < \kappa < 1, \tag{4.46}$$

$$\lim_{s \to 0} G_+(s) = 1, \quad \lim_{s \to 0} G_-(s) = 1/\kappa, \quad \text{if } \kappa \geq 1, \tag{4.47}$$

where

$$\kappa = \lim_{s \to 0} \frac{M_\mathrm{f}(s)}{M_\mathrm{r}(s)} = \frac{n_{\mathrm{f},0}}{n_{\mathrm{r},0}}. \tag{4.48}$$

Proof. First, we prove the DC gain of G_+. Since there is at least one integrator in $M_\mathrm{r}(s)$, then the limit of $\beta(s)$ given by (4.13) is

$$\lim_{s \to 0} \beta(s) = \lim_{s \to 0} \left(1 + \frac{1}{M_\mathrm{r}(s)} + \frac{M_\mathrm{f}(s)}{M_\mathrm{r}(s)} \right) = 1 + \kappa. \tag{4.49}$$

Substituting from (4.49) into (4.11) gives

$$\begin{aligned} \lim_{s \to 0} G_+(s) &= \frac{1}{2} \left(1 + \kappa - \sqrt{(1+\kappa)^2 - 4\kappa} \right) \\ &= \frac{1}{2}(1 + \kappa - |1 - \kappa|). \end{aligned} \tag{4.50}$$

The proof of the DC gain of G_- is similar. □

Another important characteristics of the AWTFs are the asymptotic stability and the H_∞ norm.

Theorem 8. *If $M_\mathrm{f}(s)$ and $M_\mathrm{r}(s)$ defined by (4.5)-(4.6) satisfy Assumption 1 and if the Nyquist plot of*

$$T_G(s) = (M_\mathrm{f}(s) - M_\mathrm{r}(s))^2 + 2M_\mathrm{f}(s) + 2M_\mathrm{r}(s) + 1 \tag{4.51}$$

does not intersect the non-positive real axis, then the AWTFs given by (4.11) and (4.12) are asymptotically stable.

Proof. The proof is based on Theorem A.2 [Curtain and Morris (2009)], which states: *A linear system is stable if and only if its transfer function*

$T(s)$ is analytic in the right-half plane and $||T||_\infty < \infty$, where $||T||_\infty = \sup_{Re(s)>0} |T(s)|$.

We have shown that the norms of $G_+(s)$ and $G_-(s)$ are bounded in the proof of Lemma 8, hence, we focus on their analyticity. We use the result of the complex function analysis, which states that the square root function $f(z) = \sqrt{z}$ is analytic everywhere except for the non-positive real axis (e.g., [Stein and Shakarchi (2010)]). The second term of $G_+(s)$ is

$$f_{2,+}(s) = \frac{1}{2}\sqrt{\beta^2(s) - 4\frac{M_f(s)}{M_r(s)}} = \frac{1}{2}\sqrt{\frac{1 + M_s(s)}{M_r^2(s)}}, \tag{4.52}$$

where $M_s = M_r^2 + M_f^2 + 2M_r + 2M_f - 2M_rM_f = (M_r - M_f)^2 + 2(M_r + M_f)$. We apply the same analysis as in Figure 1.9 of Section 1.2 of [Kelly (2006)]. Term $\sqrt{1/M_r}$ is analytic everywhere except for the non-positive real axis, where it has a branch cut. The non-analyticity is caused by functional discontinuity, which is, in this case, only a sign change. Due to that, the overlapping branch cuts of $\sqrt{1/M_r \cdot 1/M_r}$ cancel each other, which means that $\sqrt{1/M_r^2}$ is continuous and analytic even on the non-positive real axis. Then $f_{2,+}$ is analytic if and only if $\sqrt{1 + M_s}$ is analytic. Hence, if the Nyquist plot of $1 + M_s$ does not intersect the non-positive real axis, then $f_{2,+}$ is analytic.

The first terms of the AWTFs, $\alpha/2$ and $\beta/2$, are rational transfer functions. A rational function is analytic in the ORHP (open-right half plane) if and only if it has no singularities, in this case ORHP zeros and ORHP poles of M_f and M_r. Therefore, if M_f and M_r have no ORHP zeros, nor ORHP poles, then $\alpha/2$ and $\beta/2$ are analytic.

Observe that

$$G_+(s) = \frac{1}{2}\beta(s) - \frac{1}{2}\sqrt{\frac{1 + M_s(s)}{M_r^2(s)}}, \tag{4.53}$$

is an analytic function since the Nyquist plot of $(1 + M_s(s))$ does not intersect the non-positive real axis and $\beta(s)$ and $\alpha(s)$ do not have ORHP

poles due to the condition that $M_f(s)$ and $M_r(s)$ have no CRHP zeros nor CRHP poles. $\qquad \square$

Theorem 9. *If the AWTFs given by (4.11) and (4.12) are asymptotically stable, there are two integrators in $M_f(s)$ and $M_r(s)$, given by (4.5)-(4.6), and*

$$n_{f,0} \neq n_{r,0}, \tag{4.54}$$

$$d_{f,0} = d_{r,0} = 1, \tag{4.55}$$

$$n_{f,0} > 0, \ n_{r,0} > 0, \tag{4.56}$$

then either $||G_+(s)||_\infty > 1$ or $||G_-(s)||_\infty > 1$.

Proof. First, we prove that $||G_+||_\infty > 1$ if $\kappa > 1$, where $\kappa \neq 1$ due to (4.54). By ω_0 we denote a frequency that is close to 0 and evaluate the real and imaginary parts of the individual transfer functions as

$$x_1 + \jmath y_1 = \frac{M_f(\jmath\omega_0)}{M_r(\jmath\omega_0)}, \quad x_2 + \jmath y_2 = \frac{1}{M_r(\jmath\omega_0)}, \tag{4.57}$$

$x = x_1 + x_2$ and $y = y_1 + y_2$. The Taylor series expansion of (4.57) evaluated at ω_0 yield

$$x_1(\omega_0) = k_{x,1} - k_{x,2}\omega_0^2 + k_{x,3}\omega_0^4 - ..., \tag{4.58}$$

$$y_1(\omega_0) = k_{y,1}\omega_0 - k_{y,2}\omega_0^3 + k_{y,3}\omega_0^5 - ..., \tag{4.59}$$

$$x_2(\omega_0) = -l_{x,1}\omega_0^2 + l_{x,2}\omega_0^4 - l_{x,3}\omega_0^6 + ..., \tag{4.60}$$

$$y_2(\omega_0) = -l_{y,1}\omega_0^3 + l_{y,2}\omega_0^5 - l_{y,3}\omega_0^7 + ..., \tag{4.61}$$

where we assumed that M_r has two integrators. We note that $k_{x,1} = \kappa$ and $l_{x,1} = 1/n_{r,0}$. The other coefficients, $k_{x,2}$, $k_{x,3}$, etc., obtained from Taylor series are not important due to limit $\omega_0 \to 0$ as we show later in the proof.

Substituting (4.57) into (4.11) gives the real part of $G_+(\jmath\omega_0)$ as

$$\mathrm{Re}\{G_+(\jmath\omega_0)\} = \frac{1}{2}(1+x) - \frac{1}{2}\sqrt{\frac{|z| + \mathrm{Re}\{z\}}{2}}, \tag{4.62}$$

where we used $\mathrm{Re}\{\sqrt{z}\} = \sqrt{|z|/2 + \mathrm{Re}\{z\}/2}$, see e.g. Section 3.7.27 in [Abramowitz and Stegun (1964)], and

$$z = \beta^2(\jmath\omega_0) - 4\frac{M_{\mathrm{f}}(\jmath\omega_0)}{M_{\mathrm{r}}(\jmath\omega_0)}$$
$$= (1 + x^2 - y^2 + 2x - 4x_1) + \jmath(2y + 2xy - 4y_1). \tag{4.63}$$

In order to complete the proof, we show that $\mathrm{Re}\{G_+(\jmath\omega_0)\} > 1$, hence, we solve the following inequality

$$(1+x) - \sqrt{\frac{|z| + \mathrm{Re}\{z\}}{2}} > 2. \tag{4.64}$$

We simplify it as

$$\left(2(x-1)^2 - \mathrm{Re}\{z\}\right)^2 - \mathrm{Re}\{z\}^2 - \mathrm{Im}\{z\}^2 > 0, \tag{4.65}$$

substitute into it from (4.63) and obtain

$$-x_2(x_1 - 1)^2 - y_1y_2(x_1 + x_2 - 1) - 2x_2^2(x_1 - 1) - x_2^3$$
$$- y_2^2(x_1 + x_2) > 0. \tag{4.66}$$

We substitute from (4.58)-(4.61) into (4.66) and get

$$l_{x,1}(k_{x,1} - 1)^2\omega_0^2 + \mathcal{O}(\omega_0^4, \omega_0^6, \omega_0^8, ...) > 0, \tag{4.67}$$

where $\mathcal{O}(\omega_0^4, \omega_0^6, \omega_0^8, ...)$ stands for the polynomial with powers ω_0^4, ω_0^6, ω_0^8 etc. The lowest order term in (4.67) is ω_0^2. Therefore, the inequality in (4.64) holds for ω_0 close to zero if $l_{x,1} = 1/n_{\mathrm{r},0} > 0$. We assume in (4.56) that $n_{\mathrm{r},0} > 0$, hence, $\mathrm{Re}\{G_+(\jmath\omega_0)\} > 1$ and $||G_+||_\infty > 1$. Similarly, it can be shown that $||G_-||_\infty > 1$ if $0 < \kappa < 1$ and $n_{\mathrm{f},0} > 0$. Hence, if $n_{\mathrm{f},0} \neq n_{\mathrm{r},0}$ then $\kappa \neq 1$ and either $||G_+(s)||_\infty > 1$ or $||G_-(s)||_\infty > 1$. $\qquad \square$

4.3 Implications for the graphs with asymmetric coupling

In this section, we follow the argument given in the Introduction that certain features in the performance of the distributed system can be inferred from the analysis of wave propagation between the agents because of the local nature of the AWTFs.

Definition 7. *We say that the distributed system is* locally-string stable *if the AWTFs are asymptotically stable and*

$$||G_+(s)||_\infty \leq 1 \quad and \quad ||G_-(s)||_\infty \leq 1. \tag{4.68}$$

Otherwise, the system is called locally-string unstable.

Similarly to the string stabilities mentioned in the introduction, the local-string stability also deals with the performance of the distributed system. It also describes whether the disturbance acting on an agent amplifies as it propagates through the system. However, the local-string stability describes the performance from the local point of view without considering the whole distributed system. The local description is particularly advantageous for a large distributed system, where the traditional Laplacian approach is difficult to apply.

The effect of the local-string instability is illustrated in Fig. 4.5. The left panels show the response of the system with the symmetric bidirectional control, which is locally-string stable. The right panels show the response of the system with the asymmetric control, where the asymmetry is in both the position and velocity. This makes the system locally-string unstable. We can see (top-right panel) that the overshoot of the locally-string unstable system increases with the index of the agent. The more agents the wave transmits through, the larger the overshoot is, due to the fact that $||G_+(s)||_\infty > 1$. This does not happen for the locally-string stable system (top-left panel). We can see that even the locally-string stable system eventually overshoots the input signal (bottom-left panel) which is due to the reflection of the wave at the last agent.
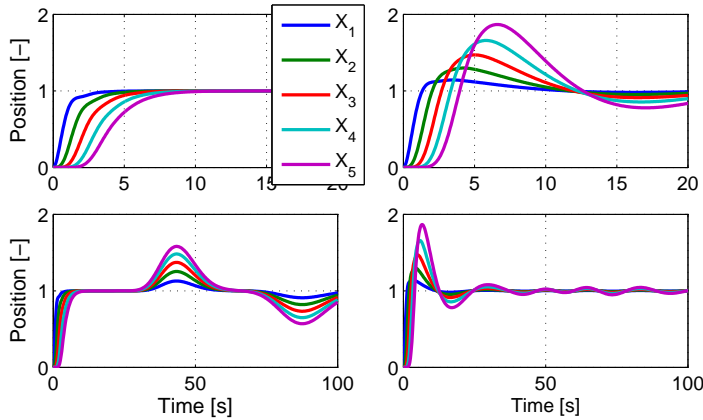
Figure 4.5: The comparison of the responses of the locally-string stable system (left panels) with the locally-string unstable system (right panels).

The main contribution of this chapter is given in the following Theorem.

Theorem 10. *If i) there are two integrators in the dynamics of the agents, ii) the AWTFs given by (4.11) and (4.12) are asymptotically stable, iii) a part of the topology of the distributed system is a path graph, and iv) the positional coupling between the agents that are lying on the path graph is asymmetric, then the distributed system is locally-string unstable.*

Proof. If the positional coupling is asymmetric, then $n_{f,0}/d_{f,0} \neq n_{r,0}/d_{r,0}$ by Definition 6. Since we can always transform $M_f(s)$ and $M_r(s)$ such that $d_{f,0} = d_{r,0} = 1$, then $n_{f,0} \neq n_{r,0}$. Therefore, $||G_+(s)||_\infty > 1$ or $||G_-(s)||_\infty > 1$, which follows from Theorem 9, and the distributed system is locally-string unstable. □

We can interpret Theorem 10 as follows. $||G_+(s)||_\infty > 1$ causes that the disturbance is amplified as it propagates from $X_i(s)$ to $X_{i+1}(s)$, from $X_{i+1}(s)$ to $X_{i+2}(s)$, from $X_{i+2}(s)$ to $X_{i+3}(s)$ etc. The larger the path graph is, the more is the disturbance amplified. Similarly, if $||G_-(s)||_\infty > 1$, then the disturbance is amplified as it propagates in the opposite direction.

Theorem 10 is in agreement with the results of [Barooah et al. (2009)], [Tangerman et al. (2012)] or [Herman et al. (2015a)], which state that if the asymmetry is in the form of $M_{\mathrm{f}}(s) = \mu M_{\mathrm{r}}(s)$ with μ being a constant gain, then the system is string unstable. However, Theorem 10 is more general since it states that the distributed system is string unstable if the DC gain of $M_{\mathrm{f}}/M_{\mathrm{r}}$ is not equal to one. Hence, it allows the asymmetry to be more complex.

We should emphasize that Theorem 10 does not disprove an asymmetry in the velocity coupling. In fact, the asymmetric velocity coupling may improve the transient of the system, as the simulation example in Section 4.4 shows.

The key part of the derivation of G_+ and G_- is that the agent has two neighbours. Therefore, we can apply the decomposition of the waves from (4.8)-(4.12) to each agent that has two neighbours. In other words, if the agents connected in a path-graph topology are parts of a system with a more complex graph topology, then G_+ and G_- are the same.

4.4 Mathematical simulations

4.4.1 Path-graph topology

The mathematical simulations compare three different control strategies for two different sizes of a path graph. The results are shown in Fig. 4.6, where the agent is modelled as a double integrator with a linear model of friction controlled by a PI controller, that is

$$M_{\mathrm{f}} = \frac{1}{3} \frac{4s + 4}{s^2(s/3 + 1)} \tag{4.69}$$

for all three cases. But

$$M_{\mathrm{r}} = M_{\mathrm{f}}, \quad M_{\mathrm{r}} = \frac{2.5}{4} M_{\mathrm{f}}, \quad M_{\mathrm{r}} = \frac{1}{3} \frac{2.5s + 4}{s^2(s/3 + 1)}, \tag{4.70 a, b, c}$$

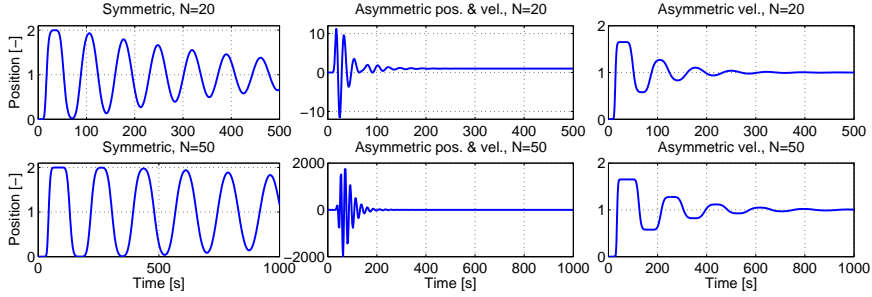for the left, middle and right panels, respectively.

Figure 4.6: The numerical simulations showing the position of the last agent in the distributed system with a path-graph topology when the leader changes its position from 0 to 1. The figure compares three different bidirectional control strategies: i) the symmetric (the left panels) defined by (4.70a), ii) the traditional asymmetric control with asymmetries in both positional and velocity couplings (the middle panels), see (4.70b), and iii) the combined symmetric positional with asymmetric velocity couplings (the right panels), see (4.70c). The top and bottom panels show the system with 20 and 50 agents, respectively.

We can see that the symmetric bidirectional control has a very long transient (the left panel), which is shortened when the asymmetry is introduced to both positional and velocity couplings (the middle panel). However, the asymmetry in the positional coupling causes a large overshoot which even scales with the size of the graph due to the local-string instability. When the positional coupling is kept symmetric and the velocity coupling asymmetric (the right panel), the overshoot is smaller than for the symmetric case. Moreover, we can see that the transient scales approximately linearly with the size of the graph.

Fig. 4.7 shows the numerical validation of Theorem 9 for M_f and M_r defined by (4.69) and (4.70b)-(4.70c). We can see that, if there is asymmetry in the positional coupling (solid line), i.e. when $n_{\mathrm{f},0} \neq n_{\mathrm{r},0}$, then the H_∞ norm of G_+ is greater than one. The norm is reduced to one by making the positional coupling symmetric (dashed line).
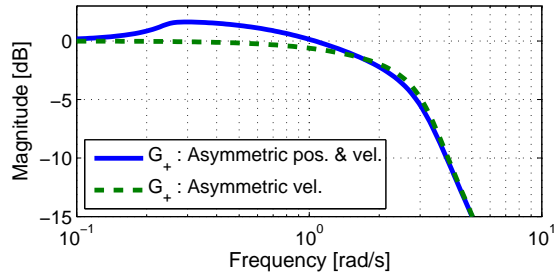
Figure 4.7: The comparison of the frequency characteristics for two different transfer functions $G_+(s)$. The asymmetries in the couplings are defined as in Fig. 4.6.

4.4.2 Complex graph topology

The numerical simulations in the previous section are carried out for a distributed system with a path graph topology. However, Theorem 10 holds also for a more complex graphs because of the local nature of the AWTFs. This can nicely be demonstrated on a graph, where a path graph is a part of a more complex graph as in Fig. 4.8. Although, the string stability is defined and studied mostly for the path graphs, we can observe the same phenomenon, that is, the amplification of a disturbance as it propagates in the system. The top panels of Fig. 4.9 show that the condition of the symmetric positional coupling is violated. Such a phenomenon is difficult to identify by the traditional state-space approach.
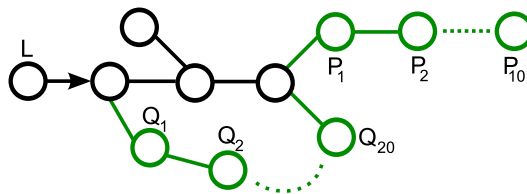

Figure 4.8: The topology of the distributed system, where the black and green nodes represent the agents with the symmetric and asymmetric couplings, respectively. The 'L'-node is the leader of the system. 'Q'-nodes lie on the same path, which differs from the path of 'P'-nodes.
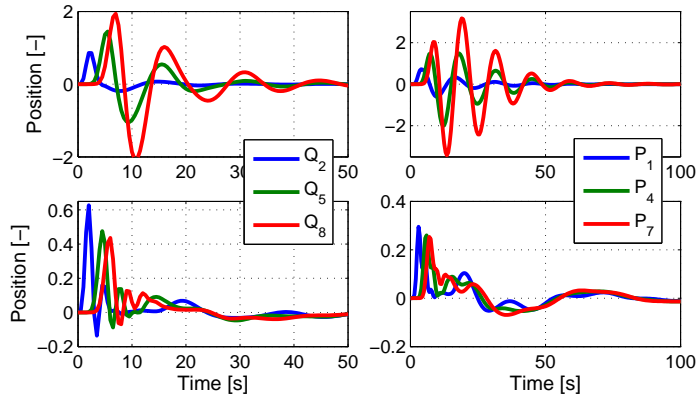
Figure 4.9: The numerical simulations showing the positions of agents Q_2, Q_5, Q_8, P_1, P_4 and P_7 of the system with the topology in Fig. 4.8. The input to the system is the Dirac pulse, which represents the noise acting on the leader. The agents at the top and bottom panels have M_f and M_r defined as in the middle and right panels in Fig. 4.6, respectively.

4.5   Conclusions

This chapter examines a multi-agent system with an asymmetric bidirectional control, where the coupling between the agents is allowed to be arbitrarily complex. The proposed approach reveals that the symmetric positional coupling, i.e. identical DC gains of the controllers, is necessary for the string stability of the multi-agent system. This finding does not disprove the asymmetry for other couplings. In fact, it is numerically shown that, if the asymmetry in the velocity coupling is adjusted properly, then the system's performance may be improved.

4.6   Appendix to the chapter

4.6.1   DC gain of T_N

This section shows how to carry out the DC gain of the transfer function describing the reflection of the wave at the rear-end agent from Lemma 9. We assume that the system has a symmetric positional coupling, i.e.

$n_{\mathrm{f},0} = n_{\mathrm{r},0}$ and $d_{\mathrm{f},0} = d_{\mathrm{r},0} = 1$, and that there are two integrators in $M_{\mathrm{f}}(s)$ and $M_{\mathrm{r}}(s)$. We note that we omit argument 's' from the equations where it is obvious.

The DC gain of $T_N(s)$ is given by

$$\kappa_{\mathrm{T},N} = \lim_{s\to 0} T_N(s) = \lim_{s\to 0} G_-(s) \lim_{s\to 0} \frac{G_+(s) - 1}{G_-(s) - 1}. \tag{4.71}$$

The DC gain of G_- and G_+ is equal to one because of the integrators in M_{f} and M_{r}. Therefore, we expand the second term of (4.71) as

$$\frac{G_+ - 1}{G_- - 1} = \frac{\left(\dfrac{1}{2}\beta - \dfrac{1}{2}\sqrt{\beta^2 - 4\dfrac{M_{\mathrm{f}}}{M_{\mathrm{r}}}} - 1\right)\dfrac{2}{s}}{\left(\dfrac{1}{2}\alpha - \dfrac{1}{2}\sqrt{\alpha^2 - 4\dfrac{M_{\mathrm{r}}}{M_{\mathrm{f}}}} - 1\right)\dfrac{2}{s}} = \frac{P_{\mathrm{n},1} - \sqrt{P_{\mathrm{n},2}}}{P_{\mathrm{d},1} - \sqrt{P_{\mathrm{d},2}}}, \tag{4.72}$$

where the definition of substituted terms $P_{\mathrm{n},1}$, $P_{\mathrm{n},2}$, $P_{\mathrm{d},1}$, $P_{\mathrm{d},2}$ is obvious.

Now we evaluate the individual terms. We start with $P_{\mathrm{n},1}$,

$$P_{\mathrm{n},1} = \frac{\beta - 2}{s} = \frac{1}{sM_{\mathrm{r}}} - \frac{1}{s} + \frac{M_{\mathrm{f}}}{sM_{\mathrm{r}}}. \tag{4.73}$$

Because of two integrators in M_{r}, $\lim_{s\to 0} \dfrac{1}{sM_{\mathrm{r}}} = 0$ and

$$\frac{M_{\mathrm{f}}}{sM_{\mathrm{r}}} - \frac{1}{s} = \frac{n_{\mathrm{f}}d_{\mathrm{r}} - n_{\mathrm{r}}d_{\mathrm{f}}}{sn_{\mathrm{r}}d_{\mathrm{f}}}, \tag{4.74}$$

where $n_{\mathrm{f}}(s)$, $d_{\mathrm{f}}(s)$, $n_{\mathrm{r}}(s)$ and $d_{\mathrm{r}}(s)$ are defined in (4.5)-(4.6). Hence,

$$\lim_{s\to 0} \frac{n_{\mathrm{f}}d_{\mathrm{r}} - n_{\mathrm{r}}d_{\mathrm{f}}}{sn_{\mathrm{r}}d_{\mathrm{f}}} = \frac{n_{\mathrm{f},0}d_{\mathrm{r},0} - n_{\mathrm{r},0}d_{\mathrm{f},0}}{0 n_{\mathrm{r},0}d_{\mathrm{f},0}} = \frac{0}{0}. \tag{4.75}$$

Applying l'Hospital rule gives

$$\frac{(n_{\mathrm{f}}d_{\mathrm{r}} - n_{\mathrm{r}}d_{\mathrm{f}})'}{(sn_{\mathrm{r}}d_{\mathrm{f}})'} = \frac{n_{\mathrm{f}}'d_{\mathrm{r}} + n_{\mathrm{f}}d_{\mathrm{r}}' - n_{\mathrm{r}}'d_{\mathrm{f}} - n_{\mathrm{r}}d_{\mathrm{f}}'}{s(n_{\mathrm{r}}d_{\mathrm{f}})' + n_{\mathrm{r}}d_{\mathrm{f}}}. \tag{4.76}$$

Then

$$\lim_{s \to 0} P_{n,1} = \frac{n_{f,1} d_{r,0} + n_{f,0} d_{r,1} - n_{r,1} d_{f,0} - n_{r,0} d_{f,1}}{n_{r,0} d_{f,0}}. \tag{4.77}$$

Similarly,

$$
\begin{aligned}
\lim_{s \to 0} P_{d,1} &= \lim_{s \to 0} \frac{1}{s M_f} - \frac{1}{s} + \frac{M_r}{s M_f} \\
&= \frac{n_{r,1} d_{f,0} + n_{r,0} d_{f,1} - n_{f,1} d_{r,0} - n_{f,0} d_{r,1}}{n_{f,0} d_{r,0}}.
\end{aligned} \tag{4.78}
$$

$P_{n,2}$ term is calculated as follows

$$
\begin{aligned}
P_{n,2} &= \frac{1}{s^2} \left(\beta^2 - 4 \frac{M_f}{M_r} \right) = \frac{1}{s^2} \left(\frac{1}{M_r^2} + \frac{2}{M_r} + 2 \frac{M_f}{M_r^2} + \left(\frac{M_f}{M_r} - 1 \right)^2 \right) \\
&= s^2 \frac{d_r^2}{n_r^2} + \frac{2 d_r}{n_r} + \frac{2 d_r^2 n_f}{n_r^2 d_f} + P_{n,3}^2,
\end{aligned} \tag{4.79}
$$

where

$$P_{n,3} = \frac{1}{s} \left(\frac{n_f d_r}{d_f n_r} - 1 \right). \tag{4.80}$$

Since $\lim_{s \to 0} P_{n,3} = 0/0$, we apply l'Hospital rule. It gives

$$
\begin{aligned}
\lim_{s \to 0} P_{n,3} &= \lim_{s \to 0} \frac{(n_f' d_r + n_f d_r') d_f n_r - n_f d_r (d_f' n_r + d_f n_r')}{d_f^2 n_r^2} \\
&= \frac{(n_{f,1} d_{r,0} + n_{f,0} d_{r,1}) d_{f,0} n_{r,0} - n_{f,0} d_{r,0} (d_{f,1} n_{r,0} + d_{f,0} n_{r,1})}{d_{f,0}^2 n_{r,0}^2}.
\end{aligned} \tag{4.81}
$$

Similarly

$$P_{d,2} = s^2 \frac{d_f^2}{n_f^2} + \frac{2 d_f}{n_f} + \frac{2 d_f^2 n_r}{n_f^2 d_r} + P_{d,3}^2, \tag{4.82}$$

and

$$\lim_{s \to 0} P_{d,3} = \frac{(n_{r,1}d_{f,0} + n_{r,0}d_{f,1})d_{r,0}n_{f,0} - n_{r,0}d_{f,0}(d_{r,1}n_{f,0} + d_{r,0}n_{f,1})}{d_{r,0}^2 n_{f,0}^2}.$$

(4.83)

Assuming $n_{f,0} = n_{r,0}$ and $d_{f,0} = d_{r,0}$ gives

$$P_{n,1} = -P_{d,1}, \quad P_{n,2} = P_{d,2}, \quad P_{n,3} = -P_{d,3}.$$

(4.84)

Then substituting (4.79) and (4.84) into (4.72) gives

$$\lim_{s \to 0} \frac{P_{n,1} - \sqrt{P_{n,2}}}{P_{d,1} - \sqrt{P_{d,2}}} = \frac{P_{n,1} - \sqrt{P_{n,3}^2 + 4\frac{d_{r,0}}{n_{r,0}}}}{-P_{n,1} - \sqrt{P_{n,3}^2 + 4\frac{d_{r,0}}{n_{r,0}}}}$$

$$= -\frac{P_{n,1}^2 - 2P_{n,1}\sqrt{P_{n,3}^2 + 4\frac{d_{r,0}}{n_{r,0}}} + P_{n,3}^2 + 4\frac{d_{r,0}}{n_{r,0}}}{P_{n,1}^2 - P_{n,3}^2 - 4\frac{d_{r,0}}{n_{r,0}}},$$

(4.85)

where (4.81) is simplified as

$$P_{n,3} = \frac{n_{r,1} - n_{f,1}}{n_{r,0}} + \frac{d_{f,1} - d_{r,1}}{d_{f,0}}.$$

(4.86)

Simplifying (4.85) and substituting it into (4.71) yields

$$\kappa_{T,N} = 1 + \frac{n_{r,0}}{2d_{r,0}} P_{n,3} \left(P_{n,3} + \sqrt{P_{n,3}^2 + 4\frac{d_{r,0}}{n_{r,0}}} \right).$$

(4.87)

We illustrate the importance of the DC gain on the response of the distributed system with a path-graph topology. Fig. 4.10 shows the response

117

of 40 agents defined by

$$M_f(s) = \frac{n_{f,1}s + n_{f,0}}{s^2}, \quad M_r(s) = \frac{n_{r,1}s + n_{r,0}}{s^2}, \tag{4.88}$$

where $n_{f,1} = 5$ and $n_{f,0} = 1$. Parameters $n_{r,1}$ and $n_{r,0}$ are changed in the simulations. We can see that the asymmetric velocity coupling significantly reduces overshoots of the system and the transient of the system is consequently shortened. The value of the overshoot is equal to $\kappa_{T,N}$, that is the DC gain of T_N (4.87). Fig. 4.11 shows that the lower the value of $n_{r,1}$ is, the lower the DC gain is.
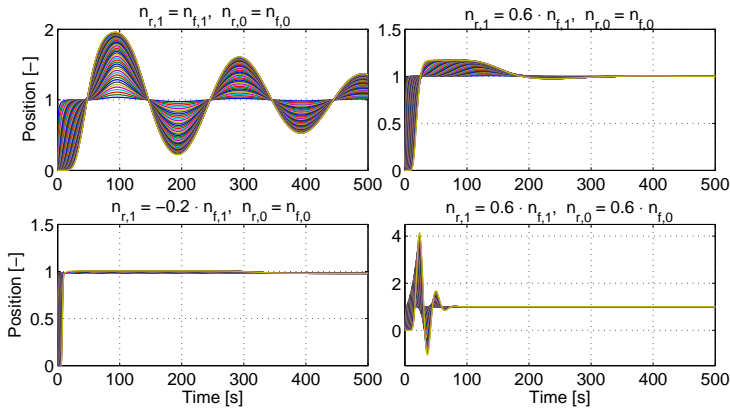
Figure 4.10: The response of the system defined in (4.88). The values of the DC gain, $\kappa_{T,N}$, carried out by (4.87), are: 1 (top-left panel), 0.17 (top-right panel) and 0.026 (bottom-left panel).
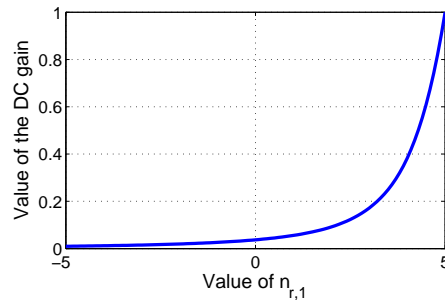

Figure 4.11: The relation between the DC gain carried out by (4.87) and the value of coefficient $n_{r,1}$ from (4.88).

5 General graph topology and the waves

This chapter generalizes the previous chapters by considering a system with a general graph topology. In comparison to the system with the path-graph topology the agent has more than two neighbours. The chapter provides a mathematical description of the reflection and transmission of travelling wave. It also presents a way how to prevent the reflection of the wave in such a system.

5.1 Mathematical preliminaries

The behaviour of nth agent in a multi-agent system is described by

$$X_n(s) = P(s)U_n(s), \tag{5.1}$$

where s is the Laplace variable, $X_n(s)$ is the output of the agent, $P(s)$ is the transfer function of the agent and $U_n(s)$ is the input to the agent that is carried out by the local controller of the agent with the task to equalize $X_n(s)$ with outputs of its neighbouring agents. We assume that each agent may have arbitrary number of neighbours, hence,

$$U_n(s) = C(s) \sum_{k \in \mathcal{N}_b} (X_k(s) - X_n(s)), \tag{5.2}$$

where $\mathcal{N}_b$ is a set of neighbouring agents of the nth agent and $C(s)$ is the transfer function of the controller. The model of the agent is then

$$X_n(s) = M(s) \sum_{k \in \mathcal{N}_b} (X_k(s) - X_n(s)), \tag{5.3}$$

where $M(s) = P(s)C(s)$ can be expressed as

$$X_n(s) = T_N(s) \sum_{k \in \mathcal{N}_b} X_k(s). \tag{5.4}$$

Here $T_N(s) = M(s)/(1 + NM(s))$ and N is the number of neighbours of nth agent.

5.2   Notation of the waves

To describe waves in a multi-agent system with a general graph topology, we need to introduce a different notation for the wave components. We replace A_n and B_n by $W_{n,n+1}^d$ and $W_{n+1,n}^a$, respectively. The first lower index is the index of the agent where the wave departs, while the second lower index is the index of the agent where the wave arrives. The upper index denotes if the wave departs from ('d') or arrives at ('a') the agent. The example is shown in Fig. 5.1.

Expressing (2.21) in the newly introduced notation gives

$$X_n(s) = W_{n,n+1}^d(s) + W_{n+1,n}^a(s) = W_{n-1,n}^a(s) + W_{n,n-1}^d(s), \tag{5.5}$$

where we assume that agents denoted $(n-1)$ and $(n+1)$ are neighbours of nth agent. Similarly, (2.22) and (2.23) are expressed as

$$W_{n,n+1}^a(s) = G(s)W_{n,n+1}^d(s), \tag{5.6}$$
$$W_{n+1,n}^a(s) = G(s)W_{n+1,n}^d(s), \tag{5.7}$$

respectively. For example, in Fig. 5.1 it holds $X_1 = W_{1,0}^d + W_{0,1}^a = W_{1,3}^d + W_{3,1}^a = W_{1,2}^d + W_{2,1}^a$ and $W_{1,2}^a = GW_{1,2}^d$ etc.
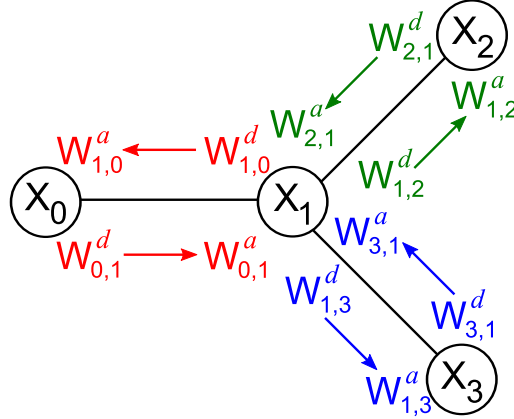
Figure 5.1: Notation of the wave components in a multi-agent system.

5.3 Mathematical description of the waves

It was shown in Chapter 2 that the wave travelling in a multi-agent system with a path graph topology and identical agents reflects only at the path-graph ends: the leader and the rear-end agent. The situation is more complicated in the case when the agent has multiple neighbours. In such a case, the wave partially reflects at the agent itself as well, which is described by the following theorem.

Theorem 11. *The transfer function, $T_{\mathrm{t},N}(s)$, describing the wave transmitting through the agent with N neighbours, and the transfer function, $T_{\mathrm{r},N}(s)$, describing the wave reflecting from the agent with N neighbours, are*

$$T_{\mathrm{t},N}(s) = \frac{W_{n,n-1}^d(s)}{W_{n+1,n}^a(s)} = \frac{T_N(s)(1 - G^2(s))}{G(s)(1 - NT_N(s)G(s))}, \; N \geq 2, \qquad (5.8)$$

$$T_{\mathrm{r},N}(s) = \frac{W_{n,n-1}^d(s)}{W_{n-1,n}^a(s)} = \frac{(N-1)T_N(s)G^2(s) + T_N(s) - G(s)}{G(s)(1 - NT_N(s)G(s))}, N \geq 1, \qquad (5.9)$$

where $(n-1)$th and $(n+1)$th are neighbouring agents of nth agent.

Proof. We substitute (5.5) into (5.4) and obtain

$$W_{n-1,n}^a + W_{n,n-1}^d = T_N \sum_{k \in \mathcal{N}_b} (W_{k,n}^d + W_{n,k}^a), \tag{5.10}$$

where we assume that $(n-1)$th agent is the neighbour of nth agent, hence $(n-1)$th agent is also a part of set $\mathcal{N}_b$. Eq. (5.5) can alternatively be expressed as

$$W_{n,k}^a = GX_n - GW_{k,n}^a = GW_{n-1,n}^a + GW_{n,n-1}^d - GW_{k,n}^a. \tag{5.11}$$

Substituting (5.11) into (5.10) and rearranging it gives

$$\begin{aligned} W_{n-1,n}^a + W_{n,n-1}^d = & T_N(G^{-1} - G) \sum_{k \in \mathcal{N}_b} (W_{k,n}^a) \\ & + NT_N G(W_{n-1,n}^a + W_{n,n-1}^d). \end{aligned} \tag{5.12}$$

Next, we separate the wave arriving from $(n-1)$th agent, that is $W_{n-1,n}^a$,

$$\begin{aligned} (1 - NT_N G)W_{n,n-1}^d = & T_N(G^{-1} - G) \sum_{k \in \mathcal{N}_b, k \neq (n-1)} (W_{k,n}^a) \\ & + (NT_N G + T_N(G^{-1} - G) - 1)W_{n-1,n}^a. \end{aligned} \tag{5.13}$$

Finally, separating the wave departing from nth agent to $(n-1)$th agent, $W_{n,n-1}^d$,

$$\begin{aligned} W_{n,n-1}^d = & \frac{T_N(1 - G^2)}{G(1 - NT_N G)} \sum_{k \in \mathcal{N}_b, k \neq (n-1)} W_{k,n}^a \\ & + \frac{(N-1)T_N G^2 + T_N - G}{G(1 - NT_N G)} W_{n-1,n}^a. \end{aligned} \tag{5.14}$$

Then

$$T_{r,N} = \frac{W_{n,n-1}^d}{W_{n-1,n}^a} = \frac{(N-1)T_N G^2 + T_N - G}{G(1 - NT_N G)} \tag{5.15}$$

is the transfer function which describes the reflection of the wave from the

nth agent, and

$$T_{t,N} = \frac{W_{n,n-1}^d}{W_{k,n}^a} = \frac{T_N(1-G^2)}{G(1-NT_NG)} \tag{5.16}$$

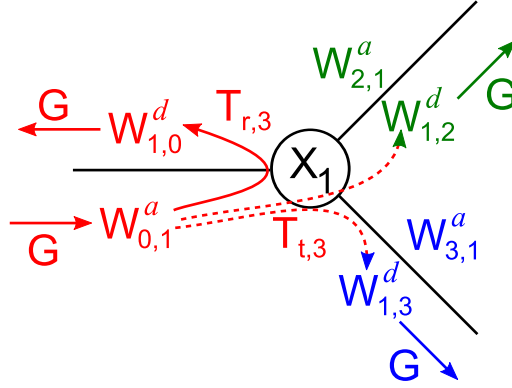describes the transmission of the wave through the nth agent. ☐

Figure 5.2: The detail of the reflection and transmission of the wave travelling from the 0th agent in Fig. 5.1, where G is the Wave transfer function from (2.24), $T_{t,3}$ and $T_{r,3}$ are the transfer functions defined by (5.8) and (5.9), respectively, with $N = 3$. Note that all agents are identical. The waves travelling from 2nd or 3rd agent are propagated analogously.

The interpretation of the theorem is as follows. If there is a wave travelling to the agent with multiple neighbours, then it is partially reflected from this agent (described by $T_{r,N}(s)$) and partially transmitted (described by $T_{t,N}(s)$). For example, the output, $X_1(s)$, of the multi-agent system in Fig. 5.2 can be expressed as

$$X_1 = (1 + T_{r,3})W_{0,1}^a + T_{t,3}W_{2,1}^a + T_{t,3}W_{3,1}^a. \tag{5.17}$$

The output is composed of three parts since the agent has three neighbours: i) wave that travels from 0th agent and reflects back to 0th agent, ii) wave that travels from 2nd agent and transmits to the 0th agent, and iii) wave that travels from 3rd agent and transmits to the 0th agent. We note that $X_1(s)$ can be expressed equivalently by calculating the reflected

wave travelling either from 2nd or 3rd agent.

5.4 Properties of the waves

Theorem 11 reveals an interesting relation between the transmitted and reflected waves. It is described by the following corollary.

Corollary 5. *The transfer functions $T_{\text{t},N}$ and $T_{\text{r},N}$ are related as follows*

$$T_{\text{t},N} - T_{\text{r},N} = 1, \tag{5.18}$$

for $N \geq 2$.

Proof. By the substitution for $T_{\text{t},N}$ and $T_{\text{r},N}$ from Theorem 11. $\qquad\square$

Theorem 11 is in agreement with the result of Section 2.3 that the wave in a multi-agent system with a path-graph topology and identical agents reflects only at the path-graph ends.

One of the important properties of the transfer function is the DC gain. The DC gain can be used to analyze the amplification/attenuation of the travelling wave as it propagates through the agent. The simulation example is shown in Section 5.5.2.

Lemma 11. *If the open-loop model of the agent, $M(s)$, has at least one integrator, then the DC gains of $T_{\text{t},N}$ and $T_{\text{r},N}$ depend only on the number of neighbours, N. Specifically,*

$$\kappa_{\text{T}} = \lim_{s \to 0} T_{\text{t},N}(s) = \frac{2}{N}, \tag{5.19}$$

$$\kappa_{\text{R}} = \lim_{s \to 0} T_{\text{r},N}(s) = \frac{2}{N} - 1, \tag{5.20}$$

where κ_{T} and κ_{R} are the DC gains of transfer functions $T_{\text{t},N}$ and $T_{\text{r},N}$, respectively.

Proof. If there is at least one integrator in the open-loop system of the agent, $M(s)$, then

$$\lim_{s \to 0} T_N = \lim_{s \to 0} \frac{M(s)}{1 + NM(s)} = \frac{1}{N} \tag{5.21}$$

and

$$\lim_{s \to 0} G = \lim_{s \to 0} \frac{1}{2} \alpha(s) - \frac{1}{2} \sqrt{\alpha^2(s) - 4} = 1, \tag{5.22}$$

since $\lim_{s \to 0} \alpha(s) = \lim_{s \to 0} 1/M(s) + 2 = 2$. Then

$$\kappa_{\mathrm{T}} = \lim_{s \to 0} T_{\mathrm{t},N} = \lim_{s \to 0} \frac{1}{G^2} \lim_{s \to 0} \frac{T_N(1 - G^2)}{G^{-1} - NT_N} = 1 \cdot \frac{0}{0}. \tag{5.23}$$

Applying l'Hopital's rule gives

$$\lim_{s \to 0} T_{\mathrm{lim}} = \lim_{s \to 0} \frac{T_N'(1 - G^2) + T_N(-2GG')}{-G^{-2}G' - NT_N'}$$

$$= \lim_{s \to 0} \frac{\dfrac{T_N'(1 - G^2)}{G'} + T_N(-2G)}{-G^{-2} - \dfrac{NT_N'}{G'}}, \tag{5.24}$$

where $'$ denotes the derivative with respect to the Laplace variable s.

We denote $M(s) = n(s)/d(s)$, where $n(s)$ and $d(s)$ are the polynomials in the numerator and denominator of $M(s)$, respectively. Then,

$$T_N'(s) = \left(\frac{n(s)}{d(s) + Nn(s)} \right)' = \frac{n'(s)d(s) - n(s)d'(s)}{(d(s) + Nn(s))^2}. \tag{5.25}$$

and

$$G' = \frac{1}{2} \alpha' - \frac{\alpha \alpha'}{2\sqrt{\alpha^2 - 4}}, \tag{5.26}$$

where

$$\alpha' = \frac{d'(s)n(s) - d(s)n'(s)}{n^2(s)}.\tag{5.27}$$

Now, we need to specify the number of integrators in $M(s)$.

One integrator in $M(s)$

One integrator in $M(s)$ causes that $\lim_{s\to 0} d'(s) \neq 0$ and $\lim_{s\to 0} d(s) = 0$, hence, $\lim_{s\to 0} T'_N \neq 0$ and $|\lim_{s\to 0} T'_N| \leq \infty$.

Moreover $\lim_{s\to 0} \alpha' \neq 0$ and consequently $\lim_{s\to 0} G' = -\infty$. Substituting for T_N, T'_N, G and G' into (5.24) gives $\lim_{s\to 0} T_{\lim} = 2/N$. Then

$$\kappa_{\mathrm{T}} = \lim_{s\to 0} T_{\mathrm{t},N} = \lim_{s\to 0} \frac{1}{G^2} T_{\lim} = 1 \cdot \frac{2}{N} = \frac{2}{N}.\tag{5.28}$$

More than one integrator in the OL

For two and more integrators, $\lim_{s\to 0} d'(s) = 0$ and $\lim_{s\to 0} T'_N = 0$, but $\lim_{s\to 0} \alpha' = 0$. Hence, we need to treat separately the limit of $\alpha'/\sqrt{\alpha^2 - 4}$ as follows

$$\begin{aligned}
\frac{\alpha'}{\sqrt{\alpha^2 - 4}} &= \frac{d'(s)n(s) - d(s)n'(s)}{n(s)\sqrt{d^2(s) + 4d(s)n(s)}} = \\
&= \frac{s^{p/2}\left(s^{(p/2)-1}\overline{d'}(s)n(s) - s^{p/2}\overline{d}(s)n'(s)\right)}{s^{p/2}n(s)\sqrt{s^p\overline{d^2}(s) + 4\overline{d}(s)n(s)}},
\end{aligned}\tag{5.29}$$

where p is the number of integrators in $M(s)$ and the overline symbol denotes the polynomial that is factored by the highest power of s, e.g.

$d(s) = s^p \overline{d}(s)$ or $d'(s) = s^{(p-1)}\overline{d'}(s)$. In view of (5.29), the limit of G' is

$$\lim_{s \to 0} G'(s) = \begin{cases} -\infty & \text{if } p = 1, \\ \lambda \in \mathbb{R} & \text{if } p = 2, \\ 0 & \text{if } p \geq 3. \end{cases} \tag{5.30}$$

Therefore, substituting from (5.30) into (5.24) gives

$$\kappa_{\mathrm{T}} = \lim_{s \to 0} T_{\mathrm{t},N} = \lim_{s \to 0} \frac{1}{G^2} T_{\lim} = 1 \cdot 2 \lim_{s \to 0} T_N = \frac{2}{N}. \tag{5.31}$$

The DC gain of the 'reflected' transfer function is inferred from (5.18) as

$$\kappa_{\mathrm{R}} = \kappa_{\mathrm{T}} - 1. \tag{5.32}$$

$\square$

5.5 The effect of the boundary in numerical simulations

5.5.1 The travelling waves

The numerical simulations are carried out for $P(s) = 1/(s(s+4))$ and $C(s) = (4s+4)/s$, which represents a second order system with a linear friction controlled by a PI controller. Hence, the complete model of the agent is $M(s) = (4s+4)/(s^2(s+4))$. The topology of the multi-agent system considered in simulations is shown in Fig. 5.3. We can see that only the agent indexed P_7 has three neighbours. We choose such a graph topology on the purpose to make the wave transmissions and reflections more transparent.

The way how the wave propagates in the system with the topology in Fig. 5.3 is shown in Fig. 5.4. The individual panels show:

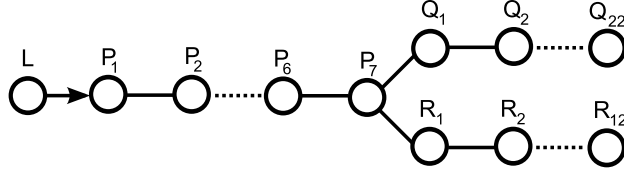- top-left – The wave is initiated by the leader and propagates to agent P_7.

Figure 5.3: The topology of the multi-agent system used in numerical simulations, where the 'L-node' is the externally controlled leader of the system.

- top-middle – The wave is being transmitted to 'Q' and 'R' parts of the graph (blue circles) and it is also reflected back to 'P' part (red crosses).
- top-right – The wave is reflected from agent R_{12} and propagates back to agent P_7 (red crosses).
- bottom-left and middle – The wave arriving to agent P_7 from 'R' part is transmitted to 'P' and 'Q' parts of the graph. We can see it by the increase of $W_{i+1,i}^a$ (red crosses) for agents P_1 - P_7 and $W_{i-1,i}^a$ (blue circles).
- bottom-right – The wave travelling from P_7 to P_1 is reflected from the leader with the negative sign and travels back to P_7. We can see it by the decrease of $W_{i-1,i}^a$ for P_1 - P_7 (blue circles).

Independent numerical validation of Theorem 11 is shown in the top panel of Fig. 5.5. We can see excellent agreement between the state-space and the wave approaches. The bottom panel shows individual waves traveling through agent P_7, where $W1 = W_{P6,P7}^a$, $W2 = T_{r,3}W_{P6,P7}^a$, $W3 = T_{t,3}W_{Q1,P7}^a$ and $W4 = T_{t,3}W_{R1,P7}^a$. In other words, $W2$ is the wave that travels from 'P' part of the graph and reflects from agent P_7, and $W3$ and $W4$ are waves that travel from 'Q' and 'R' parts of the graph, respectively, and transmit through agent P_7. Therefore,

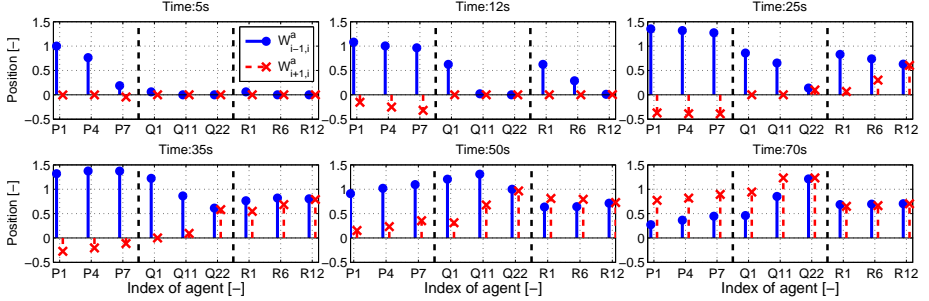$$W_{P7,P6}^d = W2 + W3 + W4 \qquad (5.33)$$

Figure 5.4: The numerical simulation of the wave propagating in the graph in Fig. 5.3. At the beginning, $t = 0$ s, all agents are at position 0 except of the leader, which changes its position from 0 to 1. At intermediate times, the wave travels to agent P_7, where it is partially transmitted to the 'Q' and 'R' parts of the graph and partially reflected back to the leader. The blue circles and red crosses represent $W_{i-1,i}^a$ and $W_{i+1,i}^a$ components of the wave on the ith agent, respectively. We can imagine these components as the left-to-right and right-to-left wave in the graph in Fig. 5.3, or as A and B components in the notation used in (2.21), respectively.

and

$$X_{P7} = W_{P6,P7}^a + W_{P7,P6}^d$$
$$= W_{P6,P7}^a + T_{\mathrm{r},3}W_{P6,P7}^a + T_{\mathrm{t},3}W_{Q1,P7}^a + T_{\mathrm{t},3}W_{R1,P7}^a. \qquad (5.34)$$

5.5.2 The effect of multiple neighbours

The local effect of the agent with more than two neighbours is demonstrated for the topology shown in Fig. 5.6. The response of the system, when the leader changes its position from 0 to 1, is given in Fig. 5.7. We can see that the more neighbours an agent has, the smaller the amplitude of the wave passing through the agent is. The figure also numerically verifies Lemma 11. Although the DC gain determines the steady state of the system, we can use it to approximate its output, in this case the position, even before the multi-agent system reaches its steady state. The transmitted wave is almost settled for time between 35 and 45 seconds and the
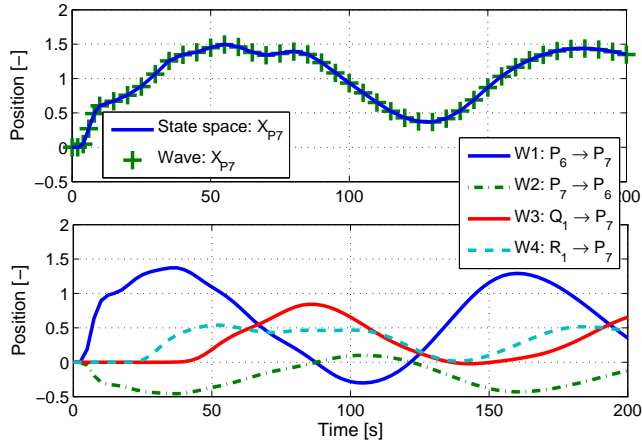
Figure 5.5: The top panel shows the comparison of the positions of agent P_7 in Fig. 5.4 simulated by the state-space approach using (5.4) (solid line) and by wave approach using (5.8) and (5.9) (plus signs). The bottom panel shows individual contributions of three waves arriving from the neighbouring agents of agent P_7.

reflected wave returns back to agent P_2 after about 45 seconds. Therefore the position of agent P_2 between 35 and 45 seconds is approximated by (5.19).

5.6   Design of an absorber for the agent

The description of the boundary allows us to design a controller that prevents reflection of the wave. The design is similar as for the soft and hard boundary in Section 3.3. We will show how to absorb the wave arriving to an agent from one direction. The design of the absorber for the other directions is analogous. We will demonstrate the design for the system shown in Fig. 5.1 by preventing the reflection of the wave travelling from the 0th agent.

First, we need to determine the response of the agent to an additional input, analogously as in Section 3.1.2. The model (5.3) of the 1st agent is
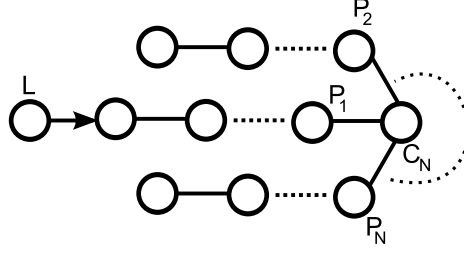
Figure 5.6: The star-graph topology of the multi-agent system. The central agent, C_N, has N neighbours. Each branch of the star graph has 20 agents with 'L-node' being the leader of the system.

modified as

$$X_1(s) = M(s) \sum_{k \in \{0,2,3\}} (X_k(s) - X_1(s)) + M(s)V_{0,1}(s), \qquad (5.35)$$

where $V_{0,1}(s)$ is the additional input of the agent as shown in Fig. 5.8.

We are interested in finding transfer function $T_{a,3}(s) = X_1(s)/V_{0,1}(s)$ for $N \to \infty$, that is, the transfer function from the additional input to the position of the agent in a system with an infinite number of agents. Hence, we do not consider the boundary conditions in the system, i.e. we disregard the waves reflected from the boundaries. Substituting $T_{a,3}$, (2.22) and (2.23) into (5.35) gives

$$\begin{aligned}
T_{a,3}(s)V_{0,1}(s) &= M(s)\left(X_0(s) + X_2(s) + X_3(s) - 3T_{a,3}(s)V_{0,1}(s) + V_{0,1}(s)\right) \\
&= M(s)\left(3G(s)T_{a,3}(s)V_{0,1}(s) - 3T_{a,3}(s)V_{0,1}(s) + V_{0,1}(s)\right).
\end{aligned} \qquad (5.36)$$

Rearranging yields

$$T_{a,3}(s) = \frac{M(s)}{1 + 3M(s) - 3M(s)G(s)}. \qquad (5.37)$$

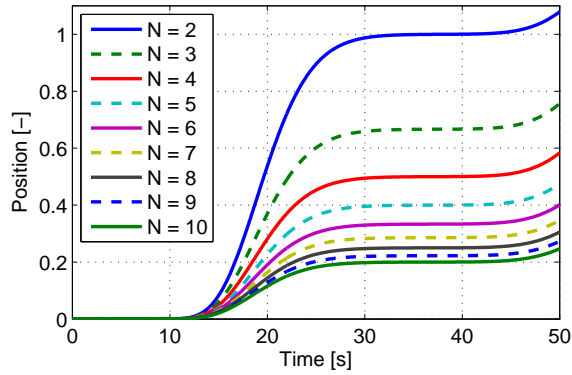The position of the 1st agent is described by (5.5), (5.8) and (5.9). We

Figure 5.7: Numerical simulations of multi-agent systems with different interaction topology. The topology is a star graph shown in Fig 5.6, where N denotes the number of neighbours of the central agent C_N. The vertical axis shows the position of agent P_2.

add the input $V_{0,1}(s)$ to the model and get

$$X_1(s) = (1 + T_{r,3}(s))W_{0,1}^a(s) + T_{t,3}(s)W_{2,1}^a(s) + T_{t,3}(s)W_{3,1}^a(s)$$
$$+ T_{a,3}(s)V_{0,1}(s). \tag{5.38}$$

The reflection of the wave travelling from the 0th agent is described by term $T_{r,3}(s)W_{0,1}^a(s)$. To eliminate the reflection, we set $V_{0,1}(s) =$
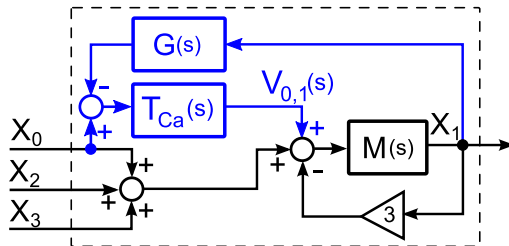

Figure 5.8: The model of 1st agent with the absorbing controller (highlighted in blue) that absorbs the wave travelling from the 0th agent, where $T_{Ca}(s) = G(s)/(1 + G(s))$ from (5.45).

$-F_a(s)W_{0,1}^a(s)$ and get

$$T_{r,3}(s)W_{0,1}^a(s) = T_{a,3}(s)F_a(s)W_{0,1}^a(s), \tag{5.39}$$

where $F_a(s)$ is the transfer function of the controller that prevents the reflection of the wave. Rearranging (5.39) gives

$$F_a(s) = \frac{-T_{r,3}(s)}{T_{a,3}(s)} = 1 - G(s). \tag{5.40}$$

The wave travelling from the 0th agent, $W_{0,1}^a(s)$, is given as in (3.64), that is

$$W_{0,1}^a(s) = \frac{G(s)}{1 - G^2(s)}X_0(s) - \frac{G^2(s)}{1 - G^2(s)}X_1(s). \tag{5.41}$$

The absorbing control law is then given as

$$\begin{aligned}
C_a(s) &= M(s)V_{0,1}(s) = M(s)F_a(s)W_{0,1}^a(s) \\
&= M(s)\frac{G(s)}{1 + G(s)}(X_0(s) - G(s)X_1(s)).
\end{aligned} \tag{5.42}$$

Substituting the control law from (5.42) into (5.38) yields

$$X_1(s) = W_{0,1}^a(s) + T_{t,3}(s)W_{2,1}^a(s) + T_{t,3}(s)W_{3,1}^a(s). \tag{5.43}$$

We can see that the wave does not reflect back to the 0th agent since $T_{r,3}(s)W_{0,1}^a(s)$ term is not present in the equation. Similarly, we can design absorbers for the waves travelling from other agents.

The results is summarized in the following theorem.

Theorem 12. *Let the agent indexed as b has $\mathcal{N}_b > 2$ neighbours. The control law that prevents the reflection of the wave travelling from the*

agent indexed as m, where $m \subset \mathcal{N}_b$, is given by

$$X_b(s) = M(s) \sum_{k \in \mathcal{N}_b} (X_k(s) - X_b(s)) + C_a(s), \tag{5.44}$$

where

$$C_a(s) = M(s) \frac{G(s)}{1 + G(s)} (X_m(s) - G(s)X_b(s)). \tag{5.45}$$

The performance of the individual control strategies of the system shown in Fig. 5.3 is compared in Fig. 5.9. We can see that the system without the absorber (top-left panel) has a very long transient. The transient can be shortened if we implement the absorber (2.53) to some of the system boundaries (bottom-left panel). The transient can further be shortened by implementing the absorber (2.53) to all agents with only one neighbour (top-right panel). However, we can see that the steady state value is changed from 1 to 2/3 due to the boundary at agent P_7. This effect is compensated by the implementation of the absorber (5.44) to agent P_7 (bottom-right panel), which prevents the reflection of the wave.

5.7   Extension for the non-identical agents

The travelling-wave approach can further be generalized for the case of non-identical agents in the multi-agent system. In such a case, the input to the agent changes from (5.2) to

$$U_n(s) = \sum_{i \in \mathcal{N}_b} C_{i,n}(s)(X_i(s) - X_n(s)), \tag{5.46}$$

where $C_{i,n}$ is the transfer function of the controller of the nth agent towards the ith agent. Therefore, (5.3) is modified as

$$X_n(s) = \sum_{i \in \mathcal{N}_b} M_{i,n}(s)(X_i(s) - X_n(s)), \tag{5.47}$$
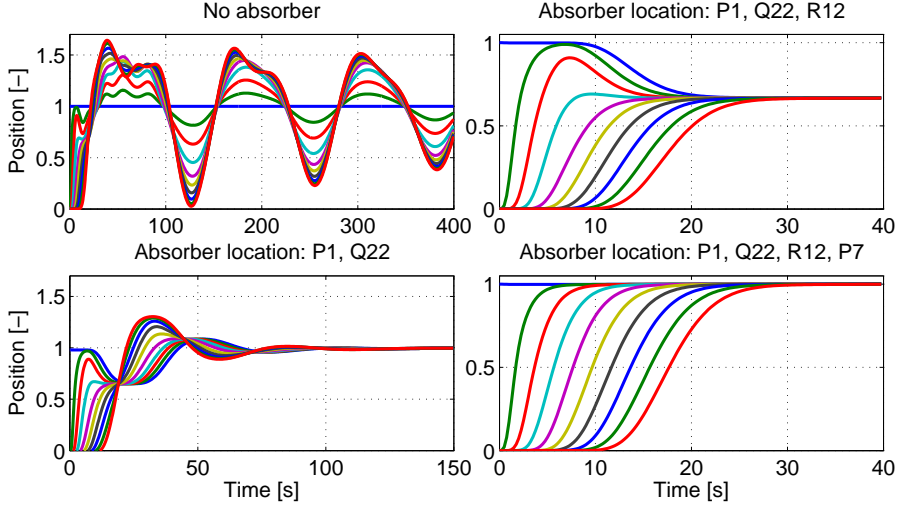
Figure 5.9: The performance comparison of individual control strategies for a multi-agent system shown in Fig. 5.3. The step response of four individual control strategies are compared. The top-left: the system with no absorber; top-right: the system with the absorber implemented to agents P_1, Q_{22} and R_{12}; bottom-left: the system with the absorber implemented to agents P_1 and Q_{22}; bottom-right: the system with the absorber implemented to agents P_1, Q_{22}, R_{12} and P_7.

where $M_{i,n}(s) = P(s)C_{i,n}$, or, alternatively,

$$X_n(s) = T_n(s) \sum_{i \in \mathcal{N}_b} M_{i,n}(s)X_i(s), \tag{5.48}$$

where $T_n(s) = \left(1 + \sum_{i \in \mathcal{N}_b} M_{i,n}(s)\right)^{-1}$. The wave transfer function describing the wave propagation is defined by

$$G_{i,n}(s) = 1 + \frac{1}{2M_{i,n}(s)} - \frac{1}{2}\sqrt{\frac{1}{M_{i,n}^2(s)} + \frac{4}{M_{i,n}(s)}}. \tag{5.49}$$

Similarly, as for the path-graph topology in Chapter 3, we need to distinguish between two cases: i) $M_{i,n}(s) \neq M_{j,n}(s)$ for $i, j \in \mathcal{N}_b$, $i \neq j$, and ii)

(a) Hard boundary on the 1st agent.

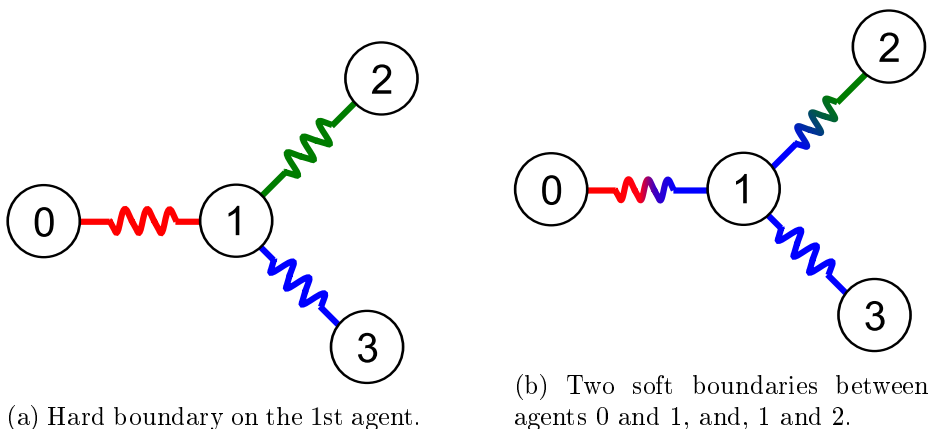(b) Two soft boundaries between agents 0 and 1, and, 1 and 2.

Figure 5.10: Boundaries in a general graph

$M_{k,n}(s) \neq M_{n,k}(s)$. We can imagine that i) as a generalization of a hard boundary for a general graph, while ii) is the soft boundary described by the same equations as in Section 3.2.1. The two boundaries are shown in Fig. 5.10.

Theorem 13. *The transfer function, $T_{\mathrm{t}}(s)$, describing the wave transmitting through the agent with more than two neighbours, and the transfer function, $T_{\mathrm{r}}(s)$, describing the wave reflecting from the agent with more than two neighbours, are*

$$T_{\mathrm{t}}(s) = \frac{W_{n,k}^d(s)}{W_{j,n}^a(s)} = \frac{T_n(s)M_{j,n}(s)\left(G_{j,n}^{-1}(s) - G_{j,n}(s)\right)}{1 - T_n(s)\sum_{i\in\mathcal{N}_b} M_{i,n}(s)G_{i,n}(s)}, \quad j \in \mathcal{N}_b \setminus k \tag{5.50}$$

$$T_{\mathrm{r}}(s) = \frac{W_{n,k}^d(s)}{W_{k,n}^a(s)} = \frac{T_n(s)M_{k,n}(s)G_{k,n}^{-1}(s)}{1 - T_n(s)\sum_{i\in\mathcal{N}_b} M_{i,n}(s)G_{i,n}(s)}$$
$$+ \frac{T_n(s)\sum_{j\in\mathcal{N}_b\setminus k} M_{j,n}(s)G_{j,n}(s) - 1}{1 - T_n(s)\sum_{i\in\mathcal{N}_b} M_{i,n}(s)G_{i,n}(s)}, \tag{5.51}$$

where k is the index of the agent where the wave transmits and $\mathcal{N}_b$ is a set of neighbouring agents to the nth agent.

136

Proof. Since the derivation is entirely carried out in the Laplace domain, we omit the argument 's' from notations.

Similarly to (5.5), we express the output of the nth agent as

$$X_n = W_{k,n}^a + W_{n,k}^d = W_{j,n}^a + W_{n,j}^d, \quad j \in \mathcal{N}_b \setminus k. \tag{5.52}$$

Hence,

$$W_{n,j}^d = W_{k,n}^a + W_{n,k}^d - W_{j,n}^a, \tag{5.53}$$

We assume there is no soft boundary between the agents, hence $G_{i,n} = G_{n,i}$, $M_{i,n} = M_{n,i}$ and

$$W_{n,i}^a = G_{i,n} W_{n,i}^d, \quad i \in \mathcal{N}_b \tag{5.54}$$
$$W_{i,n}^d = G_{i,n}^{-1} W_{i,n}^a. \quad i \in \mathcal{N}_b \tag{5.55}$$

Substituting (5.54) and (5.55) into (5.53) gives

$$W_{n,j}^a = G_{j,n} W_{k,n}^a + G_{j,n} W_{n,k}^d - G_{j,n} W_{j,n}^a. \tag{5.56}$$

Next, we substitute (5.52) into (5.48) and separate the part of the waves with index k.

$$\begin{aligned} W_{k,n}^a + W_{n,k}^d = & T_n M_{k,n} \left(W_{n,k}^a + W_{k,n}^d \right) \\ & + T_n \sum_{j \in \mathcal{N}_b \setminus k} M_{j,n} \left(W_{n,j}^a + W_{j,n}^d \right). \end{aligned} \tag{5.57}$$

Substituting from (5.54) and (5.55) for $W_{n,k}^a$ and $W_{k,n}^d$ and rearranging the result yields

$$\begin{aligned} (1 - T_n M_{k,n} G_{k,n}^{-1}) W_{k,n}^a + (1 - T_n M_{k,n} G_{k,n}) W_{n,k}^d = & \\ T_n \sum_{j \in \mathcal{N}_b \setminus k} M_{j,n} \left(W_{n,j}^a + W_{j,n}^d \right). \end{aligned} \tag{5.58}$$

Now, we substitute for $W_{n,j}^a$ from (5.56) and get

$$(1 - T_n M_{k,n} G_{k,n}^{-1}) W_{k,n}^a + (1 - T_n M_{k,n} G_{k,n}) W_{n,k}^d =$$
$$T_n \sum_{j \in \mathcal{N}_b \backslash k} M_{j,n} \left(G_{j,n} W_{k,n}^a + G_{j,n} W_{n,k}^d - G_{j,n} W_{j,n}^a + W_{j,n}^d \right). \quad (5.59)$$

Substituting for $W_{j,n}^d$ from (5.55) and rearranging the result gives

$$\left(1 - T_n M_{k,n} G_{k,n}^{-1} - T_n \sum_{j \in \mathcal{N}_b \backslash k} M_{j,n} G_{j,n} \right) W_{k,n}^a$$
$$+ \left(1 - T_n M_{k,n} G_{k,n} - T_n \sum_{j \in \mathcal{N}_b \backslash k} M_{j,n} G_{j,n} \right) W_{n,k}^d =$$
$$T_n \sum_{j \in \mathcal{N}_b \backslash k} M_{j,n} \left(-G_{j,n} + G_{j,n}^{-1} \right) W_{j,n}^a. \quad (5.60)$$

Finally, we substitute

$$- T_n M_{k,n} G_{k,n} - T_n \sum_{j \in \mathcal{N}_b \backslash k} M_{j,n} G_{j,n} = -T_n \sum_{i \in \mathcal{N}_b} M_{i,n} G_{i,n} \quad (5.61)$$

into (5.60) and obtain

$$W_{n,k}^d = \frac{T_n M_{k,n} G_{k,n}^{-1} + T_n \sum_{j \in \mathcal{N}_b \backslash k} M_{j,n} G_{j,n} - 1}{1 - T_n \sum_{i \in \mathcal{N}_b} M_{i,n} G_{i,n}} W_{k,n}^a$$
$$+ \sum_{j \in \mathcal{N}_b \backslash k} \frac{T_n M_{j,n} \left(G_{j,n}^{-1} - G_{j,n} \right)}{1 - T_n \sum_{i \in \mathcal{N}_b} M_{i,n} G_{i,n}} W_{j,n}^a. \quad (5.62)$$

$\square$

The interpretation of Theorem 13 is following. If there is a wave travelling to the agent with more than two neighbours, then the wave is partially reflected from the boundary (described by $T_r(s)$) and partially transmitted through the boundary (described by $T_t(s)$), see Fig. 5.11. Moreover, $T_t(s)$
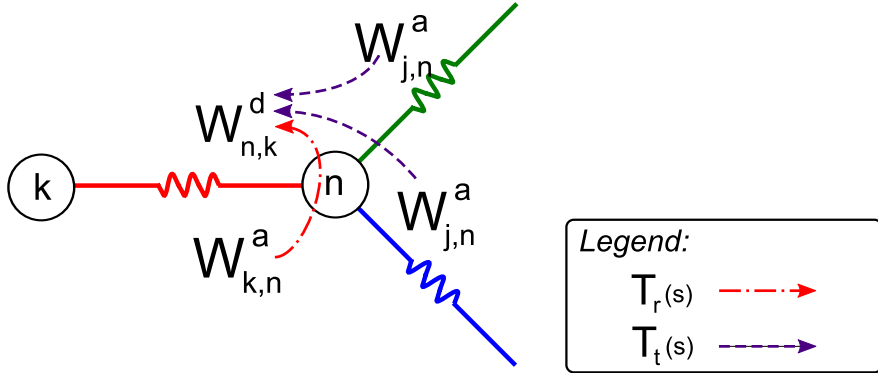
Figure 5.11: The transfer functions describing the wave reflection and transmission as stated by Theorem 13.

is independent of index k, which is the index of the agent where the wave is investigated. $T_t(s)$ changes with a change of the jth index, which means by a change of the direction where the wave travels from. Therefore, we can state the following Corollary.

Corollary 6. *The wave transmits through the hard boundary equivalently in all directions.*

However, it should be emphasized that the wave may propagate differently as it departs from the hard boundary after the transmission.

5.8 Conclusions

This chapter generalizes the travelling-wave approach to a multi-agent system with a general graph topology. It is shown that there are boundaries even in a system with identical agents. The boundaries are created at the agents with more than two neighbours. The undesired effect of the boundary can be suppressed by implementing of a wave-absorbing controller. By the numerical simulations we show that the wave-absorbing controller may significantly shorten the settling time of the system.

5.9   Appendix to the chapter

A boundary on the agent with multiple neighbours makes the analysis of a large multi-agent system cumbersome. The analysis may be simplified by introducing a similar "trick" as in Chapter 4. That is, we derive a Wave transfer function that describes waves in a multi-agent system, where each agent, except of those on the boundary, has three neighbours as shows Fig. 5.12.
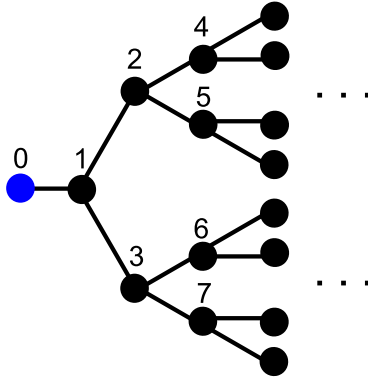

Figure 5.12: Topology of a "three-neighbours" multi-agent system. The blue circle is the leader that represents the input to the system.

The 1st agent in the system is described by

$$X_1(s) = M(s)(X_0(s) + X_2(s) + X_3(s) - 3X_1(s)). \qquad (5.63)$$

By the recursive process, identical to that described in Section 2.2.1, we get

$$\frac{X_1(s)}{X_0(s)} = \cfrac{1}{\cfrac{1+3M(s)}{M(s)} - \cfrac{2}{\cfrac{1+3M(s)}{M(s)} - \cfrac{2}{\cfrac{1+3M(s)}{M(s)} - \ddots}}}. \qquad (5.64)$$

Applying the continued-fraction expansion from (2.8), we obtain

$$\frac{X_1(s)}{X_0(s)} = G_{3\mathrm{N}}(s) = \frac{1 + 3M(s)}{4M(s)} - \frac{1}{2}\sqrt{\left(\frac{1 + 3M(s)}{2M(s)}\right)^2 - 2}, \quad (5.65)$$

which is the Wave transfer function for a multi-agent system where each agent has three neighbours. This allows us to more easily describe the way how the wave propagates in such a system. It also allows us to approximate the outputs of the agents, similarly as described in Section 3.4.2. For instance, if we change the position of the leader by $X_{\mathrm{ref}}(s)$, then

$$X_1(s) \approx G_{3\mathrm{N}}(s)X_0(s), \quad (5.66)$$

$$X_{2,3}(s) \approx G_{3\mathrm{N}}^2(s)X_0(s), \quad (5.67)$$

$$X_{4,5,6,7}(s) \approx G_{3\mathrm{N}}^3(s)X_0(s), \quad (5.68)$$
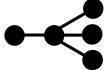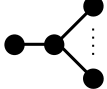
etc.

Similarly as for the three-neighbours system, we can derive a wave transfer function that describes the waves in a system, where the agents have four, five, etc. neighbours. This is summarized in Table 5.1. Their step responses are shown in Fig. 5.13.

The quadratic equation used for the Newton's approximation is, in this case, given as

$$f_N\left(G_{NN}(s)\right) = (N - 1)G_{NN}^2(s) - \frac{1 + NM(s)}{M(s)}G_{NN}(s) + 1. \quad (5.69)$$

Table 5.1: The overview of wave transfer functions for multi-agent systems, where each agent has N neighbours. The DC gain is carried out with the assumption that $M(s)$ has at least one integrator. We note that we omit the argument 's' from the "N" wave transfer functions.

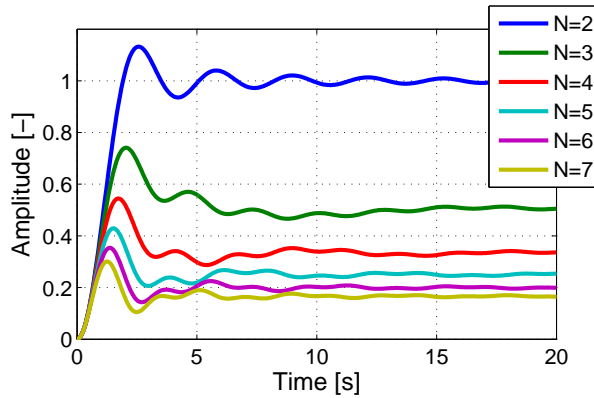| Topology	"N" wave transfer function	DC gain
	$G_{2\text{N}} = \dfrac{1+2M}{2M} - \sqrt{\left(\dfrac{1+2M}{2M}\right)^2 - 1}$	1
	$G_{3\text{N}} = \dfrac{1+3M}{4M} - \dfrac{1}{2}\sqrt{\left(\dfrac{1+3M}{2M}\right)^2 - 2}$	$\dfrac{1}{2}$
	$G_{4\text{N}} = \dfrac{1+4M}{6M} - \dfrac{1}{3}\sqrt{\left(\dfrac{1+4M}{2M}\right)^2 - 3}$	$\dfrac{1}{3}$
	$G_{NN} = \dfrac{1+NM}{2(N-1)M} - \dfrac{1}{N-1}\sqrt{\left(\dfrac{1+NM}{2M}\right)^2 - (N-1)}$	$\dfrac{1}{N-1}$

Figure 5.13: Comparison of step responses of the "N" wave transfer functions from Table 5.1 with $M(s) = 1/s^2$.

6 Conclusions

6.1 Contributions of the Wave transfer function approach

Wave transfer function

The wave approach is a complementary tool to the traditional state-space approach for the description and analysis of a multi-agent system. The wave approach gives insight into the local and temporal amplification or attenuation of the input command on the individual agents. This is particularly useful for a large-scale multi-agent system.

Let us illustrate it on the example of a multi-agent system with a path-graph topology. Let, for instance, the position of one agent of a system be externally changed due to an external reference command or a disturbance. Then this reference command also affects outputs of the neighbouring agents. We can think of this command as a 'wave' propagating in the system.The closed-form formula for the transfer function among the outputs of the agents can be found by the traditional approach, for instance, by the state-space description of the multi-agent system. As an example, we can find the transfer function $T_{1,2}(s) = X_2(s)/X_1(s)$ from the output of the first agent to the output of the second agent. However, to find this transfer function, the whole multi-agent system must be taken into consideration. Transfer function $T_{1,2}(s)$ then describes the overall behaviour of the multi-agent system since all the interactions among the agents and, in addition, the effect of boundary conditions are captured in this transfer function. This overall description is well suited for determin-

ing the asymptotic stability of a system, but it does not reveal the local behaviour of agents.

On the other hand, the transfer function $A_2(s)/A_1(s)$, or $B_1(s)/B_2(s)$, describes the interaction among the first and second agents from the local perspective, which means that it does not take into consideration neither the interactions among other agents nor the effect of the boundary conditions. The amplitude of the wave that is reflected or transmitted through the boundary can be approximated by the DC gain of the transfer functions. The approximation allows us to analyze the output of an agent before a reflected wave returns back to the agent. In other words, the wave approach provides a closed-loop formula that approximates the output of an agent. The important aspect is that the approximation is analytic allowing the mathematical analysis of its properties. Based on that, we can infer properties of the multi-agent system. The approximation is not affected by the number of agents or the interaction topology of other agents in the system. In fact, it gives exact results only until the reflected wave returns back to the agent. However, the wave approach also allows us to consider the effect of the reflected wave and extend the validity of the approximation.

An important feature of the Wave transfer function approach is that it describes the dynamics of the agent by two transfer functions ($M_f(s)$ and $M_r(s)$). This allows us to analyze even an asymmetric bidirectional control law with an arbitrary type of asymmetry and make conclusions (e.g. Theorem 10), which, the author believes, would be very challenging to make with the traditional approach.

It should be noted that the local transfer functions, i.e. the Wave or Boundary transfer functions, can also be used to provide the overall transfer function $X_2(s)/X_1(s)$ by taking $[A_2(s) + B_2(s)]/[A_1(s) + B_1(s)]$. It can be shown on the examples that this transfer function has no square root, so it is rational and is equal to $T_{1,2}(s)$. However, this calculation again requires to consider interactions among all the other agents, which is rather complicated with the wave approach.

Wave-absorbing controller

The advantage of the wave controller is that it allows the modification of the reflection conditions for the travelling waves on a boundary. Importantly, this modification does not require to change controllers of the other agents in the system and, under certain conditions, it can make the system string stable. Another advantage is that the output of the controller is only slightly modified. Therefore, the proposed control law is feasible.

The disadvantage is that the agent with the wave controller is required to know its own output, for instance, by the odometry, and the output of its immediate neighbour, which can be obtained either by the relative measurement or communication with the neighbour. Another difficulty is that the agent requires to know its own and neighbour's dynamical models. If these conditions are not satisfied, for instance, the dynamical model of neighbours is known only approximately, or the information about the neighbour's output is delayed in time, then the wave is not fully absorbed and it partially reflects back to the system. However, the numerical simulations show that the response of the system may still be improved since these schemes are relatively robust to inaccuracies. This is in agreement with experience from practical implementations of the wave absorbers, see for instance [Saigo et al. (2004)], [Kreuzer and Steidl (2011)] or [O'Connor et al. (2008)].

We consider the wave controllers as an illustration what can be achieved by the application of the wave approach. We note that, although some simpler controllers may improve the transient of a system, only the wave absorber fully absorbs the travelling wave.

Relation to the basic wave physics

The important feature of the wave approach is that it is in agreement with findings of the basic wave physics. Most of the results of this thesis can immediately be put into correspondence with known wave physics

phenomenons. For instance, i) the decomposition of the agent output into two travelling waves (Theorem 1, p. 18) vs. travelling waves and their superposition (Chapter 7 of [French (2003)]), ii) the reflections at the forced and free-end boundaries (Section 2.3, p. 23) vs. reflections at a fixed and free ends (Fig. 8-1, p. 255 of [French (2003)]), iii) the soft and hard boundaries (Section 3.2.1, p. 66) vs. wave pulses encountering the boundary between two media (Fig. 8-4, p. 260 of [French (2003)]), etc.

The fact that the links between the agents are created by the controllers allows us to generalize the Wave transfer function approach even to the asymmetric case (Chapter 4). As a result of this generalization, the wave does not propagate equally in the forward and backward directions. This makes the physical interpretation of the asymmetric link unclear, since, to the best of author's knowledge, a device such as an asymmetric spring violates the Third Newton's Law and cannot exist in nature.

It is also important to emphasize that the generalization of the wave approach to a general-graph topology (Chapter 5) cannot be interpreted in terms of waves in two or three dimensional space (part of Chapter 7 of [French (2003)]).

6.2   Contributions of the author

The goal of the thesis was to analyze the wave-based control and to generalize this approach to the field of the distributed control. This required to solve several challenging problems that were new in the field.

The first problem was to generalize the Wave transfer function for an agent with arbitrary dynamics and to use it for the design of a wave-absorbing controller that improves the performance of the system, specifically, the transient and also the string stability of the system. The generalization also required to develop a method that approximates the Wave transfer function. The results are presented in [Martinec et al. (2014a)] and [Martinec et al. (2014b)] (XIII[1] and I).

---

[1]The roman letters tag the publications of the author given on p. 169.

The second problem was to show how different dynamics of some agents in the system affect the wave travelling in the system. This was solved by introducing the soft and hard boundary concept, which led to the derivation of the local control law that prevents the wave to be reflected from these boundaries. The most challenging problem here was to show that this control law makes the system asymptotically and string stable. The results are presented in [Martinec et al. (2014d)] and [Martinec et al. (2014c)] (XIV and II).

The drawback of the approach mentioned in the previous paragraph is that we assume that the wave is travelling equivalently in both directions. This assumption is satisfactory if most of the agents use a symmetric bidirectional control law. However, if most of the agents use an asymmetric control law, then there are many boundaries in the system, which is cumbersome to handle. This drawback was resolved by generalizing the travelling wave approach for the wave travelling unequally in both directions. An unequal propagation inherently includes the boundaries on the agents caused by the asymmetric control law, which makes the description of the multi-agent system by this generalized approach significantly easier. The most important result of this problem is that the symmetric positional coupling is a necessary condition for achieving the string stability, as presented in [Martinec et al. (2015a)] (V).

The last problem that was solved in the thesis is the generalization of the travelling wave approach to a multi-agent system with a general-graph topology, i.e. to a system where an agent may have more than two neighbours. The agent with multiple neighbours represents a boundary for the travelling wave even if the agent has the identical dynamics as its neighbours. This case is presented in [Martinec et al. (2015b)] (XVIII). The thesis further elaborates the approach and presents the control law that prevents the reflection of waves. Based on the numerical simulations, it is shown that the control law shortens the transient of the system. However, due to the lack of time and space limitations, it has not been analytically derived under which conditions the system with the control law is asymptotically stable. It is likely that the proof would be similar to the proof

of Theorem 7. It has also been shown how to generalize the concept for a
non-identical agent with multiple neighbours.

6.3   Open problems

The travelling-wave approach is a new approach in the field of the dis-
tributed control. To the best of author's knowledge, the approach has not
been rigorously analyzed from the control-theory point-of-view by other
authors. Despite the new results presented in the thesis, there are other
open problems ranging from general questions regarding the asymptotic
stability of the Wave transfer function over the analysis of the multi-agent
system properties to potential applications of the wave absorbers.

Here is a list of some of open problems:

Mathematical open problems

- Derive necessary conditions for the asymptotic stability of the Wave
  transfer function. The conditions given by Lemma 4 are only sufficient.
- Find an exact analytical impulse response of the Wave transfer func-
  tions. The state-of-the-art software is not capable to perform the in-
  verse Laplace transform of an irrational transfer function (discussion
  on p. 21).
- Based on the author's experience and numerical simulations, the New-
  ton's method (Section 2.7.2) is numerically a more reliable method for
  an approximation of the Wave transfer functions than other methods.
  However, it remains open in which sense (norm) the approximation by
  Newton's method converges to the Wave transfer function. It is also
  not solved yet how to choose the initial guess of Newton's iterations
  and why the relative order of the initial guess determines the root to
  which the method converges.

Open problems related to the control theory

- It is well described how the location of poles and zeros of a rational transfer function affect its time response. Regarding the irrational transfer function, it is still a challenge for investigations ([Curtain and Morris (2009)]). Similarly, it would be also worth to analytically investigate how the model of an agent affects the impulse/step/Bode response of the Wave transfer function (Fig. 2.20, p. 61).
- The numerical simulations (Fig. 1.1, p. 8) of the symmetric bidirectional control law show that the outputs of the agents oscillate between zero and two if they respond to the unit step in x_{ref}. However, the proof of that is yet to be shown. The wave approach may be a suitable tool for the proof since it shows that the H_∞ norm of the Wave transfer function is bounded by one (Lemma 3, p. 34).
- Theorem 10 (p. 110) gives the condition for the local-string stability of the system. However, the numerical simulations show that the multi-agent system is locally-string unstable but asymptotically stable even in the cases when the Asymmetric Wave transfer function tends to be asymptotically unstable. Therefore, it seems that the boundary conditions, that is the first and the last agents, asymptotically stabilize a multi-agent system. The way how and why it is possible is to be solved.
- Section 5.6 derives the wave-absorbing controller for a multi-agent system with a general-graph topology. The numerical simulations show that the controller may shorten the settling time. However, if the graph has a limit cycle, then the controller may even destabilize the whole system, which raises the question. What is the optimal number and locations of the absorbers?
- It is shown in Section 5.6 that the Wave transfer function description of a system with an asymmetric bidirectional control is complicated since there are two boundaries between the neighbouring agents. This problem is solved by introducing the Asymmetric wave transfer function. The same problem occurs in a system with the general-graph topology since the wave also reflects at each agent with more than two neighbours. For some topologies, the problem can be solved by the ap-
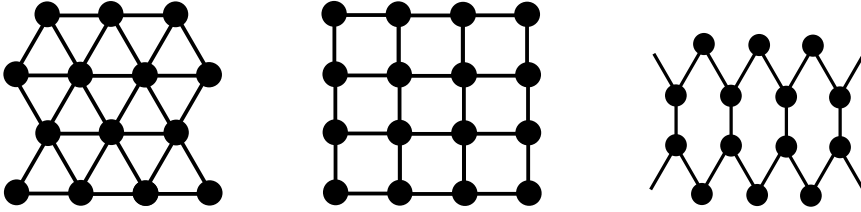
Figure 6.1: Examples of topologies

proach introduced in Section 5.9. It is not clear how to apply the same trick for more general topologies, for instance, those shown in Fig. 6.1. The largest difficulty seems to be due the cycles that are present in the graph.

- It is not discussed in this thesis that the control effort of the wave-absorbing controller is closely related to the zero-vibration input shapers. The preliminary results, mostly based on the numerical simulations, are given in [Martinec et al. (2015c)] (XVII). However, a thorough analytical comparison is yet to be carried out.

- Examine the possibility to generalize the Wave transfer function for a nonlinear system.

General open problems

- Carry on in the investigation of properties of the topologies given in Table 5.1 (p. 142). An asymmetric coupling between the agents may possibly be also treated by this approach. It would be worth to investigate it since systems with a general-graph topology are not well explored and the simplification of their description may reveal interesting properties similar to 'necessity of symmetric positional coupling' treated by Theorem 10 (p. 110).

- The physical interpretation of the 'necessity of symmetric positional coupling' (Theorem 10, p. 110) is still unclear.

- Examine possible practical applications of the wave-absorbing controllers (Theorems 2, 5 and 6, pages 31, 78 and 80).

- The authors of [Cantos and Veerman (2014)] analyze the transient of

a large array of linear oscillators. They argue that a wave behaviour is apparent in the response of the system and give an analytic estimate of the so-called *signal velocity*, which represents the speed of the wave. It may be possible that a similar analytic measure of the wave speed could be obtained by the travelling-wave approach presented in the thesis.

7 Appendix

7.1 Wavebox

The current state-of-the-art software (see the discussion in Section 2.2.3, p. 21) is not capable to carry out the inverse Laplace transform of an irrational transfer function such as the wave transfer function. To be able to run numerical simulations, the author implemented a set of functions with examples in Matlab. Therefore, the reader can run the simulations without the necessity of implementing the approximation methods. The set of functions, called *WaveBox*, is available for download at Matlab Central [Martinec (2015)].

The current version of the WaveBox (ver 1.1) contains:

Examples

Example1 – This example demonstrates the absorption of the wave in a multi-agent system with a path-graph topology where all agents are identical (see Section 2.5, p. 38). The wave is absorbed on the leader, which has no dynamics.

Example2 – The same as in *Example1* but the leader has its own internal dynamics.

Example3 – This example demonstrates the absorption of the wave in a multi-agent system with a path-graph topology where the agents are not identical. One soft boundary is assumed to be in the system (see Section 3.4, p. 83).

Example4 – The same as in *Example3* but with the hard boundary.

Example5 – This example is a combination of *Example3* and *Example4*. It shows behaviour of the system with a complex boundary (combination of the soft and hard boundaries).

Example6 – This example demonstrates the absorption of the wave in a multi-agent system with a general topology where the agents are identical but can have multiple neighbours (see Section 5.5, p. 127).

Methods

approximate_ AWTF– Approximates the Asymmetric wave transfer functions by (4.11)-(4.12) (p. 98).

approximate_ BGTF – Approximates the transfer functions describing the transmission and reflection of the waves, $T_{t,N}(s)$ and $T_{r,N}(s)$ (Theorem 11, p. 121), on an agent with multiple neighbours.

approximate_ BTF – Approximates the Boundary transfer functions for prescribed front and rear agent transfer functions (see (3.3), p. 65).

approximate_ WTF – Approximates the Wave transfer function for the given open-loop model of the agent (Sections 2.5 and 2.7.2, p. 38 and p. 49).

decompose_ waves – Decomposes the outputs of two neighbouring agents into two travelling waves A and B (Theorem 1, p. 18).

init_ absorber_ BGTF – Initializes the wave absorber for a boundary on an agent with multiple neighbours (Theorem 12, p. 133).

init_ absorber_ BTF – Initializes the wave absorber for the soft and hard boundaries (Theorems 5 and 6, p. 78 and p. 80).

init_ absorber_ leader – Initializes the wave absorber for the leader or the rear-end agent (Theorem 2, p. 31).

It should be noted that, in some cases, the approximation methods may run into a numerical instability. This exhibits as a sudden instability after seemingly settled response. The problem is usually resolved by a change of the number of iterations or the time-length of the approximation.

7.2 Overview of the results from distributed control - Table 7.1

Comments to Table 7.1

PF1 - The eigenvalues of the system do not converge to 0 as for (SB1).

PF2, SB2 and PA2 - [Martinec et al. (2014b)] analytically shows that the transient of identical systems connected in a series (PF2) grows better than linearly with the number of agents. The same paper numerically shows that the transient of the symmetric bidirectional control (SB2) scales quadratically. (SB2) is also supported by the results of [Barooah et al. (2009)] that the least stable eigenvalue, i.e. the smallest eigenvalue of the system approaches 0 as $\mathcal{O}(1/N^2)$. In contrast, the eigenvalues in PF2 are multiplied and do not converge to 0. The least stable eigenvalue in PA2 is also bounded away from zero and converges as $\mathcal{O}(1/N)$, see [Hao and Barooah (2012a)], therefore, its transient is faster than of the SB2.

PF3, PF4 and PF5 - The closed loop transfer function from the input to the output of the nth agent is $T^n(s) = (M(s)/(1 + M(s)))^n$, where $M(s)$ has one, two or three integrators. A proper choose of the numerator of $M(s)$ can asymptotically stabilize $T^n(s)$.

PF6 and PF8 - The closed loop transfer function from the input to the output of the nth agent is $T^n(s) = (M(s)/(1 + M(s)))^n$, where $M(s)$ has one integrator. If $||T(s)||_\infty \leq 1$, then the system is string (PF6) and flock (PF8) stable.

PF7, PF9, PF10 proved by [Seiler et al. (2004)].

SB1, SB3, SB6 and SB8 - [Barooah and Hespanha (2005)] proved that, if the open-loop model has one integrator and the deviation of the leader's trajectory from a constant velocity is bounded in L_2 norm, then the spacing errors between the vehicles is bounded, irrespective of the number of

Table 7.1: The table summarizes the state-of-the-art of a linear control of a multi-agent system with the path-graph topology. Only algorithms that require no agent-to-agent communication are shown. Legend: F - fast transient, M - medium transient, S - slow, M_+ - better than medium transient, M_- - worse than medium transient. The ✓ says that the property can be achieved. The ✗ says that the property can not be achieved. If the symbol is in the circle, then the property is analytically proved. The properties that are not circled are based on the numerical simulations. The questionmark symbolizes the property that is expected by author's experience but yet not analyzed. The parts highlighted in red and squared are the results of this thesis. The lower index at some of the properties refers to the explanation bellow the table.

Algorithm	Transient		Asymptotic stability			String stability		Flock stability		
	1 int.	≥2 int.	1 int.	2 int.	≥3 int.	1 int.	>2 int.	1 int.	2 int.	≥3 int.
Predecessor following	Ⓕ PF1	Ⓕ PF2	✓⃝ PF3	✓⃝ PF4	✓⃝ PF5	✓ PF6	✗⃝ PF7	✓ PF8	✗⃝ PF9	✗⃝ PF10
Symmetric bidirectional	Ⓜ SB1	Ⓢ SB2	✓⃝ SB3	✓⃝ SB4	✗⃝ SB5	✓ SB6	✗⃝ SB7	✓ SB8	✓⃝ SB9	✗⃝ SB10
Proportional asymmetry	Ⓕ PA1	Ⓜ₊ PA2	✓⃝ PA3	✓⃝ PA4	✓⃝ PA5	✓ PA6	✗⃝ PA7	✓ PA8	✗⃝ PA9	✗⃝ PA10
More Laplacians, $c_{f,0}=c_{r,0}$	F	M-	✓	✓	✗?	✓	✗ Ls7	✓	✓ Ls9	✗⃝ Ls10
More Laplacians, $c_{f,0}\neq c_{r,0}$	F	M+	✓	✓	✓?	✓	☒ La7	✓	☒ La9	✗⃝ La10
$C_f(s)\neq C_r(s)$, but $c_{f,0}=c_{r,0}$	?	?	✓?	✓?	?	✓?	✗? SO7	✓?	✓? SO9	✗?
$C_f(s)\neq C_r(s)$, and $c_{f,0}\neq c_{r,0}$	?	?	✓?	✓?	?	✓?	☒ AO7	✓?	☒ AO9	✗?

vehicles. Hence, we call the system string and flock stable.

SB4 - It was shown in [Barooah et al. (2009)] that the system with two integrators can be made stable and that the least stable eigenvalue of the system approaches 0 as $\mathcal{O}(1/N^2)$.

SB5 can not be made asymptotically stable as showed in [Barooah and Hespanha (2005)].

SB10, PA5, Ls10 and La10 - [Herman et al. (2015b)] showed that a circular system where the agents has three integrators is asymptotically unstable, which was also showed in [Cantos and Veerman (2014)] for one particular system. However, a path-graph can be made asymptotically stable, for instance, by the predecessor following algorithm. [Herman et al. (2015b)] further numerically confirms the conjecture of [Cantos and Veerman (2014)] that, if the circular system is asymptotically unstable, then the path-graph system is either asymptotically or flock unstable. The reasoning is that a disturbance inside the circular system grows as it propagates from its origin. If the disturbance acts inside the path-graph system, then the boundary conditions (the first and the last agents) may asymptotically stabilize the system. Therefore, a sufficiently high value of N leads to asymptotically unstable path-graph system, however, if N is small then the system can be made asymptotically stable.

SB7 and SB9 - It was shown in [Veerman et al. (2007)] that the peak in the Bode characteristics grows approximately linearly with the number of agents.

PA1 and PA3 - The system has eigenvalues on the negative real axis, see for instance [Herman et al. (2014b)].

PA4 - It was shown in [Hao and Barooah (2012a)] that the least stable eigenvalue of the system is bounded away from 0 and the eigenvalue approaches it as $\mathcal{O}(1/N)$.

PA6 and PA8 - It was shown in [Herman et al. (2014b)] that at most one integrator in the open-loop model is a necessary condition for the string

stability. Although the condition is not sufficient, the appropriate choice of the controller makes the system string stable.

PA7, PA9 and PA10 follows from the product form shown in [Herman et al. (2014a)] and [Herman et al. (2015a)] that two integrators in the agent's model cause the harmonic instability. PA7 and PA9 are also independently verified by [Martinec et al. (2015a)].

Ls7, Ls9, SO7 and SO9 - The system with a path-graph topology can be made locally-string stable as shown in [Martinec et al. (2015a)]. It seems that the system is string unstable due to the boundary conditions, that is, the first and the last vehicles, as in the case of (SB7). If that is true, then it should be flock stable since the disturbance in the system is not going to scaled exponentially with the number of vehicles.

La7, La9, AO7 and AO9 - It was shown in [Martinec et al. (2015a)] that the symmetric positional coupling ($c_{\mathrm{f},0} = c_{\mathrm{r},0}$) is a necessary but not sufficient condition for the string stability. Otherwise, the travelling wave in the system is exponentially amplified as it propagates in the system.

Bibliography

Abramowitz, M. and Stegun, I. (1964). *Handbook of mathematical functions: with formulas, graphs, and mathematical tables*. Dover Publications.

Amat, S., Busquier, S., and Plaza, S. (2004). Review of some iterative root-finding methods from a dynamical point of view. *Scientia*, 10, 3–35.

Arcak, M. (2007). Passivity as a Design Tool for Group Coordination. *IEEE Transactions on Automatic Control*, 52(8), 1380–1390.

Asmar, N.H. (2004). *Partial Differential Equations with Fourier Series and Boundary Value Problems*. Pearson Prentice Hall, New Jersey, 2nd editio edition.

Bamieh, B., Jovanovic, M.R., Mitra, P., and Patterson, S. (2012). Coherence in Large-Scale Networks: Dimension-Dependent Limitations of Local Feedback. *IEEE Transactions on Automatic Control*, 57(9), 2235–2249.

Barooah, P., Mehta, P., and Hespanha, J. (2009). Mistuning-Based Control Design to Improve Closed-Loop Stability Margin of Vehicular Platoons. *IEEE Transactions on Automatic Control*, 54(9), 2100–2113.

Barooah, P. and Hespanha, J. (2005). Error amplification and disturbance propagation in vehicle strings with decentralized linear control. In *44th IEEE Conference on Decision and Control*, theorem 3, 4964–4969.

Bibliography

Bateman, H. and Erdélyi, A. (1954). *Tables of integral transforms.* California Institute of technology. Bateman Manuscript project. A. Erdélyi, editor. W. Magnus, F. Oberhettinger, F. G. Tricomi, research associates. McGraw-Hill, New York.

Brancik, L. (1999). Programs for fast numerical inversion of Laplace transforms in MATLAB language environment. *Conference MATLAB*, 27–39.

Briegel, B., Zelazo, D., Bürger, M., and Allgöver, F. (2011). On the zeros of consensus networks. *50th IEEE Conference on Decision and Control and European Control Conference*, 1890–1895.

Cantos, C.E. and Veerman, J.J.P. (2014). Transients in the Synchronization of Oscillator Networks. *eprint arXiv:1308.4919.*

Cao, M., Zhang, S., and Camlibel, M.K. (2012). A Class of Uncontrollable Diffusively Coupled Multiagent Systems with Multichain Topologies. (February 2013), 465–469.

Carlson, G. and Halijak, C. (1964). Approximation of Fractional Capacitors $(1/s)^{(1/n)}$ by a Regular Newton Process. *IEEE Transactions on Circuit Theory*, (5), 210–213.

Cayley, A. (1879). Application of the Newton-Fourier method to an imaginary root of an equation. *Quarterly Journal of Pure and Applied Mathematics*, 16, 179–185.

Chiang, M. (2012). *Networked Life: 20 Questions and Answers.* Cambridge University Press, New York.

Chopra, N. and Spong, M.W. (2006). Passivity-Based Control of Multi-Agent Systems. In *Advances in Robot Control*, 107–134. Springer Berlin Heidelberg.

Chu, K.c. (1974). Decentralized control of high-speed vehicular strings. *Transportation Science*, 8(4), 361–384.

Corless, R.M., Gonnet, G.H., Hare, D.E.G., Jeffrey, D.J., and Knuth, D.E. (1996). On the Lambert W Function. In *Advances in Computational Mathematics*, 329–359.

Cosgriff, R. (1969). The asymptotic approach to traffic dynamics. *IEEE Transactions on Systems Science and Cybernetics*, (4), 361–368.

Curtain, R. and Morris, K. (2009). Transfer functions of distributed parameter systems: A tutorial. *Automatica*, 45(5), 1101–1116.

Das, S. (2011). *Functional fractional calculus*. Springer Berlin Heidelberg.

de Hoog, F.R., Knight, J.H., and Stokes, A.N. (1982). An Improved Method for Numerical Inversion of Laplace Transforms. *SIAM Journal on Scientific and Statistical Computing*, 3(3), 357–366.

Dhaene, T. and Zutter, D.D. (1992). Selection of lumped element models for coupled lossy transmission lines. *IEEE Transactions on Computer-Aided Design of Integrated Circuits and Systems*, (July), 805–815.

Dwivedy, S.K. and Eberhard, P. (2006). Dynamic analysis of flexible manipulators, a literature review. *Mechanism and Machine Theory*, 41(7), 749–777.

Egerstedt, M., Martini, S., and Cao, M. (2012). Interacting with networks: How does structure relate to controllability in single-leader, consensus networks? *IEEE Control systems magazine*, (July), 66–73.

Elwakil, A. (2010). Fractional-order circuits and systems: an emerging interdisciplinary research area. *IEEE Circuits and Systems Magazine*, 40—-50.

Eyre, J., Yanakiev, D., and Kanellakopoulos, I. (1998). A Simplified Framework for String Stability Analysis of Automated Vehicles. *Vehicle System Dynamics*, 375–405.

Flotow, A.H. (1986a). Disturbance propagation in structural networks. *Journal of Sound and Vibration*, 106(3), 433–450.

Bibliography

Flotow, A.H. (1986b). Traveling wave control for large spacecraft structures. *Journal of Guidance Control and Dynamics*, 9(4), 462–468.

French, A.P. (2003). *Vibration's and Waves*. M.I.T. introductory physics series. CBS Publishers & Distributors, New Delhi.

Halevi, Y. (2005). Control of Flexible Structures Governed by the Wave Equation Using Infinite Dimensional Transfer Functions. *Journal of Dynamic Systems, Measurement, and Control*, 127(4), 579.

Halevi, Y. and Wagner-Nachshoni, C. (2006). Transfer function modeling of multi-link flexible structures. *Journal of Sound and Vibration*, 296(1-2), 73–90.

Hao, H. and Barooah, P. (2010). Control of large 1D networks of double integrator agents: Role of heterogeneity and asymmetry on stability margin. In *49th IEEE Conference on Decision and Control (CDC)*, 7395–7400. IEEE.

Hao, H. and Barooah, P. (2012a). On Achieving Size-Independent Stability Margin of Vehicular Lattice Formations With Distributed Control. *IEEE Transactions on Automatic Control*, 57(10), 2688–2694.

Hao, H. and Barooah, P. (2012b). Stability and robustness of large platoons of vehicles with double-integrator models and nearest neighbor interaction. *International Journal of Robust and Nonlinear Control*, 23(18), 2097–2122.

Hao, H., Yin, H., and Kan, Z. (2012). On the robustness of large 1-D network of double integrator agents. In *American Control Conference (ACC)*, 6059–6064.

Herman, I., Martinec, D., Hurak, Z., and Sebek, M. (2015a). Nonzero Bound on Fiedler Eigenvalue Causes Exponential Growth of H-Infinity Norm of Vehicular Platoon. *IEEE Transactions on Automatic Control*, 60(8), 2248–2253.

Herman, I., Martinec, D., Hurák, Z., and Šebek, M. (2014a). Harmonic instability of asymmetric bidirectional control of a vehicular platoon. In *Control Conference (ACC), 2014 American*, 5396–5401.

Herman, I., Martinec, D., Hurák, Z., and Šebek, M. (2014b). Scaling in bidirectional platoons with dynamic controllers and proportional asymmetry. *Submitted to IEEE Transactions on Automatic Control*, 1–12.

Herman, I., Martinec, D., Veerman, J.J.P., and Sebek, M. (2015b). Stability of a circular system with multiple asymmetric Laplacians. In *5th IFAC Workshop on Distributed Estimation and Control in Networked Systems (NecSys)*.

Jones, W.B. and Thron, W.J. (1984). *Continued Fractions: Analytic Theory and Applications*. Encyclopedia of Mathematics and its Applications. Cambridge University Press, New York.

Jovanovic, M. and Bamieh, B. (2005). On the ill-posedness of certain vehicular platoon control problems. *IEEE Transactions on Automatic Control*, 50(9), 1307–1321.

Kelly, J.J. (2006). *Graduate Mathematical Physics*. Wiley-VCH, Weinheim.

Kreuzer, E. and Steidl, M. (2011). Controlling torsional vibrations of drill strings via decomposition of traveling waves. *Archive of Applied Mechanics*, 82(4), 515–531.

Lesieutre, B. (2002). Impedance matching controllers to extinguish electromechanical waves in power networks. *IEEE International Conference on Control Applications*, 25–30.

Lestas, I. and Vinnicombe, G. (2007). Scalability in heterogeneous vehicle platoons. *2007 American Control Conference*, (M), 4678–4683.

Levine, W. and Athans, M. (1966). On the optimal error regulation of a string of moving vehicles. *IEEE Transactions on Automatic Control*, 11(3), 355–361.

Lin, F., Fardad, M., and Jovanovic, M.R. (2012). Optimal Control of Vehicular Formations With Nearest Neighbor Interactions. *IEEE Transactions on Automatic Control*, 57(9), 2203–2218.

Bibliography

Lunze, J. (2012). Synchronization of Heterogeneous Agents. *IEEE Transactions on Automatic Control*, 57(11), 2885–2890.

Lunze, J. (2013). A method for designing the communication structure of networked controllers. *International Journal of Control*, 86(9), 1489–1502.

Malti, R., Melchior, P., Lanusse, P., and Oustaloup, A. (2012). Object-oriented CRONE toolbox for fractional differential signal processing. *Signal, Image and Video Processing*, 6(3), 393–400.

Martinec, D. (2015), WaveBox. MATLAB Central File Exchange (http://www.mathworks.com/matlabcentral/fileexchange/51958), Retrieved November 27, 2015.

Martinec, D., Herman, I., Hurák, Z., and Šebek, M. (2014a). Refinement of a bidirectional platooning controller by wave absorption at the leader. In *Control Conference (ECC), 2014 European*, 2845–2850.

Martinec, D., Herman, I., Hurák, Z., and Šebek, M. (2014b). Wave-absorbing vehicular platoon controller. *European Journal of Control*, 20, 237–248.

Martinec, D., Herman, I., and Sebek, M. (2014c). A travelling wave approach to a multi-agent system with a path-graph topology. *submitted to Automatica*.

Martinec, D., Herman, I., and Sebek, M. (2014d). Two-sided wave-absorbing control of a heterogenous vehicular platoon. In *Proceedings of the 19th IFAC World Congress, 2014*, 1986, 8091–8096.

Martinec, D., Herman, I., and Sebek, M. (2015a). On the necessity of symmetric positional coupling for string stability. *submitted to IEEE Transactions on Control of Network Systems*, 1–7.

Martinec, D., Herman, I., and Sebek, M. (2015b). Travelling waves in a multi-agent system with general graph topology. *5th IFAC Workshop on Distributed Estimation and Control in Networked Systems (NecSys)*, (4), 1–6.

164

Martinec, D., Hromčík, M., Herman, I., Vyhlídal, T., and Šebek, M. (2015c). On zero-vibration signal shapers and a wave-absorbing controller for a chain of multi-agent dynamical systems. In *2015 European Control Conference*, 1025–1030.

Martinec, D., Sebek, M., and Hurak, Z. (2012). Vehicular platooning experiments with racing slot cars. *2012 IEEE International Conference on Control Applications*, 166–171.

Mei, C. (2011). Wave control of vibrations in multi-story planar frame structures based on classical vibration theories. *Journal of Sound and Vibration*, 330(23), 5530–5544.

Melzer, S. and Kuo, B. (1971). A closed-form solution for the optimal error regulation of a string of moving vehicles. *IEEE Transactions on Automatic Control*, 16(1), 50–52.

Mesbahi, M. and Egerstedt, M. (2010). *Graph theoretic methods in multiagent networks*. Princeton Series in Applied Mathematics. Princeton University Press, New Jersey.

Middleton, R.H. and Braslavsky, J.H. (2010). String Instability in Classes of Linear Time Invariant Formation Control With Limited Communication Range. *IEEE Transactions on Automatic Control*, 55(7), 1519–1530.

Moreau, L. (2005). Stability of multiagent systems with time-dependent communication links. *IEEE Transactions on Automatic Control*, 50(2), 169–182.

Nagase, K., Ojima, H., and Hayakawa, Y. (2005). Wave-based Analysis and Wave Control of Ladder Networks. *44th IEEE Conference on Decision and Control*, 5298–5303.

O'Connor, W.J. (2006). Wave-echo control of lumped flexible systems. *Journal of Sound and Vibration*, 298(4-5), 1001–1018.

O'Connor, W.J. (2007). Wave-Based Analysis and Control of Lump-Modeled Flexible Robots. *IEEE Transactions on Robotics*, 23(2), 342–352.

Bibliography

O'Connor, W.J., Ramos de la Flor, F., McKeown, D.J., and Feliu, V. (2008). Wave-based control of non-linear flexible mechanical systems. *Nonlinear Dynamics*, 57(1-2), 113–123.

Ojima, H., Nagase, K., and Hayakawa, Y. (2001). Wave-based analysis and wave control of damped mass-spring systems. *40th IEEE Conference on Decision and Control*, 8(December), 2574–2579.

Olfati-Saber, R., Fax, J., and Murray, R. (2007). Consensus and cooperation in networked multi-agent systems. *Proceedings of the IEEE*, (January), 215–233.

Ortigueira, M. (2008). An introduction to the fractional continuous-time linear systems: the 21st century systems. *IEEE Circuits and Systems Magazine*, 8(3), 19–26.

Oustaloup, A., Melchior, P., Lanusse, P., Cois, O., and Dancla, F. (2000). The CRONE toolbox for Matlab. In *CACSD. Conference Proceedings. IEEE International Symposium on Computer-Aided Control System Design*, 190–195. IEEE.

Peled, I., O'Connor, W., and Halevi, Y. (2012). On the relationship between wave based control, absolute vibration suppression and input shaping. *Mechanical Systems and Signal Processing*, 1–11.

Petras, I. (2008). Stability of fractional-order systems with rational orders. *Fractional Calculus and Applied Analysis*, 269—-298.

Ploeg, J., van de Wouw, N., and Nijmeijer, H. (2014). Lp String Stability of Cascaded Systems: Application to Vehicle Platooning. *IEEE Transactions on Control Systems Technology*, 22(2), 786–793.

Ren, W., Beard, R.W., and Atkins, E. (2007). Information consensus in multivehicle cooperative control. *IEEE Control systems magazine*, (April), 71–82.

Saigo, M., Tanaka, N., and Nam, D.H. (2004). Torsional vibration suppression by wave-absorption control with imaginary system. *Journal of Sound and Vibration*, 270(4-5), 657–672.

Seiler, P., Pant, A., and Hedrick, K. (2004). Disturbance Propagation in Vehicle Strings. *IEEE Transactions on Automatic Control*, 49(10), 1835–1841.

Shaw, E. and Hedrick, J.K. (2007). Controller design for string stable heterogeneous vehicle strings. In *46th IEEE Conference on Decision and Control*, 2868–2875. IEEE.

Singhose, W., Derezinski, S., and Singer, N. (1996). Extra-insensitive input shapers for controlling flexible spacecraft. *Journal of Guidance, Control, and Dynamics*, 19(2), 385–391.

Sirota, L. and Halevi, Y. (2014). Wave based vibration control of membranes. *2014 American Control Conference*, 2729(4), 2729–2734.

Sirota, L. and Halevi, Y. (2015). Fractional order control of the two-dimensional wave equation. *Automatica*, 59, 152–163.

Stein, E.M. and Shakarchi, R. (2010). *Complex Analysis*. Princeton lectures in analysis. Princeton University Press, New Jersey.

Swaroop, D. and Hedrick, J.K. (1999). Constant Spacing Strategies for Platooning in Automated Highway Systems. *Journal of Dynamic Systems, Measurement, and Control*, 121(3), 462.

Swaroop, D. and Hedrick, J. (1996). String stability of interconnected systems. *IEEE Transactions on Automatic Control*, 41(3), 349–357.

Tangerman, F., Veerman, J., and Stosic, B. (2012). Asymmetric decentralized flocks. *IEEE Transactions on Automatic Control*, 57(11), 2844–2853.

Thorp, J., Seyler, C., and Phadke, A. (1998). Electromechanical wave propagation in large electric power systems. *IEEE Transactions on Circuits and Systems*, 7122(June), 614–622.

Vaughan, D.R. (1968). Application of Distributed Parameter Concepts to Dynamic Analysis and Control of Bending Vibrations. *Journal of Basic Engineering*, 90(2), 157–166.

Bibliography

Veerman, J., Stosic, B.D., and Olvera, A. (2007). Spatial instabilities and size limitations of flocks. *Networks and Heterogeneous Media*, 2(4), 647–660.

Vinagre, B., Podlubny, I., and Feliu, V. (2000). Some approximations of fractional order operators used in control theory and applications. *Journal of Fractional Calculus and Applied Analysis*, 231—-248.

Vyhlídal, T., Kučera, V., and Hromčík, M. (2013). Signal shaper with a distributed delay: Spectral analysis and design. *Automatica*, 49(11), 3484–3489.

Weeks, W.T. (1966). Numerical Inversion of Laplace Transforms Using Laguerre Functions. *Journal of the ACM*, 13(3), 419–429.

Wieland, P., Sepulchre, R., and Allgöwer, F. (2011). An internal model principle is necessary and sufficient for linear output synchronization. *Automatica*, 47(5), 1068–1074.

Yamamoto, K. and Smith, M. (2013). Mass chains with passive interconnection: Complex iterative maps and scalability. In *52nd IEEE Conference on Decision and Control*, 37–42.

Zamani, M., Helmke, U., and Anderson, B.D. (2015). Zeros of networked systems with time-invariant interconnections. *Automatica*, 61, 97–105.

Zelazo, D. and Mesbahi, M. (2011). Edge Agreement: Graph-Theoretic Performance Bounds and Passivity Analysis. *IEEE Transactions on Automatic Control*, 56(3), 544–555.

Zhang, H., Lewis, F.L., and Qu, Z. (2012). Lyapunov, Adaptive, and Optimal Design Techniques for Cooperative Systems on Directed Communication Graphs. *IEEE Transactions on Industrial Electronics*, 59(7), 3026–3041.

Publications of the author

Journal publications

I. D. Martinec, I. Herman, Z. Hurák, M. Šebek. Wave-absorbing vehicular platoon controller. *European Journal of Control*, 20:237–248, 2014. Co-authorship: 50%.

II. D. Martinec, I. Herman, M. Šebek. A travelling wave approach to a multi-agent system with a path-graph topology. *Submitted to Automatica (2nd revision)*, 2014. Co-authorship: 65%.

III. I. Herman, D. Martinec, Z. Hurák, M. Šebek. Scaling in bidirectional platoons with dynamic controllers and proportional asymmetry. *Submitted to IEEE Transactions on Automatic Control*, 2014. Co-authorship: 30%.

IV. I. Herman, D. Martinec, Z. Hurák, M. Šebek. Nonzero bound on Fiedler eigenvalue causes exponential growth of H-infinity norm of vehicular platoon. *IEEE Transactions on Automatic Control*, 60(8):2248–2253, 2015. Co-authorship: 30%.

V. D. Martinec, I. Herman, M. Šebek. On the necessity of symmetric positional coupling for string stability. *Submitted to IEEE Transactions on Control of Network Systems (2nd revision)*, 2015. Co-authorship: 65%.

VI. I. Herman, D. Martinec, M. Šebek. Transfer functions in consensus systems with higher-order dynamics and external inputs. *Submitted*

to IEEE Transactions on Control of Network Systems, 2015. Co-authorship: 30%.

VII. I. Herman, D. Martinec, J.J.P. Veerman. Transients of platoons with asymmetric and different Laplacians. *Submitted to Systems and Control Letters*, 2015. Co-authorship: 30%.

Conference publications

VIII. D. Martinec, Z. Hurák. Vehicular platooning experiments with LEGO MINDSTORMS NXT. *IEEE International Conference on Control Applications (CCA), (MSC)*, 927–932, 2011. Co-authorship: 50%.

IX. D. Martinec, M. Šebek, Z. Hurák. Vehicular platooning experiments with racing slot cars. *IEEE International Conference on Control Applications (CCA), (MSC)*, 166–171, 2012. Co-authorship: 50%.

X. I. Herman, D. Martinec, Z. Hurák, M. Šebek. Equalization of intervehicular distances in platoons on a circular track. *International Conference on Process Control 2013*, 47–52, 2013. Co-authorship: 30%.

XI. D. Martinec, M. Bundzel. Evolutionary Algorithms and Reinforcement Learning in Experiments with Slot Cars. *International Conference on Process Control 2013*, 159–162, 2013. Co-authorship: 50%.

XII. I. Herman, D. Martinec, Z. Hurák, M. Šebek. PDdE-based analysis of vehicular platoons with spatio-temporal decoupling. *4th IFAC Workshop on Distributed Estimation and Control in Networked Systems (NecSys)*, 144–151, 2013. Co-authorship: 30%.

XIII. D. Martinec, I. Herman, Z. Hurák, M. Šebek. Refinement of a bidirectional platooning controller by wave absorption at the leader. *European Control Conference 2014*, 2845–2850, 2014. Co-authorship: 50%.

XIV. D. Martinec, I. Herman, M. Šebek. Two-sided wave-absorbing control of a heterogenous vehicular platoon. *Proceedings of the 19th IFAC World Congress*, 8091–8096, 2014. Co-authorship: 65%.

XV. I. Herman, D. Martinec, Z. Hurák, M. Šebek. Harmonic instability of asymmetric bidirectional control of a vehicular platoon. *American Control Conference 2014*, 5396–5401, 2014. Co-authorship: 30%.

XVI. I. Herman, D. Martinec, M. Šebek. Zeros of transfer functions in networked control with higher-order dynamics. *Proceedings of the 19th IFAC World Congress*, 9177–9182, 2014. Co-authorship: 30%.

XVII. D. Martinec, M. Hromčík, I. Herman, T. Vyhlídal, M. Šebek. On zero-vibration signal shapers and a wave-absorbing controller for a chain of multi-agent dynamical systems. *European Control Conference 2015*, 1025–1030, 2015. Co-authorship: 50%.

XVIII. D. Martinec, I. Herman, M. Šebek. Travelling waves in a multi-agent system with general graph topology. *5th IFAC Workshop on Distributed Estimation and Control in Networked Systems (NecSys)*, 2015. Co-authorship: 65%.

XIX. I. Herman, D. Martinec, J.J.P. Veerman, M. Šebek. Stability of a circular system with multiple asymmetric Laplacians. *5th IFAC Workshop on Distributed Estimation and Control in Networked Systems (NecSys)*, 2015. Co-authorship: 30%.